Secular evolution of galaxies

XXIII Canary Islands Winter School of Astrophysics

Edited by

J. Falcón-Barroso and J. H. Knapen

Galaxy morphology

Ronald J. Buta

Department of Physics and Astronomy, University of Alabama
Box 870324, Tuscaloosa, AL 35487, USA
buta@sarah.astr.ua.edu

Abstract

Galaxy morphology has many structures that are suggestive of various processes or stages of secular evolution. Internal perturbations such as bars can drive secular evolution through gravity torques that move gas into the central regions and build up a flattened, disk-like central bulge, or which may convert an open spiral pseudoring into a more closed ring. Interaction between individual components of a galaxy, such as between a bar and a dark halo, a bar and a central mass concentration, or between a perturbation and the basic state of a stellar disk, can also drive secular transformations. In this series of lectures, I review many aspects of galaxy morphology with a view to delineating some of the possible evolutionary pathways between different galaxy types.

2.1 Introductory remarks

A principal goal of extragalactic studies has been to understand what drives the morphology of galaxies. It is important to determine the dynamical and evolutionary mechanisms that underlie the bewildering array of forms that define the various galaxy classification schemes used today (e.g., Sandage & Bedke 1994; Buta *et al.* 2007), because this will allow us to establish the relationships, if any, between different galaxy types. Physical interpretations of galaxy morphology have revolved around two different domains: (1) formative evolution, where rapid, violent processes, such as hierarchical clustering and merging, led to formation of major galactic components, such as bulges, disks, haloes, and presumably, the Hubble sequence (e.g., White & Rees 1978; Firmani & Avila-Reese 2003); and (2) secular evolution, where disk material is slowly rearranged through the collective interaction of instabilities, such as bars, ovals, spirals, and triaxial dark matter haloes

(Kormendy & Kennicutt 2004, hereafter KK04). KK04 argued that the Universe is in a state of transition, where secular evolution is becoming the dominant process of morphological change.

Galaxy morphology is a classical subject with a rich history in astronomy. Associated with many famous names, such as the Herschels, Lord Rosse, Curtis, Shapley, Hubble, Lundmark, Reynolds, Sandage, Morgan, and de Vaucouleurs, morphology and classification are the first step in the study of galaxies as fundamental units of matter in space. As elegantly noted by Peng *et al.* (2002), clues to galaxy formation and evolution 'are hidden in the fine details of galaxy structure.'

With this series of lectures, I not only have the great privilege of laying out the fine details of galaxy morphology in the tradition of these earlier observers, but also I must do so in the context of secular evolution. This is very challenging, not just because the subject is so broad, but because we are only beginning to understand how secular processes operate in galaxies. Fortunately, my colleagues at this School bring a considerable expertise on this subject, and I feel like I can cover galaxy morphology at the level of detail that I think is needed.

Galaxy morphology may be a classical subject in astronomy, but it has a surprising freshness that has defied predictions of its impending irrelevance to true understanding of galaxies. Classical galaxy morphology and classification have survived into the modern era for several reasons: the *Hubble Space Telescope* (*HST*), the Sloan Digital Sky Survey (SDSS), and the improved understanding of the meaning of different morphological types through extensive theoretical and observational studies. There can be little doubt that morphology holds the key to recognising the processes of galactic evolution, and that it will continue to provide insight as the relationships between different types of galaxies become better established.

My goals with this series of lectures on galaxy morphology are to: (1) provide a historical overview of galaxy morphology and classification; (2) illustrate phenomenology and highlight notation; (3) introduce non-optical galaxy classification; (4) describe interpretative galaxy classification; (5) describe environmental impacts on galaxy morphology; (6) describe the important quantitative tools used for modern morphological studies and the use of large surveys to explore morphology on an unprecedented scale; and finally (7) highlight the importance and relevance of morphology to the evidence for secular evolution in galaxies.

In describing morphology, I will draw heavily on two recent sources: the de Vaucouleurs Atlas of Galaxies (dVA, Buta *et al.* 2007) and the major

review on galaxy morphology by Buta (2013, hereafter B13) for the new series: Planets, Stars, and Stellar Systems.

2.2 How is morphology relevant to secular evolution?

Morphology is the key to understanding secular processes. Galaxies are susceptible to internal instabilities or component interactions that can affect a galaxy's basic structure and slowly change it over time. Even subtle interactions with the environment can produce long-term secular evolution (Kormendy & Bender 2012). Relevant questions are like this: when you see a galaxy of type SA(s)b or SB(r)c, etc., has the galaxy always had this type, or have these types evolved from other types? Is there a specific direction of evolution, e.g., from late to early type, from barred to nonbarred, from pseudoringed to ringed, from spiral to nonspiral? What guidance can we get from theory regarding these questions?

It is not hard to find speculative examples of possible morphological evolution. For example, Fig. 2.1 shows two morphologically similar galaxies that differ in a few ways: one (NGC 3351) is a clear intermediate-type spiral while the other (NGC 2859) is a 'late' S0; the spiral has very little bulge while the S0 has a more prominent bulge; the bar in the S0 looks weaker than that in the spiral, while the rings in the spiral are better described as pseudorings compared to what is seen in the S0. Looking at these two galaxies, one might wonder if a galaxy like NGC 2859 might be a possible end-product of some long-term evolutionary process in a galaxy like NGC 3351. Indeed, it was from examining such possible relationships that Kormendy (1979) first proposed the idea that secular evolution takes place in barred galaxies: he noticed a special relationship between bars and features called 'lenses' that suggested to him that bars may dissolve over time into a more axisymmetric state, the engine of dissolution being an interaction between the spheroidal component and the bar. This idea was not far off the mark: Bournaud & Combes (2002) examined bar dissolution and rejuvenation in models with and without external gas accretion. In the models without accretion, the bar evolves to a lens-like structure.

In examining the impact of secular evolution on galaxy morphology, we should be mindful of the intrinsic and extrinsic factors that have an impact on morphology. Here is a brief summary of these factors:

Random orientations of symmetry axes. Inclination of the symmetry plane to the line of sight, and the accompanying projection effects and enhanced influence of dust obscuration, is probably the most important

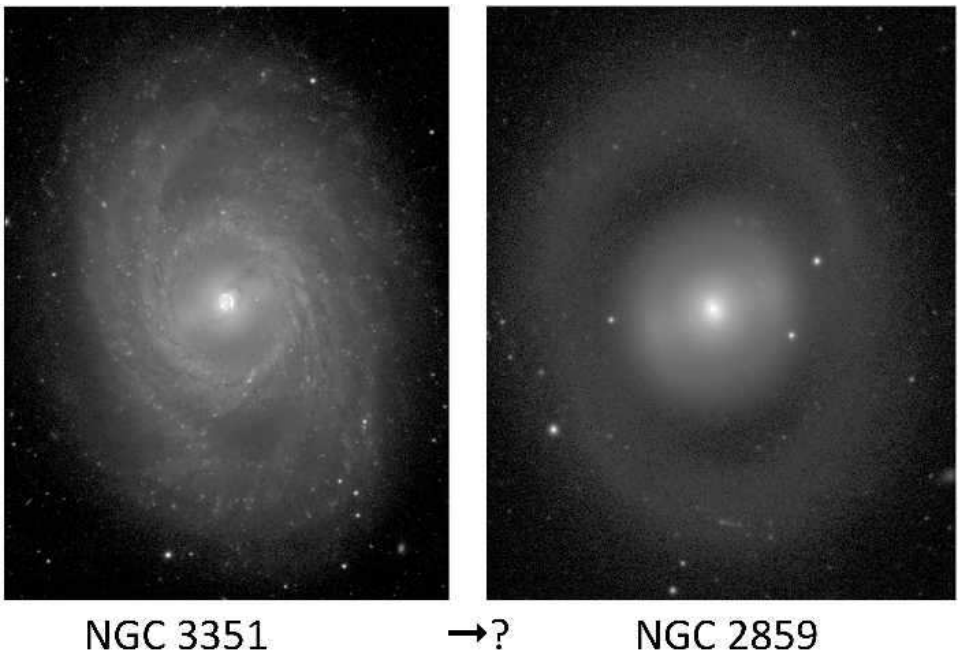

Fig. 2.1. Does the similarity between these two galaxies, one an intermediate-type spiral and the other a late S0, imply an evolutionary connection?

extrinsic factor affecting the morphology of nearby galaxies. As a disk-shaped galaxy is viewed from a face-on orientation to an edge-on orientation, the appearance of familiar morphological features can change. For example, a bar may become so foreshortened that it is not recognisable. If a bar has significant three-dimensional structure, its face-on shape can be lost while its edge-on shape becomes its distinguishing characteristic. Rings and spiral patterns can be lost or less recognisable, although, as shown in B13, these features may still be evident even at inclinations as high as 81°.

Wavelength of observation. The influence of dust and star formation on spiral galaxy morphology has a strong wavelength dependence (Fig. 2.2). The blue (B) band, the historical waveband of galaxy classification studies, is sensitive to reddening and extinction by dust, and to the hot blue stars associated with star-forming regions. As wavelength increases from B to the near-infrared (IR), the dust becomes more transparent, reddening and extinction are reduced, and the influence of star-forming regions diminishes, giving spiral galaxies a smoother appearance in the red and near-IR. However, a curious thing happens in the mid-IR. In this wavelength domain, the ultraviolet energy absorbed by dust grains in star-forming regions is

Fig. 2.2. NGC 5364 in two passbands. The B-band emphasises dust and star formation, while the I-band is less sensitive to dust and emphasises an older, more smoothly distributed stellar population.

re-emitted strongly, and is already evident at 3.6μm by the return of the prominence of star-forming regions even as the extinction diminishes to only 5% of that in the V-band. As is shown in Lecture 3 (Section 2.6), 3.6μm galaxy morphology is astonishingly similar to B-band morphology, absent the effects of extinction and reddening.

Total mass and luminosity. Figure 2.3 shows the strong dependence of galaxy morphology on total mass and luminosity. M 81 is a giant spiral having a B-band absolute magnitude of -21.1 and shows extremely organised and well-developed high-surface brightness structure. DDO 155, a dwarf having $M_B^o = -12.1$, is in contrast a very small, low surface brightness, irregular-shaped galaxy. Van den Bergh (1960a,b) and Sandage & Tammann (1981) effectively used such differences to define galactic *luminosity classes* (van den Bergh 1998; dVA; B13).

Environmental density, interaction, and merger history. The strong correlation between environmental density and galaxy morphology was first described by Hubble & Humason (1935) and studied in greater detail by Dressler (1980). The morphology-density relation, as it is called, is such that denser environments like rich galaxy clusters have a preponderance of early-type (E, S0) galaxies compared to lower-density environments (Fig. 2.4).

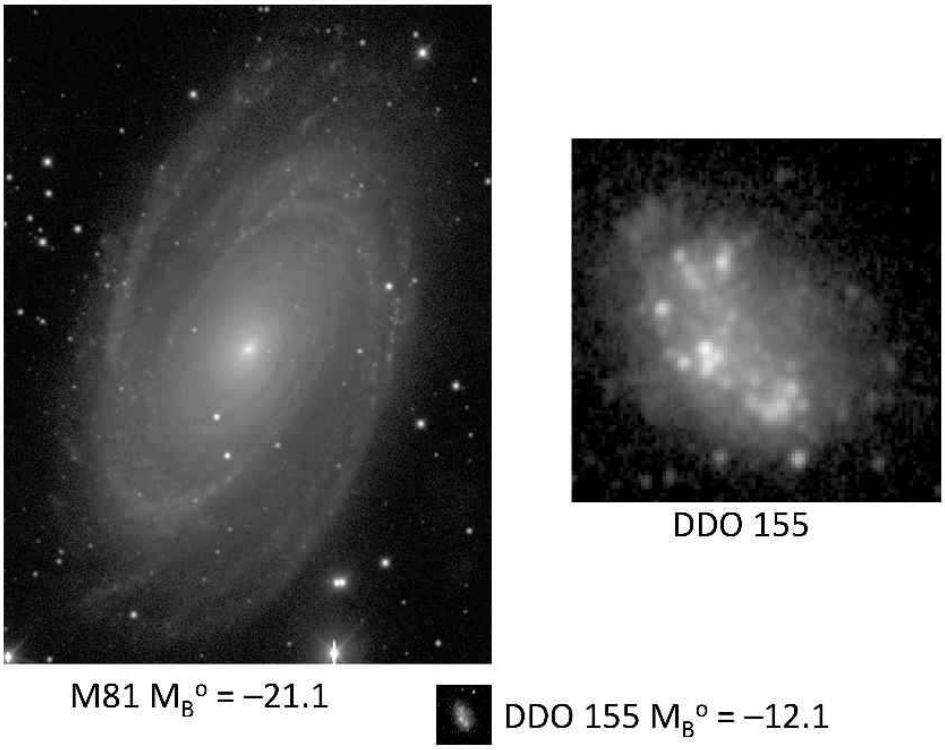

Fig. 2.3. The effect of luminosity on *B*-band morphology, comparing the giant spiral M 81 with the nearby dwarf irregular DDO 155 (shown on the same scale in the lower-left panel).

Even in lower-density environments where spirals are abundant, such as the Virgo cluster, morphology can show evidence of an interaction with the intra-cluster medium (e.g., Koopmann & Kenney 2004; see Lecture 4, Section 2.7).

Star formation history. Galaxies that formed all of their stars many Gyr ago tend to look very different from those that did not. Galaxies which are not currently forming any stars are redder, smoother, more centrally concentrated, and more symmetric than those which are. The bluest normal galaxies are Magellanic spirals and irregulars.

Lookback time. Morphology can be significantly affected by the lookback time to a galaxy. When the redshift is high, the lookback time can be so great that we see an early phase of morphological evolution. Galaxies tend

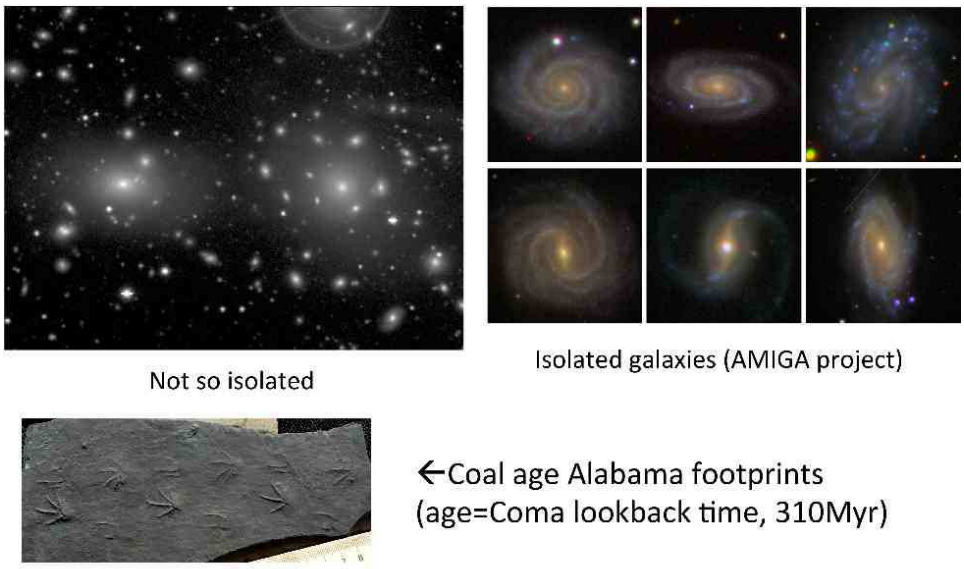

Fig. 2.4. A high-density environment like the central region of the Coma cluster is rich in early-type galaxies, while spirals are more prevalent in less dense environments. The Analysis of the Interstellar Medium in Isolated Galaxies (AMIGA) project is described by Verdes-Montenegro *et al.* (2005).

to have more irregular shapes and relatively small linear sizes for $z \geq 1$ (see B13 and Lecture 4, Section 2.7).

2.3 Historical overview

Galaxy morphology became evident when large and effective telescopes began to be used to observe the sky. In the late 18th century, English astronomer William Herschel built 18.7 in speculum metal reflectors which he used to 'sweep' the sky for anything out of the ordinary, such as 'nebulae'. Herschel and those who followed him saw different kinds of nebulae: those that appeared to lie within the band of light called the Milky Way ('galactic nebulae'), and those which were found mainly away from the Milky Way ('non-galactic nebulae'). For a while, all types of nebulae were thought to be distant but unresolved stellar systems, a popular but largely speculative idea at the time. Prior to the 1870s, all illustrations of nebulae were visual sketches based on what was seen through an eyepiece. One of the most detailed early sketches was that of M 51 made by Herschel's son John in the 1820s (Hoskin 1982).

The non-galactic nebulae seen by Herschel had a variety of interesting

shapes, ranging from round to highly elongated, and showed varying degrees of central brightness. Herschel invented a simple descriptive classification of these objects based on brightness, size, shape, and central concentration. This approach was also used by John Herschel to describe all nebulous objects compiled to the 1860s (Herschel 1864).

Even though the Herschel telescopes could reveal thousands of non-galactic nebulae, the finer details of galaxy morphology were largely elusive. Galaxy morphology 'came alive' in 1845 when William Parsons, 3rd Earl of Rosse, observed nebulae with a much larger telescope, the 1.8 m 'Leviathan of Parsonstown'. This telescope was constructed on the grounds of Birr Castle in central Ireland, and was the largest telescope in the world for nearly 75 years. The Leviathan observations are replete with visually seen details of galaxy morphology, and from the sketches that were made, one can tell that the observers had seen spiral arms, bars, rings, dust lanes, star-forming regions, tidal features, even Magellanic barred spirals. In the extensive set of notes published by the 4th Earl (Parsons 1880), one can determine that spiral structure was seen in 75 'nebulae' later found to be galaxies. Figure 2.5 shows what could be viewed as the first galaxy morphology *atlas*: a compilation of Birr Castle Leviathan sketches made by a variety of observers.

Although the Leviathan of Parsonstown was the most powerful telescope of its day, it was not capable of guided photography and therefore could not get long exposure images of things like spiral nebulae. Nebular photography became possible in the 1880s with the availability of silver bromide dry emulsion plates and telecopes designed for accurate guiding. Isaac Roberts (1829–1904) obtained in 1888 the first long-exposure photograph of the Andromeda Nebula, which first revealed the spiral structure in the faint outer parts of the nebula (Roberts 1893). As the number of plates accumulated, the first classification systems emerged. Max Wolf (1863-1932) published a simple system of letters to describe 17 different types of non-galactic nebulae, ranging from amorphous inclined types to patchy, well-developed spirals (Wolf 1908). This system was used over a period of 30 years by a number of well-known nebular researchers, including Hubble who thought it was a useful temporary system until accumulation of more data allowed something better to come along.

A big photographic survey described by Curtis (1918) helped set the stage for the Hubble classification system. Photographs of hundreds of nebulae, galactic and non-galactic, were taken over a nearly 20-year period with the the 36 inch Lick Crossley reflector by, in addition to Curtis, well-known photographers James E. Keeler and Edward E. Barnard. The main specific

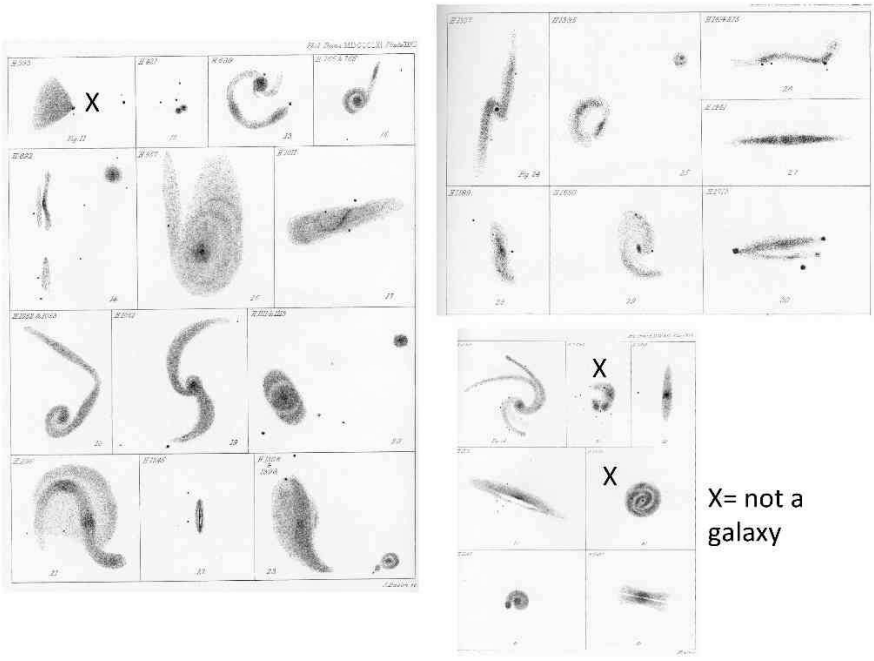

Fig. 2.5. The first galaxy morphology atlas, based on visual sketches made with the Birr Castle 'Leviathan' (Parsons 1880).

galaxy morphology Curtis recognised was 'ϕ-type spirals', later renamed barred spirals by Hubble (1926). Curtis believed all non-galactic nebulae were spirals and that any that didn't look spiral would eventually be found to be such. Hubble (1922) disputed this conclusion; he noted that genuine bright but definitely non-spiral non-galactic nebulae existed. After obtaining and inspecting many available plates, Hubble (1926) published a new classification system to replace the Wolf (1908) system. This system placed galaxies on a sequence ranging from amorphous elliptical-shaped objects to well-developed, patchy-armed spirals. The spiral part of the sequence was split between non-barred ('normal') and barred spirals. However, Hubble believed that his 1926 system was flawed because the transition from the flattest-looking E galaxies to Sa spirals looked too sharp to be real. He hypothesised that there had to be armless but highly flattened disk-shaped galaxies in the transition from types E to Sa. This was shown in his famous 'tuning fork' illustration in his book, The Realm of the Nebulae, published in 1936 (Fig. 2.6, left). It is thought that Hubble was inspired to illustrate

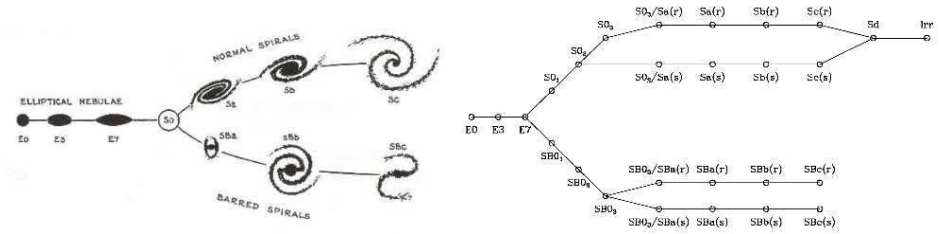

Fig. 2.6. The original Hubble (1936) 'tuning fork' classification (left), and a schematic of the revised tuning fork outlined in the Hubble Atlas (Sandage 1961; Buta *et al.* 2007).

his classification this way because this is how Sir James Jeans illustrated it in his 1928 book, *Astronomy and Cosmogony* (Block et al. 2004). Sandage (2005) has also noted that the arrangement of galaxies on a sequence ranging from amorphous to highly structured spirals was outlined independently by Reynolds (1920), but never referenced by Hubble.

Hubble had planned to revise his classification system further but died before completing it. Allan Sandage used Hubble's notes to prepare the monumental *Hubble Atlas of Galaxies* (Sandage 1961). This firmly cemented Hubble's ideas into astronomy. Inclusion of S0 galaxies, as well as splitting each tuning fork prong into ringed and non-ringed varieties, made the classification more complicated. Van den Bergh (1976) commented that the addition of S0s destroyed the 'simple beauty' of the original 1926 classification. The revised Hubble-Sandage (RHS) system was later expanded and further revised in the *Carnegie Atlas of Galaxies* (Sandage & Bedke 1994).

S0 galaxies, probably the most enigmatic type in the whole Hubble sequence, are thoroughly described in the Hubble Atlas and Carnegie Atlas. An excellent example of an S0 is NGC 2784, shown in Fig. 2.7, while the RHS classification of S0s is summarised in Fig. 2.8. The three main components of an S0 are the *nucleus*, the *lens*, and the *envelope*. A lens is a distinct feature that appears as a well-defined region having a shallow brightness gradient interior to a sharp edge. The enhancement can be very slight as in NGC 2784, or more distinct as in NGC 1411 (Fig. 2.8, top middle). The RHS subclassification of nonbarred S0s, $S0_1$, $S0_2$, and $S0_3$, depends on structure differentiation, while that for barred S0s: $SB0_1$, $SB0_2$, and $SB0_3$, is based on the development of the bar. The differences between nonbarred and barred S0s are important. For example, dust rings are a common feature of type $S0_3$, while they may not factor in at all in type $SB0_3$.

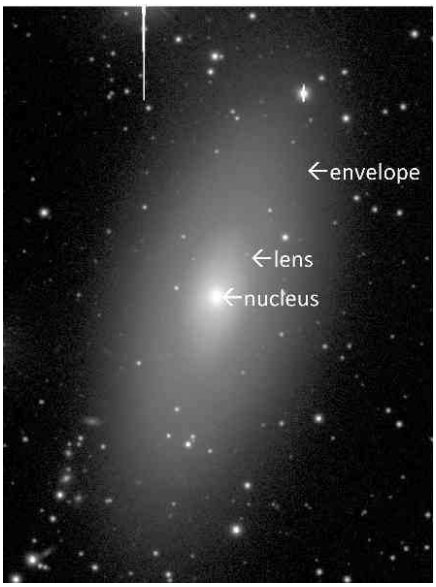

Fig. 2.7. NGC 2784 displays the main elements – nucleus, lens, and envelope, that define an S0 galaxy (Sandage 1961).

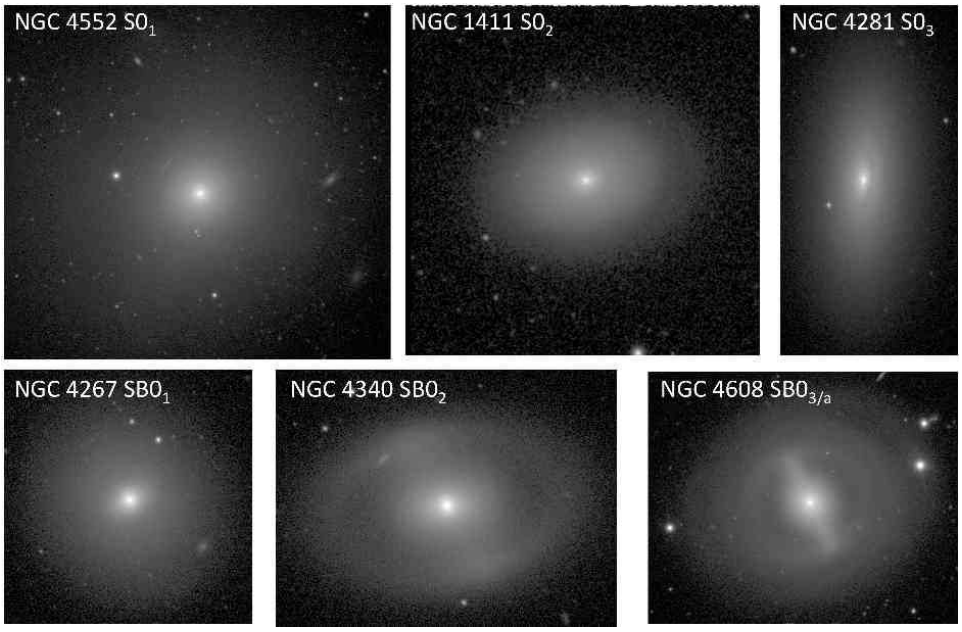

Fig. 2.8. These galaxies show the main S0 galaxy categories descibed in the Hubble and Carnegie atlases of galaxies.

Around the same time as the Hubble Atlas was being prepared, W.W. Morgan (1906-1994) proposed a classification system that combined galaxy form with stellar population defined by (Morgan 1958):

(a) *population group*: a, af, f, fg, g, gk, k for dominant spectral types A, AF, F, FG, G, GK, and K. This is estimated solely from *central concentration*;
(b) *form family*: S (spirals), B (barred spirals), E (ellipticals), I (irregulars), D (like S0s), plus others;
(c) inclination class flattening index.

In Fig. 2.9, a Morgan sequence of population groups, based on classifications from Morgan (1958) and illustrated using SDSS colour images, shows the effectiveness of his approach. The sequence a through k is a colour sequence from bluish to yellow-orange. The system did not have the impact that Hubble's did, perhaps because the population groups were closely analogous to Hubble types Sa, Sb, and Sc. For example, in Fig. 2.9, NGC 3389 (type aS4) is Hubble type Sc, NGC 3583 (type fgS4p) is Hubble type Sb, and NGC 4260 (type gkB4) is Hubble type Sa.

The most recognisable and important of Morgan's form classes is the cD galaxy, a *supergiant* version of the D form family found in the centres of rich clusters (Fig. 2.10). These objects, also known as 'brightest cluster members', were extensively studied by Schombert (1986, 1987, 1988).

In 1953, non-Palomar firebrand Gerard de Vaucouleurs (1918-1995) carried galaxy morphology into the southern hemisphere, developing his own interpretation of the Hubble-Sandage classifications on the way. Figure 2.11 shows de Vaucouleurs's (1959) 'classification volume' (the VRHS, or 'three-pronged swirling two-handled tuning fork'). The long axis defines the 'stages' E, E^+, $S0^-$, $S0^o$, $S0^+$, S0/a, Sa, Sab, Sb, Sbc, Sc, Scd, Sd, Sdm, Sm, Im.

De Vaucouleurs viewed galaxy morphology as a continuous sequence of forms. He was also artistically talented and made a sketch (see Kormendy's contribution, this volume) of a cross-section of his classification volume in 1962. The sketch shows the arrangement of families (apparent bar strength) and varieties (presence or absence of an inner ring) near stage Sb. Families and varieties can be thought of as continuous secondary traits (de Vaucouleurs 1963); Fig. 2.12 shows the use of the underline notation for these characteristics.

The *stage* is the primary dimension of the VRHS. Elliptical galaxies are amorphous systems with a smoothly declining brightness gradient (Fig. 2.13). They are not disk-shaped. Elliptical galaxies have two VRHS stages: E and E^+. The number after the letter E, as in E2, is the flattening

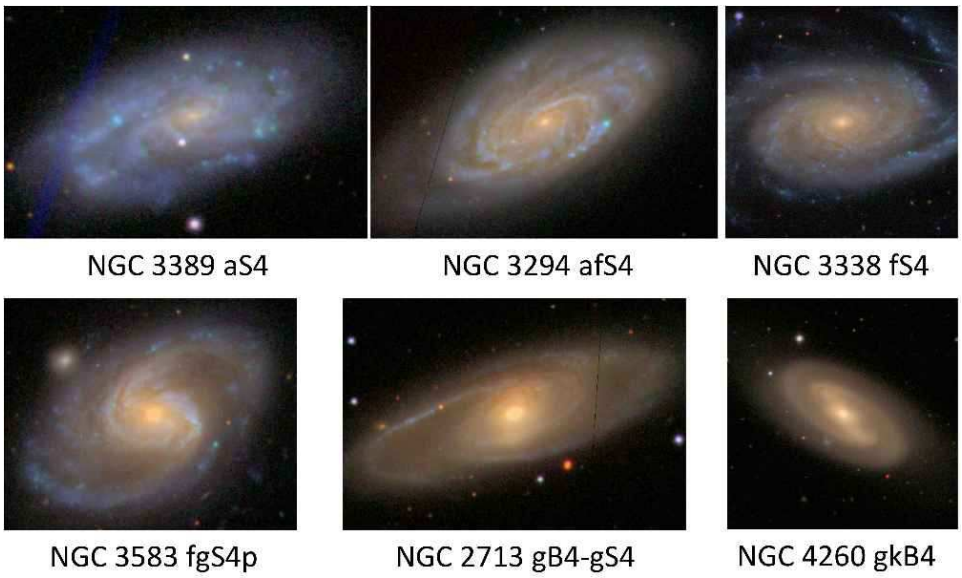

Fig. 2.9. Examples of the stellar-population/form class classification of Morgan (1958).

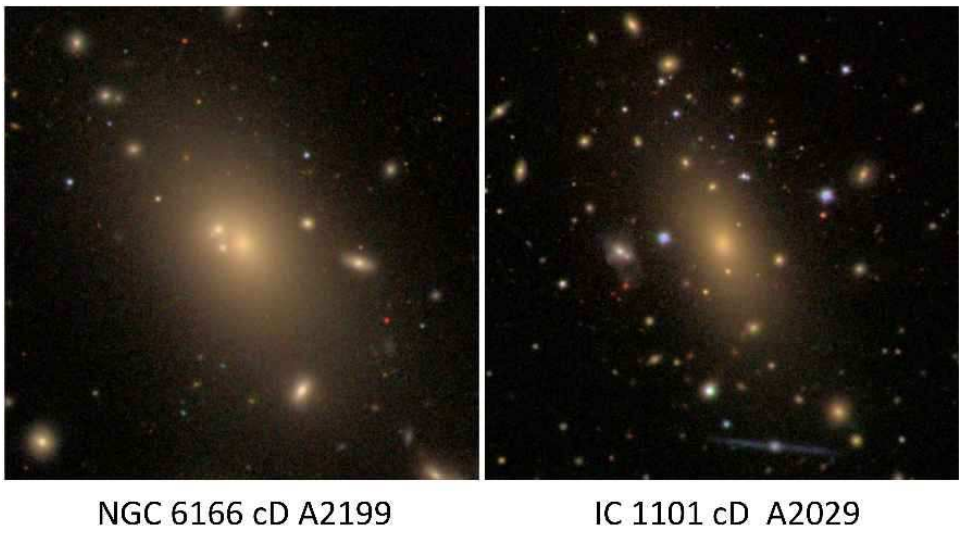

Fig. 2.10. The Morgan cD class of supergiant galaxies.

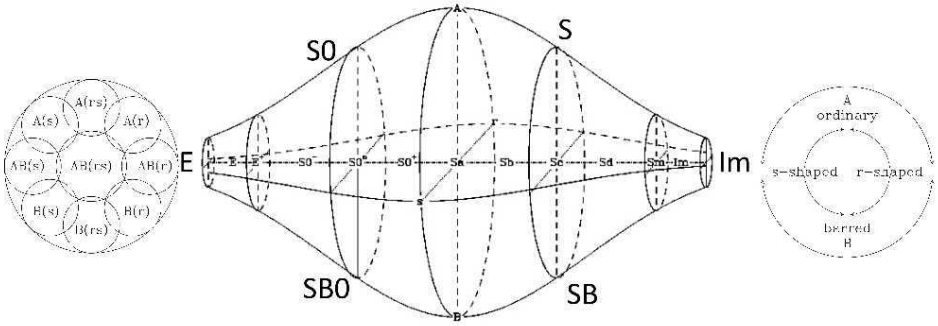

Fig. 2.11. The de Vaucouleurs (1959) revised Hubble-Sandage classification system.

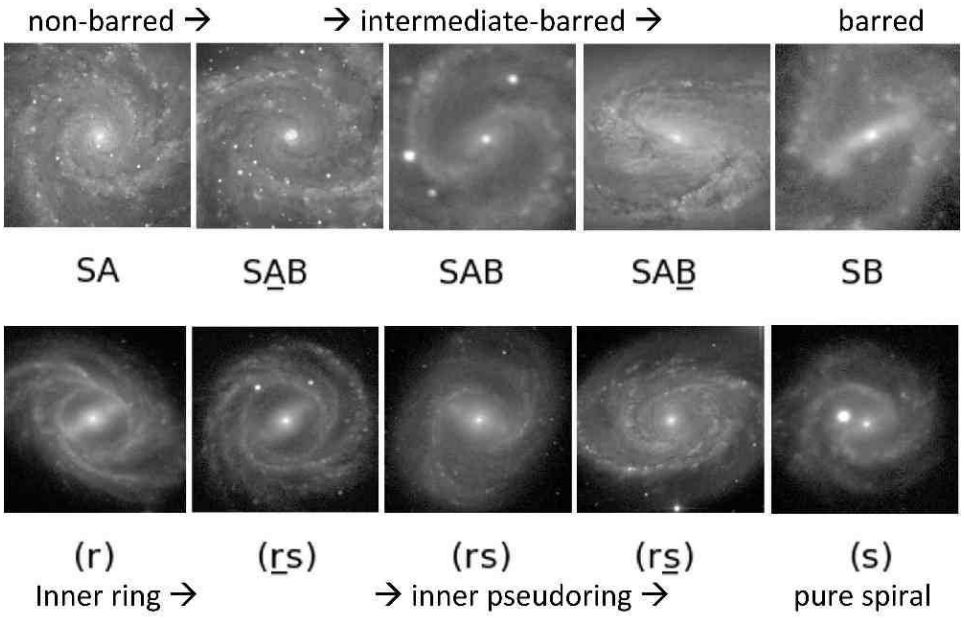

Fig. 2.12. Family and variety in the VRHS as continuous characteristics (from B13).

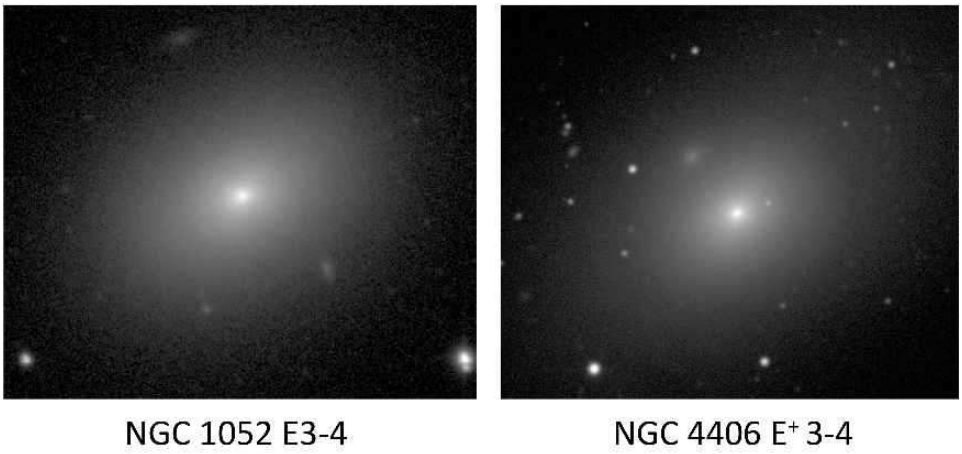

Fig. 2.13. An elliptical galaxy (E) and a 'late elliptical' galaxy (E^+).

index $n = 10(1 - b/a)$, a numerical specification of how elliptical the galaxy is. The E*n* sequence is not, however, physically significant. Type E^+ is a transition stage to the S0 class. These are E-like galaxies showing slight traces of differentiated structure, usually subtle evidence of lenses or faint outer envelopes. Type E^+ has also been used by de Vaucouleurs as a 'home' for Morgan cD galaxies.

In the VRHS, S0 galaxies have three stages: $S0^-$, $S0^o$, and $S0^+$, in a sequence of increasing structure. Type $S0^-$ generally has barely differentiated structure, often in the form of subtle lenses. Type $S0^o$ tends to have stronger lenses and is more obvious as an S0. Type $S0^+$ often has well-defined ring structures, both inner and outer, but can also have subtle spiral structure. Types such as SB(r)0^o and SB(s)0^+ are possible, as are SAB types. Note that this sequence is based on development of structure and NOT on bulge-to-total luminosity ratio.

In the VRHS, spirals have 9 stages: S0/a, Sa, Sab, Sb, Sbc, Sc, Scd, Sd, Sdm, and Sm. These are still recognised using Hubble's three criteria: the relative size of the bulge, the degree of openness of the spiral arms, and the degree of resolution of the arms into knots. Small-bulge early-type galaxies, especially barred spirals, are the biggest violators of these rules. The VRHS introduces *extreme late-type spirals*: Sd, Sdm, and Sm, to the Hubble sequence. Figure 2.14 shows how well these types fit into the sequence with clear, easily distinguishable characteristics. The intermediate spiral types (like Sab, Sbc, etc.) are almost as common as the main types. The most common spirals in magnitude-limited samples are of types

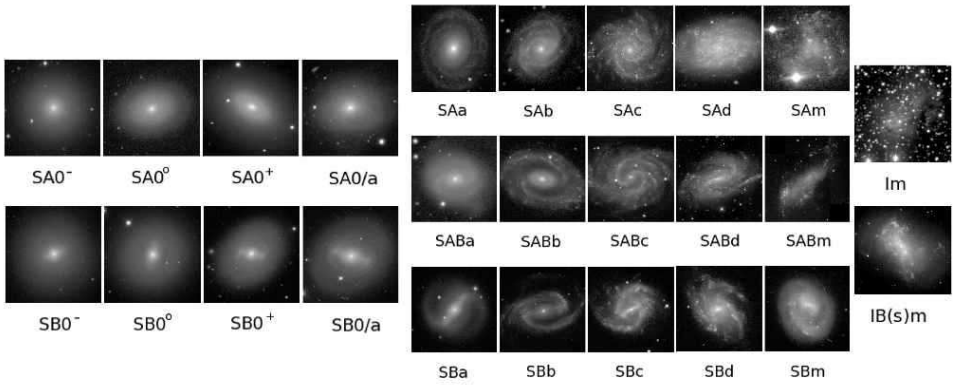

Fig. 2.14. Examples of the S0 and spiral stages along the VRHS sequence.

Sb–Sc. A special hallmark of the VRHS is the recognition of the Magellanic Clouds as extreme late-type barred spirals of the type SB(s)m that show a characteristic one-armed asymmetry and offset bar (de Vaucouleurs & Freeman 1972). Magellanic irregulars form the last major stage along the VRHS, and are often barred (i.e., classified as type IBm or IB(s)m, implying a subtle spiral variety). Examples highlighting the S0, spiral, and irregular sequences are shown in Fig. 2.14.

Spiral and S0 stages are still recognisable in edge-on galaxies, but Fig. 2.15 shows one case that is distinctive. NGC 3115 is an original Hubble E7 type that was reclassified as type $S0_1$ in the Hubble Atlas. It is now recognised as an S0 with a 'thick' disk, although it looks more like an E galaxy with an *embedded* disk (Fig. 2.15).

The outer ring classification is the final original dimension of the VRHS. Closed outer rings are symbolised by (R) preceding the other type symbols. The hallmark of VRHS classifications is the recognition of outer pseudorings (R′) made of variable pitch angle outer spiral arms. Examples are illustrated and described in Lecture 2 (Section 2.5).

The genesis of a galaxy classification is shown in Fig. 2.16. The main features of the galaxy are labelled and its basic type is (R)SAB(r)0/a. However, its bulge is inconsistent with the type S0/a as is often the case for early-type barred galaxies.

The VRHS has had some additions and revisions in recent years. For example, inner and outer lenses were added to the classification by Buta (1995) using notation suggested by Kormendy (1979). Inner lenses are found roughly in the same location as inner rings, while outer lenses are found

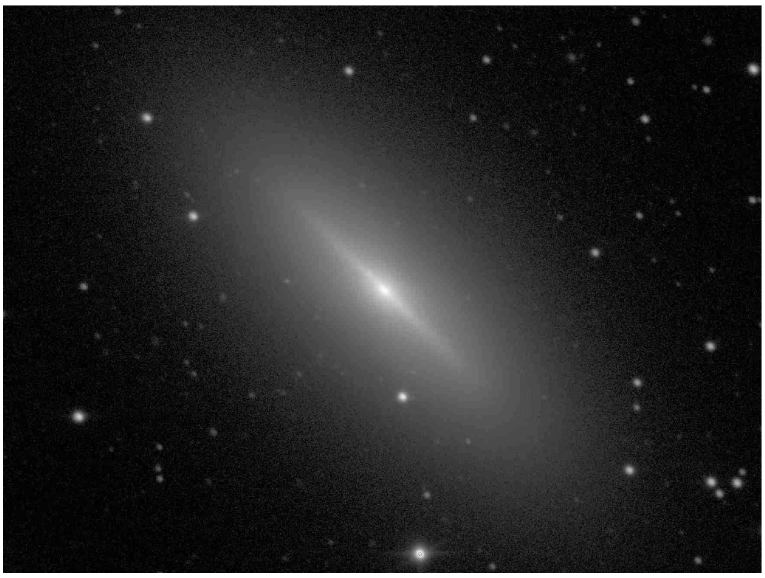

Fig. 2.15. Edge-on S0 galaxy NGC 3115 (V-band).

where outer rings often are seen. Figure 2.17 shows that there is a morphological continuity between rings and lenses, and one possible interpretation is that some lenses are highly evolved former star-forming rings.

The effect of total mass and luminosity on galaxy morphology was characterised by van den Bergh (1960a,b) in terms of *luminosity classes*. (An illustration of the luminosity class standards, van den Bergh 1998, is given in B13). The classes are applicable only to intermediate to late-type spirals and are analogous to those used in stellar spectral classification: luminosity class I: supergiant spirals; II: bright giant spirals; III: giant spirals; IV: subgiant spirals; and V: dwarf spirals and Magellanic irregulars. The main idea is that more luminous spiral galaxies have the most well-organised structure (Fig. 2.3). In massive, luminous spirals, the structure is more symmetric and more ordered. In lower-mass spirals, the structure is more chaotic; in fact, in dwarfs the spiral structure can be so weak or absent that surface brightness is used as the criterion of luminosity classification.

Dwarf galaxies in the Virgo cluster were the subject of an exceptional study by Binggeli *et al.* (1985). The main types of dwarfs classified by these authors are: cE - compact ellipticals; dE - dwarf ellipticals; dE,N - nucleated dwarf ellipticals; dS0 - dwarf S0s; dS0,N - nucleated dwarf S0; BCD - blue compact dwarf; and 'large dE' or large dwarf ellipticals (all illustrated in B13). If the dEs and dS0s were actually dwarf versions of normal E and S0

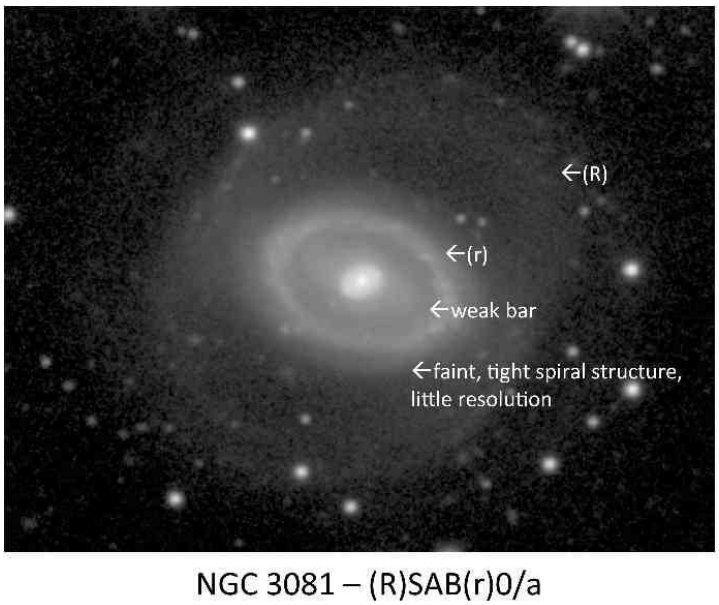

Fig. 2.16. Classification of NGC 3081.

galaxies, their existence would widen the parameter space at the left end of the VRHS. However, recent studies have indicated that dEs and dS0s are likely not connected to actual E or S0 galaxies but to Magellanic irregulars. Kormendy & Bender (2012) have suggested that dEs and dS0s are environmentally modified Magellanic irregulars, and that the true dwarf members of the E galaxy class are objects like the compact Es in Fig. 2.78. Kormendy & Bender have proposed renaming all dE and dS0 galaxies 'spheroidals'. This connects these objects directly to galaxies referred to as 'dwarf spheroidals' and dwarf irregulars in the Local Group. Detailed studies of Local Group dwarf spheroidals and irregulars reveal systems with a complex star formation history (Mateo 1998).

Dwarf spirals are a controversial subject; only a few genuine cases are known. IC 3328, a dE, was shown to be a true dwarf spiral by Jerjen *et al.* (2000). NGC 3928 was recognised as a dwarf spiral by van den Bergh (1980). It is shown relative to the supergiant spiral UGC 6614 in Fig. 2.18.

2.4 Tuning fork controversy

The RHS and VRHS classifications have always had a problem with early-type galaxies:

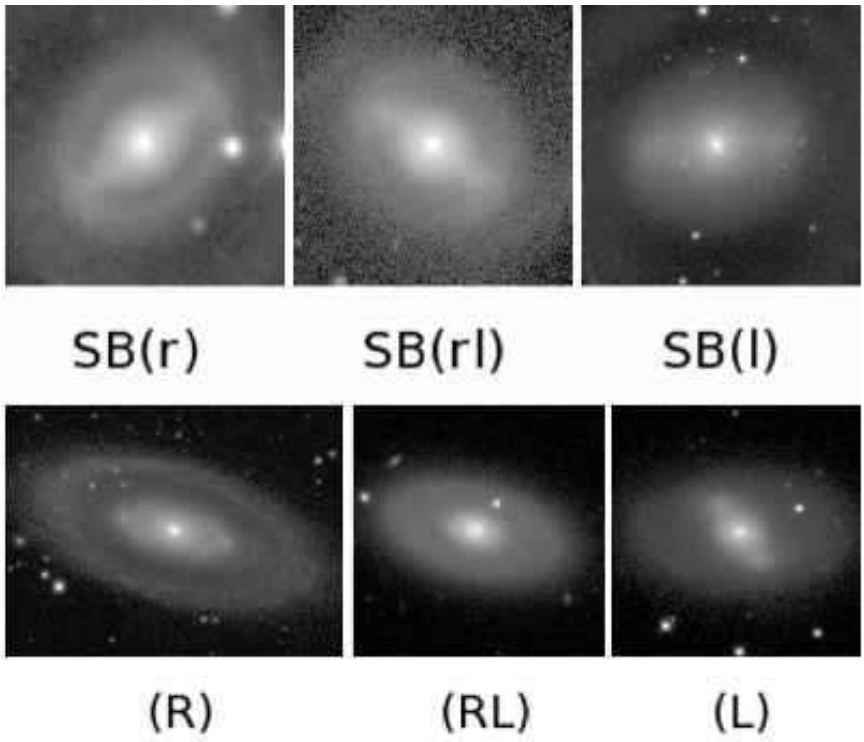

Fig. 2.17. Examples showing the continuity of ring and lens morphologies. Other examples may be found in B13.

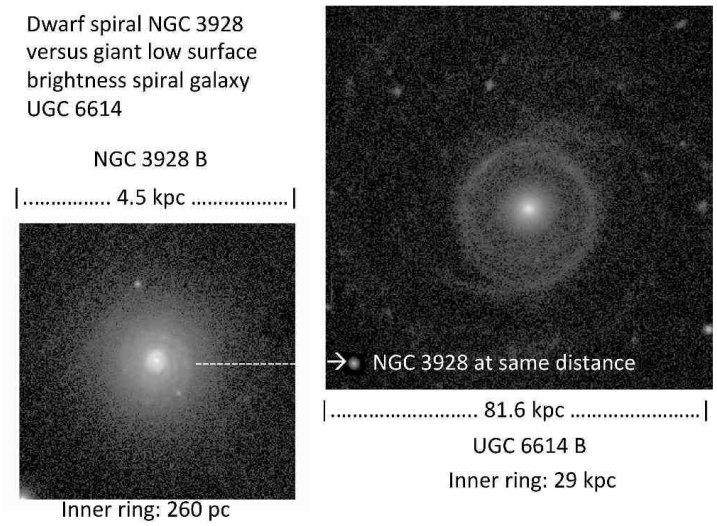

Fig. 2.18. Dwarf spiral NGC 3928 as compared to the supergiant spiral UGC 6614.

(a) the E*n* classification has no physical significance, unlike the stage classification for spirals;
(b) the properties of S0s do not support the idea of them being a transition class between ellipticals and Sa, SBa galaxies (van den Bergh 1976, 1998).

Van den Bergh (1976) challenged the tuning fork by following the suggestion of Spitzer & Baade (1951; also Baade 1963) that S0s probably form a sequence parallel to spirals, rather than being in the juncture of the tuning fork between ellipticals and spirals. In a revised classification, van den Bergh proposed that S0s be classified as a sequence S0a – S0b – S0c parallel to the regular Hubble spiral sequence classification Sa – Sb – Sc (Fig. 2.19, lower left). In between these two sequences is a sequence of 'anemic spirals': Aa – Ab – Ac, meaning spirals whose lower than average star formation rate and dust content implied a deficiency of HI gas (discussed further in Lecture 4, Section 2.7). This view of the S0s is called 'parallel sequence classification'. Although a reasonable point of view, the van den Bergh sequence did not gain much traction at least in part because of the absence, until recently, of any S0s than might be identified as type S0c.

Several recent studies have provided strong support for the parallel sequence idea:

(a) Kormendy & Bender (2012): Sph galaxies & E galaxy dichotomies; edge-on disks embedded in environmentally modified Sph galaxies; S0c galaxy identified;
(b) Cappellari *et al.* (2011): ATLAS^{3D} kinematic classifications;
(c) Laurikainen *et al.* (2011): Near-IR S0 Survey (revised view of S0 bulges and identification of some of the first van den Bergh S0c galaxies).

The problem with the E*n* classification was at least partly solved by Kormendy & Bender (1996) who modified the Hubble E galaxy sequence to distinguish boxy versus disky Es (Fig. 2.19, upper right). Boxy Es show isophotes that have a negative value of the relative Fourier radius parameter a_4/a (Jedrezjewski 1987), are more luminous, have less rotation, and more velocity dispersion anisotropy than disky Es, which have a positive value of a_4/a. Figure 2.19 (upper left) shows two extreme examples of boxy and disky Es where the character is evident by eye. The E(b)5 is NGC 7029 while the E(d)5 is NGC 4697.

Further studies of E galaxies revealed that galaxies classified as dwarf ellipticals in the Virgo cluster are NOT the low-luminosity versions of regular ellipticals (Kormendy 1985; Kormendy *et al.* 2009). Instead, as we noted in the previous section, dE and dS0 galaxies are the progeny of late-type galaxies. Kormendy & Bender's (2012) reclassification of these objects as

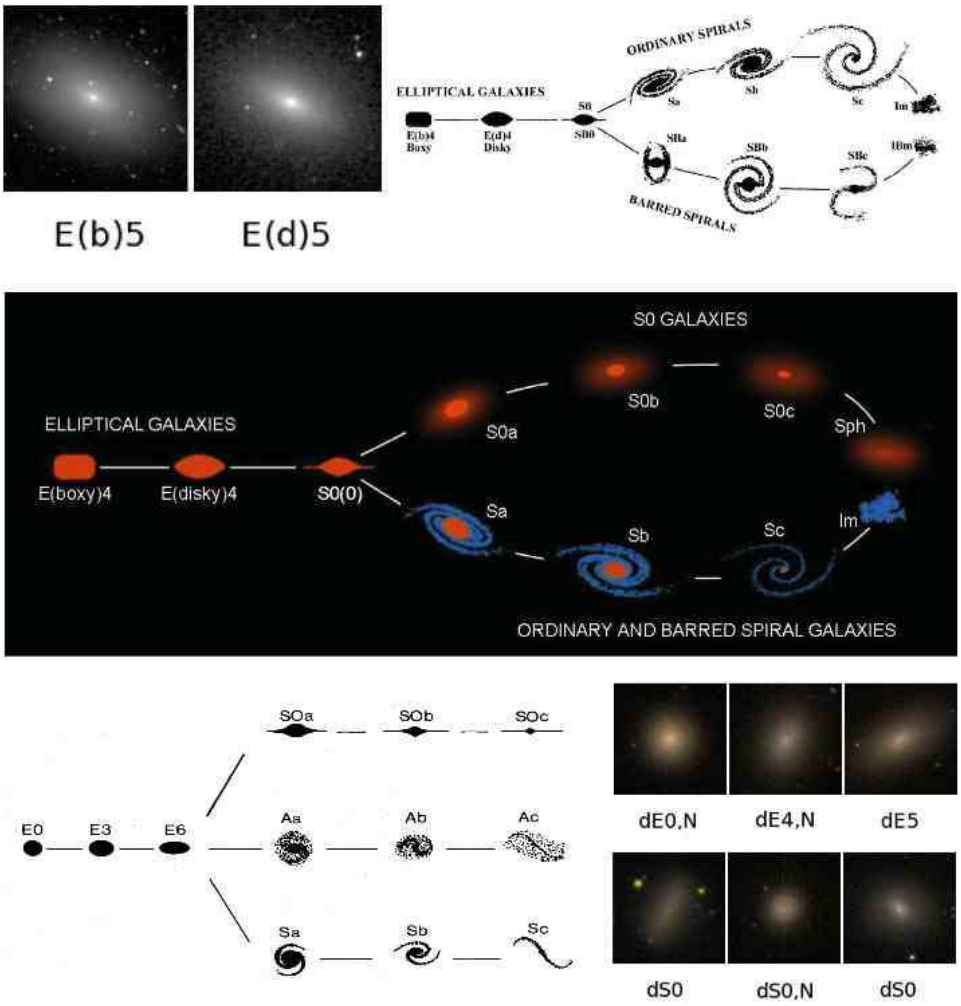

Fig. 2.19. Two revisions of the Hubble tuning fork by Kormendy & Bender (1996, 2012). The van den Bergh (1976) parallel sequence classification schematic is shown at lower left, and several Sph galaxies are shown at lower right. All three modified tuning forks are reproduced with permission of the authors

Sph galaxies, and their suggested location in parallel sequence classification is shown in Fig. 2.19, middle. Several examples are shown in Fig. 2.19, lower right.

Kormendy *et al.* (2009) carried out a very detailed study of high- and low-luminosity E galaxies and Sph galaxies. An E galaxy dichotomy exists in the sense that luminous Es have a 'core' (an inner radial zone of what seems

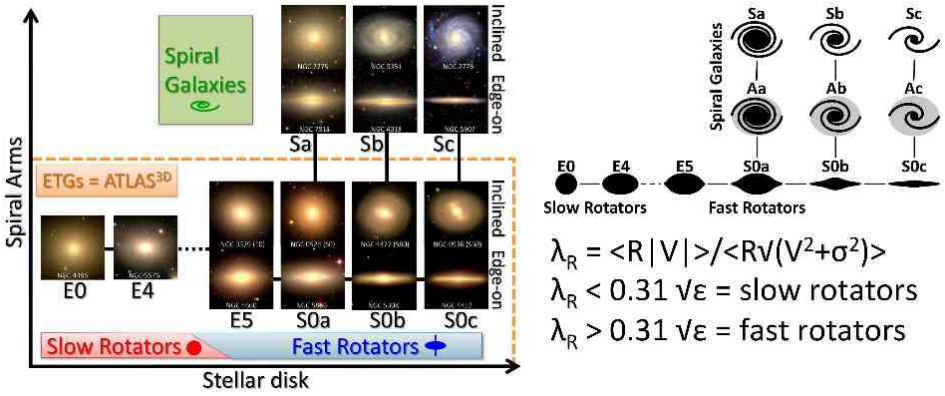

Fig. 2.20. Atlas^{3D} kinematic basis for parallel sequence classification, from Cappellari *et al.* (2011, reproduced with permission).

like 'missing light', like a cone cut off at the top), while lower-luminosity Es appear to lack this missing light core, instead showing 'extra light' in the manner of a power-law excess. B13 shows a comparison between three nucleated Sph galaxies and three genuine E galaxies (one of the core type, and two of the power-law type). Although the subtle differences are evident directly, the distinctions are best seen in the profiles and parameter correlations described by Kormendy *et al.* (2009).

ATLAS^{3D} was a massive study of the detailed kinematics of 260 early-type galaxies (Emsellem *et al.* 2007, 2011; Cappellari *et al.* 2011). Based on a kinematic parameter, λ_R, Cappellari *et al.* (2011) independently came to the same conclusion as Kormendy & Bender (2012): the correct placement of S0s is parallel to spirals. Cappellari *et al.* (2011) showed that the best way to order early-type galaxies is kinematically, not morphologically. Their proposed revision to the Hubble tuning fork is shown in Fig. 2.20.

The contribution of Laurikainen *et al.* (2011) to the parallel sequence classification idea involves the use of sophisticated two-dimensional photometric decomposition that led to both a revised view of the significance of S0 bulges (bulge-to-total luminosity ratio) and the discovery of a few genuine S0c galaxies. This is discussed further in Lecture 3 (Section 2.6).

Note that none of this necessarily completely negates the value of tuning fork classifications, because types such as En, S0$_1$, S0$_2$, S0$_3$, or E^+n, S0$^-$, S0°, and S0$^+$ are still morphologically valid visual categories. A galaxy may be classified as type SA(rl)0$^+$ and S0b, and the two classifications are more complimentary than contradictory. The same is true for the dE and

dS0 categories. The revised tuning fork clarifies relationships between types and, most importantly, finds a proper 'home' for the enigmatic Sph/dE/dS0 galaxies in the Hubble sequence.

The revisions to the tuning fork represent the coming to fruition of *quantitative* and *interpretive* galaxy classification. Quantitative morphology relies on derived photometric or kinematic parameters to determine relations between galaxy types such as, for example, the relation between spheroidal galaxies and Magellanic irregular galaxies, normal ellipticals and compact ellipticals, disky ellipticals and disk galaxies, and between spirals and S0s. Interpretive galaxy classification means 'with a particular idea in mind', such as the nature versus nurture origin of S0 galaxies, or, for example, different subtypes of outer pseudorings (see Lecture 2, Section 2.5).

2.4.1 Does the continuity of galaxy morphology imply that secular evolution must be occurring?

To some extent it probably does, but apparent continuity can be misleading. For example, the VRHS classification of S0s from featureless systems with only a trace of a lens to systems with obvious rings or traces of spiral structure is clear continuity in galaxy morphology, but it does not necessarily mean that the placement of S0s between ellipticals and spirals is correct. The type 'S0/a' automatically suggests a correct placement. Even so, some aspects of the VRHS could imply secular evolution, such as:

(a) The smooth variation in bar strength (with numerous examples filling the continuum of forms from SA to SB). Does this imply evolution from SB to SA or vice-versa, or both? The simulations of Bournaud & Combes (2002) suggest that bar destruction by increasing central mass concentration followed by bar rejuvenation by external gas accretion could keep 'apparent bar strength' as a continuum of forms just as recognised in the VRHS.

(b) The seemingly smooth connection between rings and lenses. These features are found in the same general locations relative to bars, and in particular the radial profile of a lens can be very much like a ring of lower contrast on a steeply declining background [e.g., the lens of NGC 1553 (Kormendy 1984); as compared to the bright stellar inner ring of NGC 7702 (Buta 1991; see Fig. 20 of Buta & Combes 1996)]. Do lenses simply represent the dissolution of bars or bar-like features, or could many lenses be diffused (highly evolved) former rings? The latter could follow from the mere existence of inner, outer, and nuclear lenses in the same manner as inner, outer, and nuclear rings. Nevertheless, the virtually one-to-one connection between the sizes of bars and the diameters of inner lenses still suggests, as noted by Kormendy (1979), that such

lenses formed by bar dissolution. A study of lens colours would aid greatly in further establishing these connections.

(c) The smooth variations in ring morphologies, ranging from completely closed features to no ring at all, with a continuum of 'pseudorings' in between. Does this mean that pseudorings evolve secularly into closed rings? Does it also mean that a galaxy with no ring could eventually become ringed? Even the simplest numerical simulations, such as those of Schwarz (1981, 1984a), Simkin *et al.* (1980), and Byrd *et al.* (1994), suggest that it might be possible for gravity torques acting on spiral segments to evolve a pseudoring pattern and eventually close it. It is not clear from such simulations, however, that pure (s)-variety spirals could evolve into pure (r)-variety spirals. Such evolution could depend on the evolution of the bar pattern speed as well.

(d) The smooth variations in morphology along the spiral type sequence. Could a spiral evolve along this sequence? Could it do this without also evolving along the family and variety dimensions of the VRHS? Stage evolution is perhaps the most important question we could ask about secular galaxy evolution, because it brings us into the realm of bulge formation and evolution. If many bulges are built up by secular movement of disk material (as opposed to multiple mergers), then secular evolution from late-to-early would indeed be possible (KK04). A big question is, how many 'steps' in stage could a galaxy evolve in this way during a Hubble time? I did not discuss 'pseudobulges' during my actual lectures since these were covered in some detail by Kormendy (this volume), but in the next set of notes I will describe the morphologies of such bulges.

2.5 Lecture 2: Barred and spiral galaxies

In my second lecture I would like to introduce the important morphological and evolutionary issues connected with bars and spirals in galaxies. Although related morphologically, bars are often considered as major dynamical components of galaxies, while spirals are seen as features possibly driven by bars (e.g., Kormendy 1979; Kormendy & Norman 1979). Even so, a significant fraction of normal galaxies are unbarred and still spiral. The role of bars and spirals in secular evolution of galaxies is clearly important.

Barred galaxies can be considered 'the ultimate' in galaxy morphology, by which I mean they have some of the most organised structures known. This is shown by the examples in Fig. 2.21. In these galaxies the bar is obviously a major perturbation, and one of the first questions we may ask is, how many galaxies are barred? A large number of studies have examined this question, often focussing on infrared observations since these penetrate dust and make some obscured bars more visible. One such study by Eskridge *et al.* (2000) found the following: from H-band (1.65 μm) images of 186 bright nearby

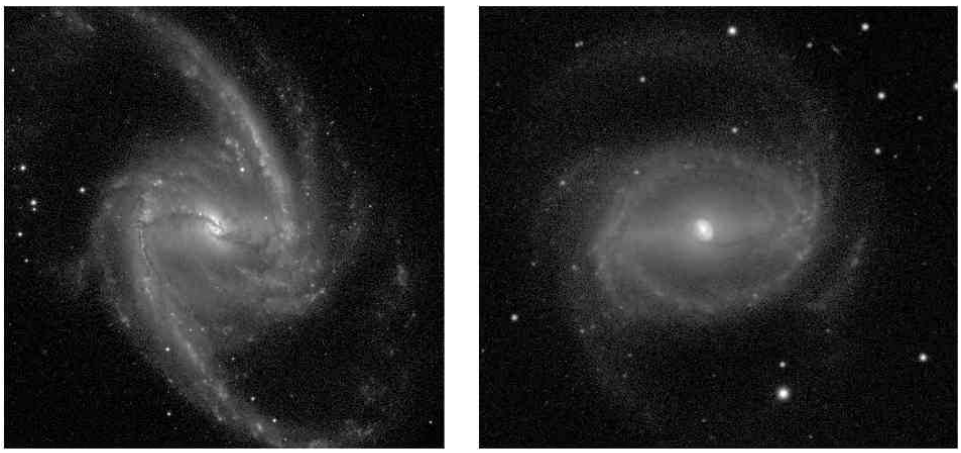

Fig. 2.21. The bars in these galaxies are stronger than average and each shows characteristics, such as the presence of a 'pseudobulge', that suggest secular evolution has occurred.

galaxies, 56% were visually classified as 'strongly barred', 16% were classified as 'weakly barred', and 27% were 'unbarred'. Although it seems that strong bars are more common than weak ones, this is an illusion. An optically classified SA galaxy may show a weak bar in the IR and get a new classification of SAB, and an optically classified SAB galaxy may show a more prominent bar in the IR and get classified as SB. However, even though the bar of an optically classified SB galaxy may also look stronger in the IR, it has no new classification bin to be placed in. Thus, IR imaging does not really change the *rankings* of bars. All bars in spirals at least look stronger in the IR, and the rankings (what is actually strong and what is actually weak) remain about the same. From many studies (see Buta *et al.* 2010b for a recent summary), and including both SAB and SB types, the bar fraction ranges from 50-70%.

Bars are characterised by their different morphologies and non-elliptical shapes. A typical normal bar in an early-type galaxy has two sections: a broad inner zone, and narrower ends (e.g., NGC 4314 in Fig. 2.22). The inner zone can be round or elliptical and can be mistaken for a large bulge. The broad section is not seen in late-type galaxies generally (e.g., NGC 4731 in Fig. 2.22). Athanassoula *et al.* (1990) fitted generalised ellipses to the isophotal shapes of early-type galaxy bars and demonstrated the typical boxy character of these features. In early-to-intermediate-type galaxies, bars are made of an old stellar population, while in very late-type galaxies, bars

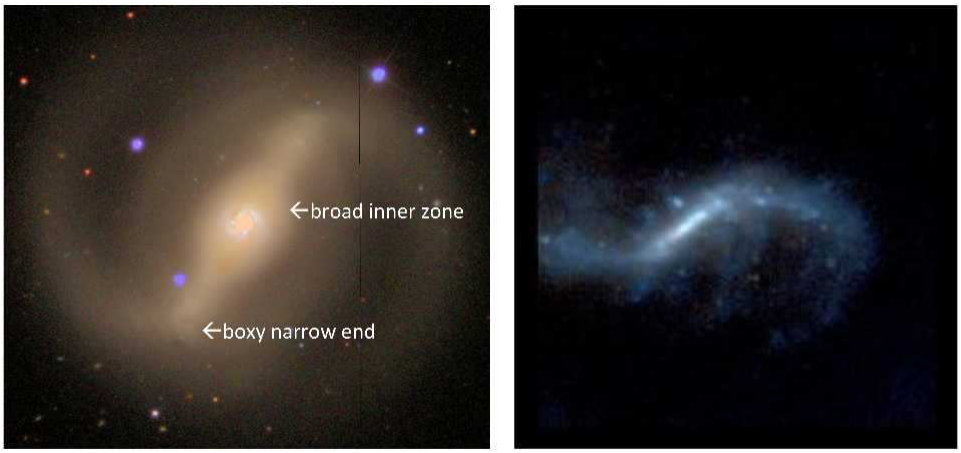

Fig. 2.22. NGC 4314 shows the characteristic features of an early-type galaxy bar, including the broad inner zone and the boxy narrow ends, while NGC 4731 shows a typical late-type galaxy bar which lacks a broad zone and has a much younger stellar population.

can include a much younger stellar population. These characteristics are well shown by the examples in Fig. 2.22.

In an ansae-type bar, the broad inner zone and the bar ends may be separated or at least more distinct (Fig. 2.23). Ansae bars are found in 40% of early-type barred galaxies (Martínez-Valpuesta *et al.* 2007) and are very rare in later types. Even so, exceptional examples of ansae in intermediate-type spirals are known, such as the SBb galaxy NGC 5375 shown in the upper left frame of Fig. 2.23. Particularly intriguing, and not really well understood, is the variety of ansae morphologies seen in early-type barred galaxies. Some are roundish spots, others are relatively linear enhancements, while still others are narrow arcs that appear to blend into an inner ring or lens. In colour SDSS images or colour index maps like that shown for NGC 7098 in Fig. 2.23, ansae are seen to be made of old stars, although NGC 4151 provides a counter example where the ansae are blue and irregular due to star formation.

What are the three-dimensional shapes of ansae? The galaxy NGC 4216 (Fig. 2.24) shows a boxy bulge with bright enhancements that look like ansae in a 3.6 μm image. If this is what the enhancements are, then it appears that ansae are flatter than the inner sections of bars.

The appearance of ansae, and the existence of many bars which do not have them, suggests a possible interpretation of the features in terms of secular evolution (Fig. 2.25). We can ask: are ansae bars merely a distinct type

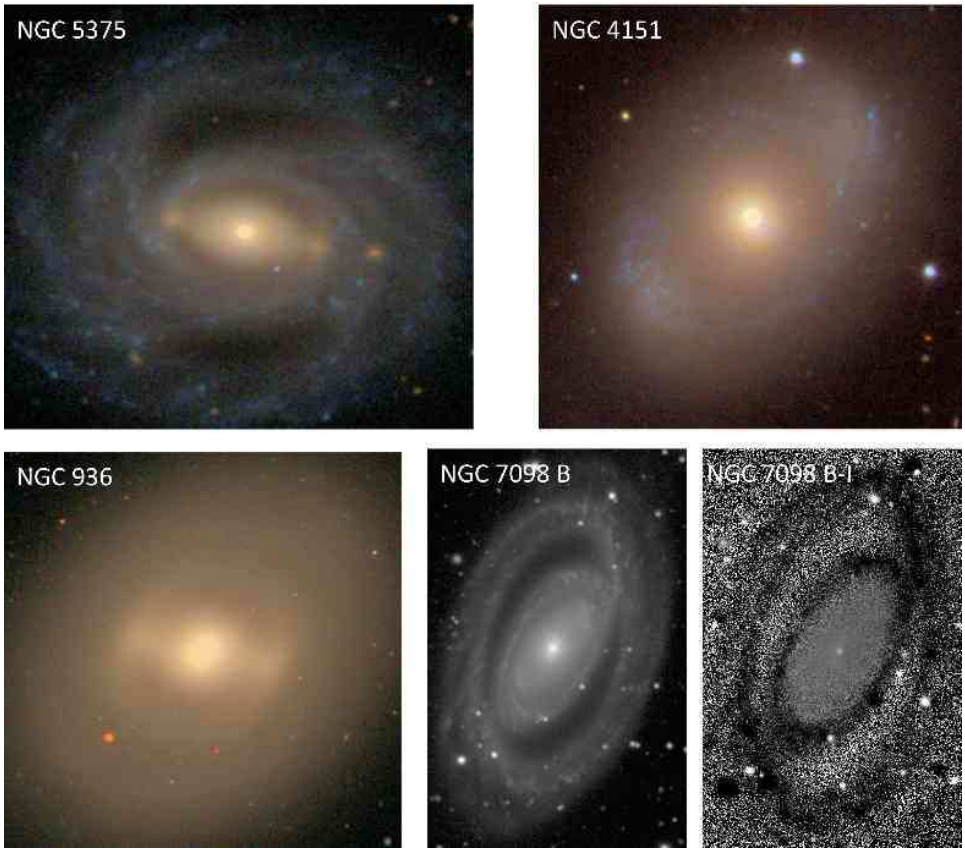

Fig. 2.23. Colour SDSS images of three galaxies with ansae-type bars, and a colour index map of one, that shows how ansae are often made of an old stellar population but can include young stars, as in NGC 4151. The $B - I$ colour index map of NGC 7098 is coded such that bluer features are dark and redder features are light.

of bar, related to some aspect of bar formation, or is there a process that changes a normal bar (e.g., as in NGC 4608) into an ansae bar (e.g., as in NGC 2859)? Can this process separate the two parts of a normal bar and eventually stretch the ansae into arcs?

Ovals are broad, bar-like features having little Fourier amplitude above m=2, as shown by the example in Fig. 2.26. Other examples are illustrated by KK04 and B13. The effect of an oval on galaxy morphology can be similar to that of a conventional bar (KK04). The similarity between some oval galaxies and SB galaxies with outer rings suggests that the oval is driving ring formation in the same manner as a bar would. The oval is a bar-like feature sitting in the same place where a bar and an inner ring would be.

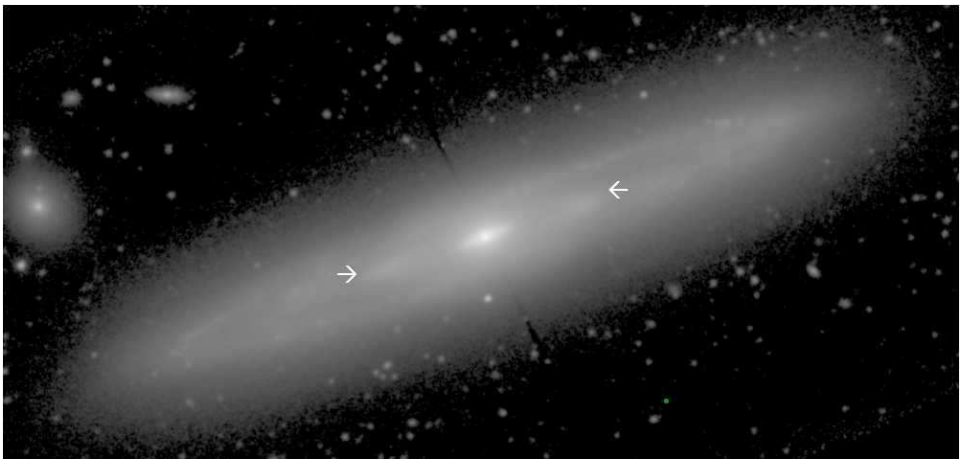

Fig. 2.24. In this 3.6 μm image, the nearly edge-on Sb spiral NGC 4216 shows likely ansae (arrows) flanking an inner boxy zone.

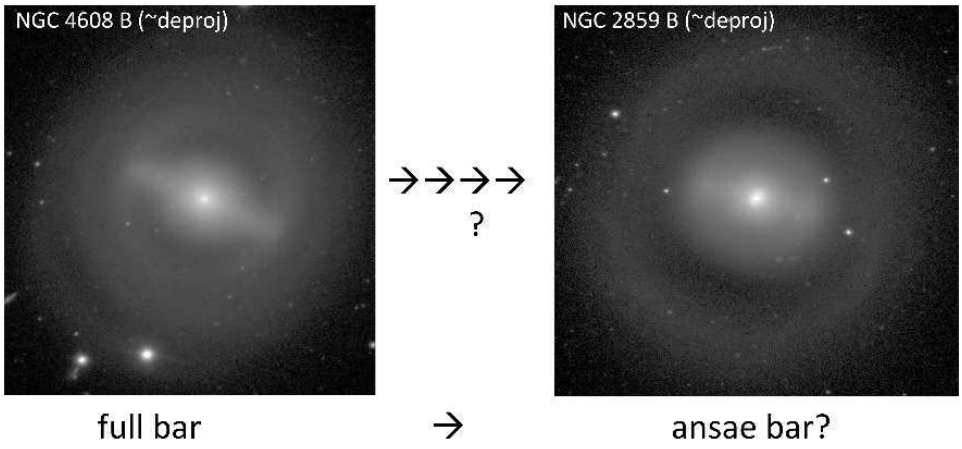

Fig. 2.25. Possible scenario of secular evolution where a full bar evolves to where the broad inner zone and the ends separate.

When a bar or an oval is viewed at an angle intermediate between end-on and broadside on, the isovelocity contours bend towards the bar as in NGC 6300 (Buta 1987). Similar bending can be used to identify an oval in an inclined galaxy (KK04).

Boxy or X-morphologies (Fig. 2.27) are commonly seen in edge-on disk galaxies. Considerable evidence supports the idea that these features are simply the projections of the vertical structure of bars (Bureau & Freeman 1999; Bureau & Athanassoula 1999; Athanassoula & Bureau 1999). How-

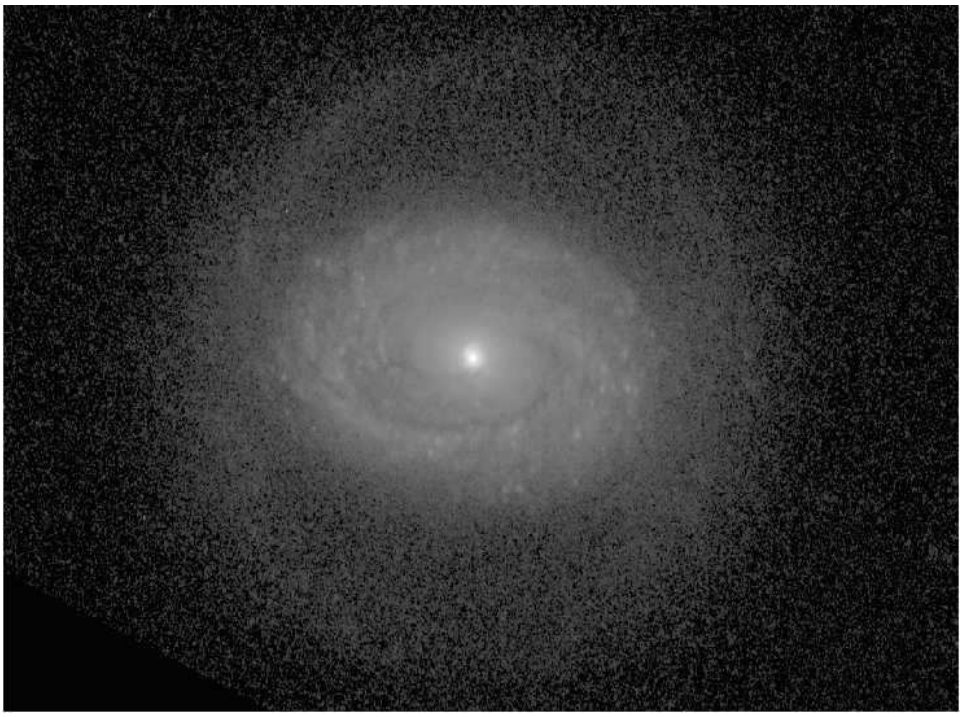

Fig. 2.26. Deprojected blue light image of NGC 4941, an outer-ringed galaxy with a prominent inner oval disk.

ever, X-morphologies can also be seen in galaxies inclined less than 50°, e.g., IC 5240 (Buta *et al.* 2007, see Fig. 2.27, lower right) and IC 4290 (Buta & Crocker 1991). In such cases, the boxy/X-morphology affects only the broad inner section and not the narrower ends, another argument in favour of the ends of bars being flatter than their middle sections.

Barred galaxies are well-known for their ring morphologies. The bar usually fills one dimension of an inner ring, as in NGC 2523 and NGC 1398 (Fig. 2.28). The inner ring of NGC 1398 especially shows a tight spiral morphology that is mostly distinct from the rest of the galaxy's extensive spiral structure.

Outer rings (R) are usually about 2–2.5 times the size of an inner ring/bar. Usually there is only one (R), but very rare cases have two (Fig. 2.29). The stellar populations in outer rings are potentially very interesting. In NGC 2273, the two outer rings are smooth and both may be characterised mostly by an older stellar population. However, the double outer ring in NGC 1211 has a population dichotomy that is well shown in an SDSS colour image (Fig. 2.30). The outer outer ring is blue while the inner outer ring,

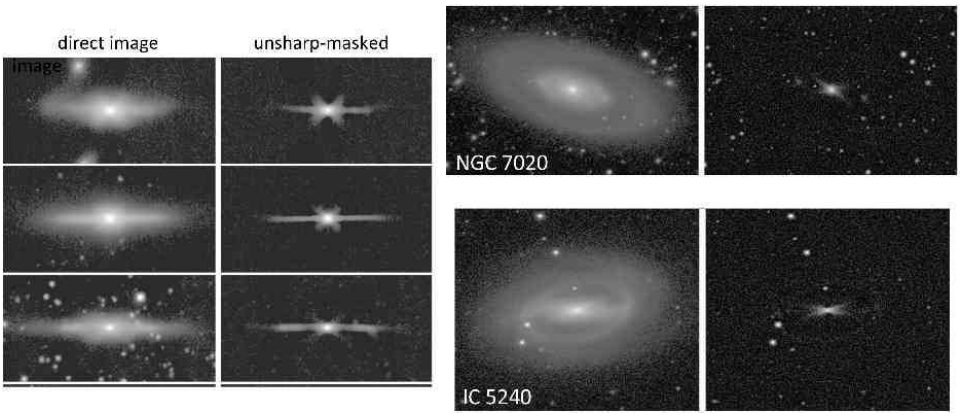

Fig. 2.27. Examples of edge-on and non-edge-on X-galaxies.

the inner ring, the bar, and the bulge are defined by a much older and redder stellar population. The suggestion is that the outer outer ring is a recent acquisition, possibly an accretion feature where the material from a disrupted companion has settled into the disk plane of a host (R)SB(rl)0^+ galaxy. Alternatively, NGC 1211's outer structure may be related to what Buta (1995) referred to as an 'R_1R_2'' morphology, or double outer ring/pseudoring (Buta *et al.* 2007). These also can show a population dichotomy with the R_1 component being redder and made of older stars than the R_2' component. This kind of morphology has been linked to the outer Lindblad resonance, and is described further later in this lecture.

The outer spirals in barred galaxies often have variable pitch angle and close into what de Vaucouleurs referred to as an outer pseudoring, (R′). These features are most common among early- to intermediate-type spirals (Buta & Combes 1996). The morphologies of these features are distinctive enough to merit special attention, as shown by the R_1R_2' morphology. This is also discussed later in this lecture.

Rings are likely products of secular evolution in galaxies, in the following sense. As reviewed by Buta & Combes (1996), the best interpretation of barred galaxy rings is that they form by gas accumulation at resonances, under the continuous action of gravity torques due to the bar. In the presence of a bar potential, gas clouds try and settle into the parent orbits of the potential, but cannot do so without crossing other orbits. This leads to a spiral that slowly can be torqued into rings near orbital resonances (Schwarz 1981, 1984a).

The resonance idea is not the only interpretation of barred galaxy rings

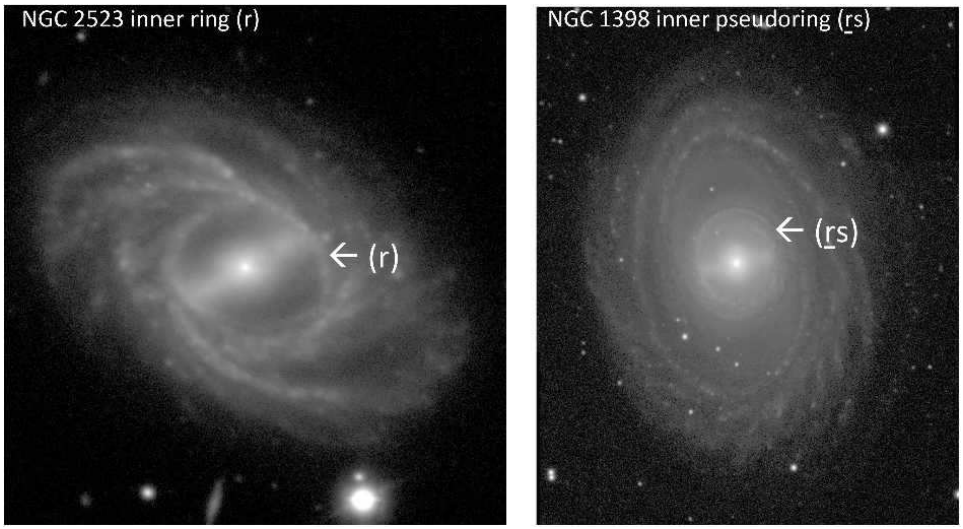

Fig. 2.28. NGC 2523 and NGC 1398, two galaxies with conspicuous inner rings.

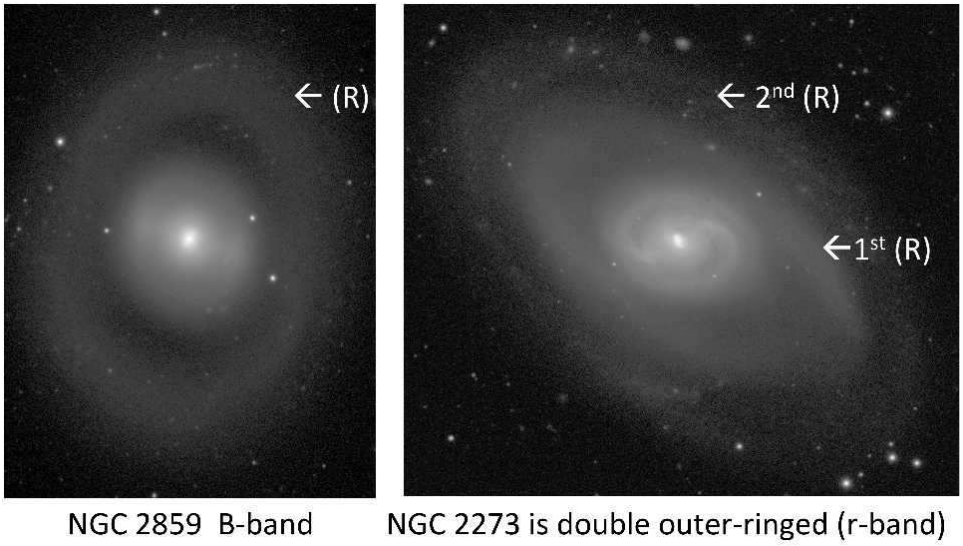

Fig. 2.29. Two galaxies with conspicuous outer rings.

that has been put forward (see summary in B13 and also Athanassoula, this volume), but it makes a number of predictions with respect to morphology that are easily testable. To do so, we need to find a reliable way to judge the intrinsic shapes and orientations of inner and outer rings. The way this can

be done is to obtain *distributions of apparent axis ratios and relative bar-ring position angles*, and then to model these distributions under the assumptions of random orientations of the disk planes and zero vertical thickness. The latter assumption is not unreasonable given that rings in spirals are often zones of active star formation.

The Catalogue of Southern Ringed Galaxies (CSRG, Buta 1995) was designed to evaluate the intrinsic shapes and orientations of inner and outer rings in this manner. Inner SB rings are oval with intrinsic axis ratio $\langle q_o \rangle = 0.81 \pm 0.06$ and are aligned parallel to the bar (Fig. 2.31, left panel). The velocity field of the nearby galaxy NGC 1433 (Buta *et al.* 2001) beautifully demonstrates this characteristic alignment. The large inner ring in this galaxy has $q_o = 0.63$, much more elongated than average. The velocity field betrays this shape by a kinematic line of nodes that is nearly along the minor axis of the ring. Bars may also underfill an inner ring or pseudoring, as in NGC 7098 (Fig. 2.31, right panel). Bars generally do not overfill inner rings, making H. Curtis's 'ϕ-type' characterisation not quite appropriate.

Although parallel alignment is clearly the 'rule' for SB inner rings, misalignments are sometimes seen. These are recognised in nearly face-on galaxies as clear cases of inner pseudorings crossed at a large angle by a bar. A kinematically confirmed example is ESO 565-11 (Fig. 2.31, middle panel; see Buta *et al.* 1995a). Other likely examples are NGC 309 (Sandage 1961) and CSRG 1052 (Buta 1995).

ESO 565-11 is such an extreme case that it suggests a possible evolutionary effect. The galaxy is not only a misaligned bar-inner ring system, but also a misaligned bar-oval system, because the inner pseudoring lies around the rim of a massive oval, from which stellar outer arms emerge. Since long-term, stable misalignment of massive nonaxisymmetric components is unlikely, the suggestion is that the bar of ESO 565-11 is relatively new, and that it formed within a pre-existing oval that itself is a remnant of a past bar episode. Evidence in support of this idea is the presence of the large and very unusual nuclear ring (Buta *et al.* 1999). The extreme elongated shape and size of this feature (more than 3 kpc in radius) are likely indicators of its youth.

For SB outer rings/pseudorings, statistics favor $\langle q_o \rangle = 0.82 \pm 0.07$ and both parallel and perpendicular alignments (Buta 1995). The different alignments are shown with deprojected inner rings in Fig. 2.32. In each, note the exclusive parallel alignment of the inner rings in the same galaxies.

Nuclear rings (nr) are found well inside bars (Fig. 2.33). Nuclear rings average 1.5 kpc in diameter, and have roughly circular intrinsic shapes and a morphology that can be shaped by dust. According to Knapen (2005) and Comerón *et al.* (2010) nuclear rings are found in 20% of galaxies in the type

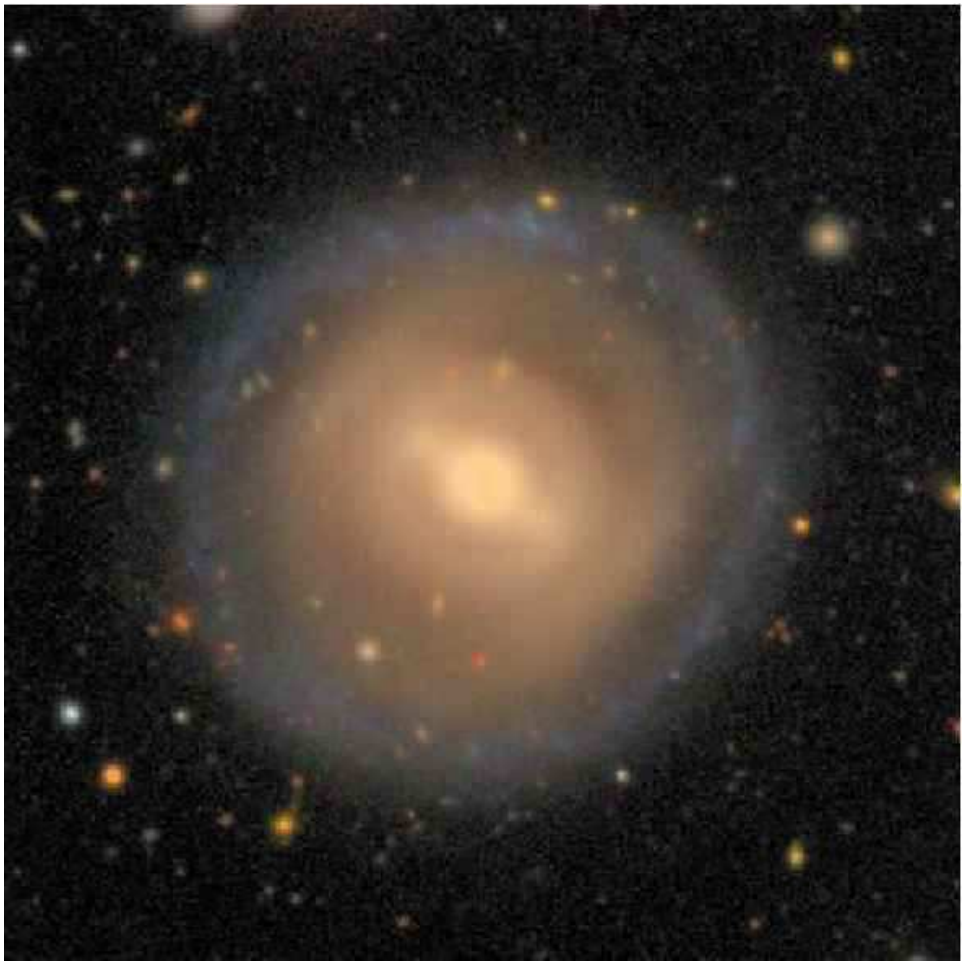

Fig. 2.30. NGC 1211, a double outer-ringed galaxy with an obvious stellar population dichotomy.

range S0$^-$ to Sd. Figure 2.34 shows two results from Comerón *et al.* (2010): that nuclear rings have a wide range of linear diameters, from 200 pc to several kpc, and that stronger bars tend to host smaller nuclear rings, while weaker bars can host small and large rings. The connections between bars and the properties of nuclear rings are discussed further in Knapen (2010).

Found in the same area as nuclear rings are nuclear (secondary) bars (nb) (Fig. 2.35). According to Erwin (2004, 2011), double bars are found in ∼20% of S0-Sb galaxies. The sense of a nuclear bar, tipped ahead of (leading) or behind (trailing) a primary bar can be judged from the sense of winding of spiral arms (assumed to be trailing). The existence of both types of nuclear

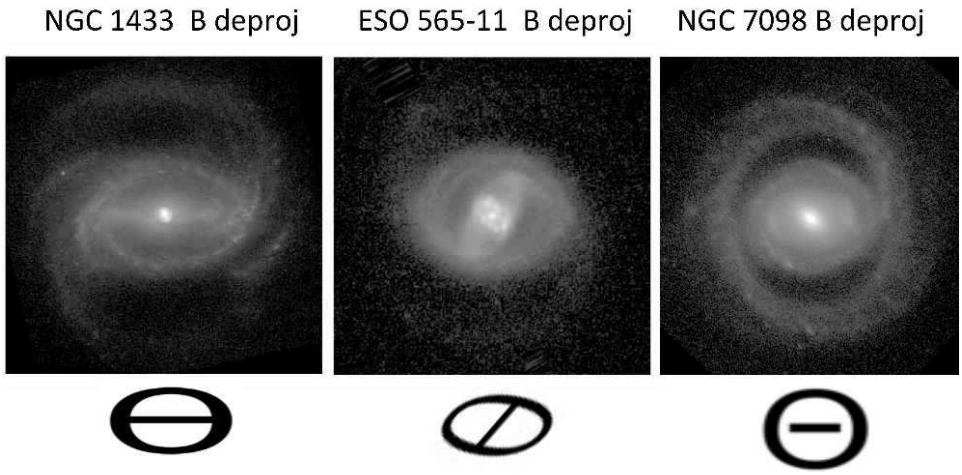

Fig. 2.31. Intrinsic inner ring shapes and orientations in barred galaxies.

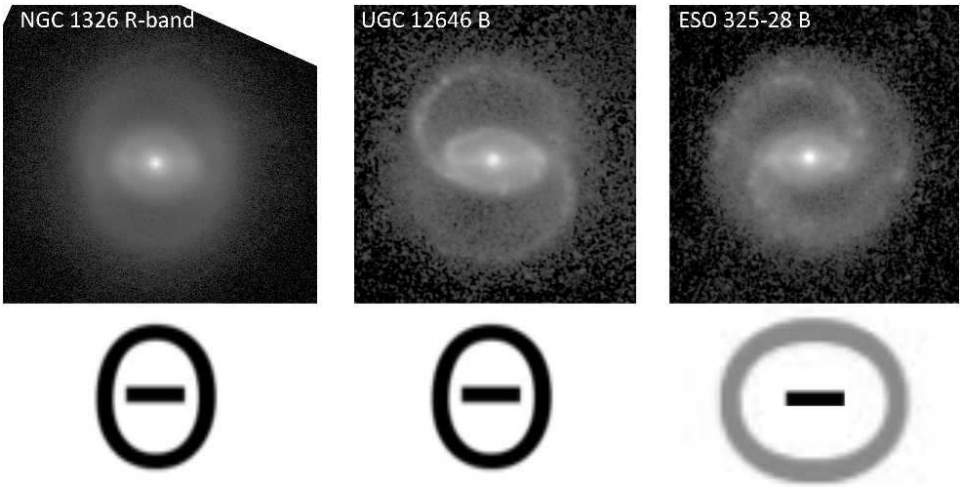

Fig. 2.32. Intrinsic outer ring and pseudoring shapes and orientations in barred galaxies, as compared with deprojected images.

bars argue that these features have a different pattern speed from the primary bar. Erwin (2004, 2011) shows that alignments between nuclear and primary bars are random (Fig. 2.36), and Corsini *et al.* (2003) find direct kinematic evidence for it in NGC 2950.

In terms of secular evolution, nuclear rings are in a different domain from inner and outer rings. Outer rings are thought to have a long timescale

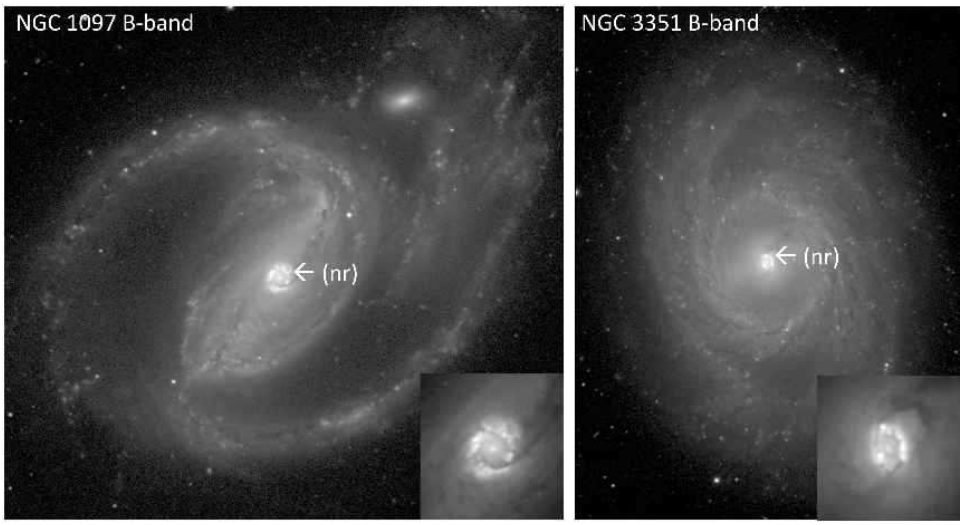

Fig. 2.33. Two barred galaxies with nuclear rings.

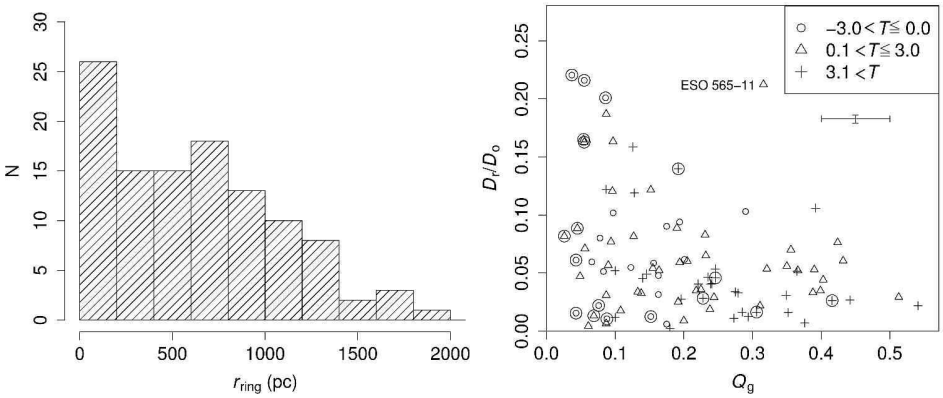

Fig. 2.34. Two graphs from Comerón *et al.* (2010, reproduced with permission) showing the wide range of linear sizes of nuclear rings and the sensitivity of relative ring size to relative bar torque strength Q_g.

(requiring more than a few Gyr to form; Schwarz 1981; Rautiainen & Salo 2000), while nuclear rings, being much closer to the centre, have a timescale of only a few times 10^8 years (Combes 1991). Only nuclear rings are prone to extreme bursts of star formation. The presence of a nuclear bar inside a star-forming nuclear ring (as, e.g., in NGC 6782) should produce gravity torques that could evolve the central regions (Shlosman *et al.* 1989). Also, the coexistence of nuclear, inner, and outer rings, each with a very different

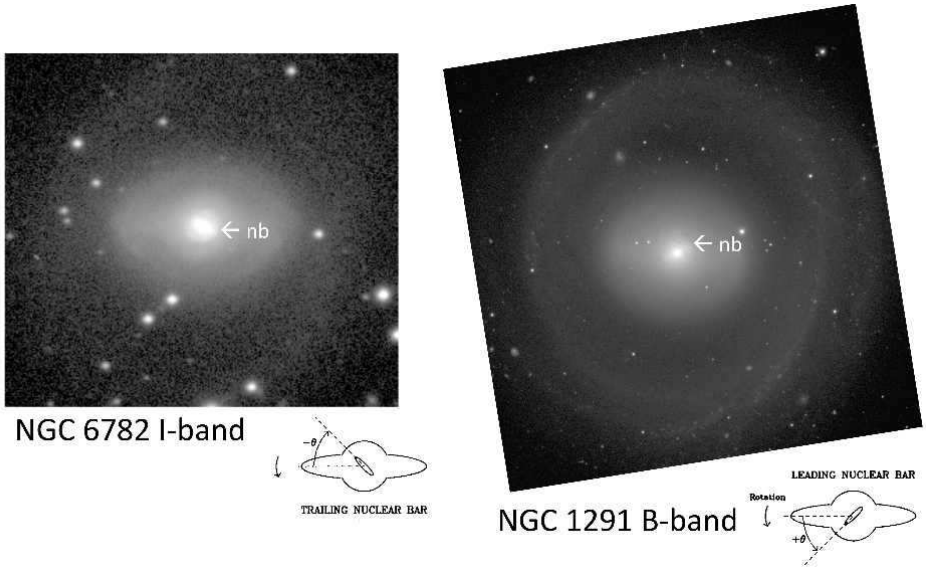

Fig. 2.35. Two barred galaxies with secondary or nuclear bars. The one in NGC 6782 is tipped behind the primary bar and is called trailing, while the one in NGC 1291 is tipped ahead and called leading. Schematics are from Buta & Crocker (1993a).

time scale, in the same galaxy, suggests a persistent means of funnelling gas towards the central regions.

2.5.1 Quantifying bar strength

One of the major goals de Vaucouleurs had during his long career was to find ways of quantifying the three dimensions of the VRHS. He imagined setting the stage $T = f$ (colour, surface brightness, HI content, etc.), where f is a numerical function of measured parameters, each of which correlate individually with stage but with a large scatter. However, no effective way of doing this was ever really found. T is still best estimated visually. In contrast, there is more than one way of reliably quantifying bars. Doing this would be useful for several reasons: (1) to judge the actual significance of a bar within its disk; (2) to examine the connection between bars and spirals (e.g., we can ask: do the former 'drive' the latter?); and (3) to investigate how measureable properties of bar-associated features like rings correlate with bar strength.

Relative Fourier intensity amplitudes can quantify the light perturbation effectively. Two examples involving early-type barred galaxies are shown

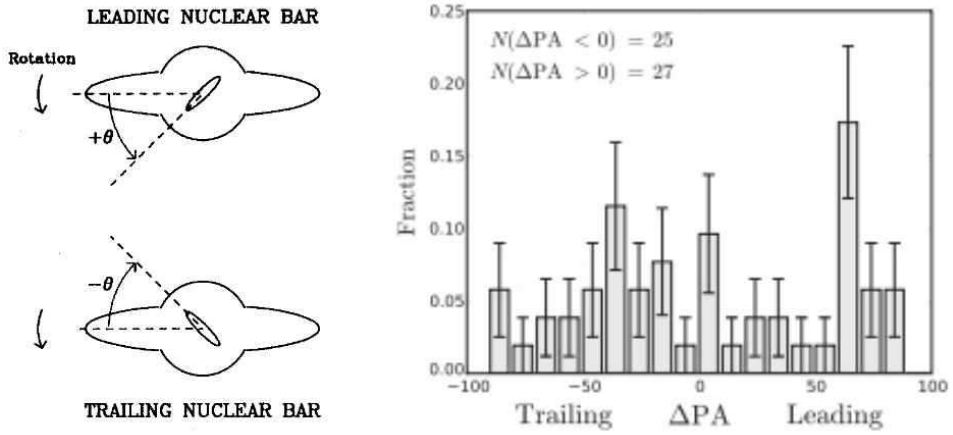

Fig. 2.36. The schematic at left shows the definitions of the terms 'leading' and 'trailing' as applied to nuclear bars in terms of the sign of the angle θ (Buta & Crocker 1993a). The graph at right shows the distribution of θ values for a large sample of secondary bars from Erwin (2004, reproduced with permission).

in Fig. 2.37. A_2 is the maximum of the relative $m = 2$ Fourier amplitude I_2/I_0. The amplitudes are derived from a Fourier expansion of the brightness distribution:

$$I(R,\phi) = I_0(R) + \Sigma_{m=1}^{\infty} I_m(R)\cos[m(\phi - \phi_m(R))]. \tag{2.1}$$

With such an expansion, the sine and cosine amplitudes are derived as

$$\begin{aligned} I_{mc}(R) &= 2 < I(R,\phi)\cos(m\phi) > \\ I_{ms}(R) &= 2 < I(R,\phi)\sin(m\phi) > \\ I_m(R) &= \sqrt{I_{mc}(R)^2 + I_{ms}(R)^2} \\ \phi_m(R) &= \frac{1}{m}\tan^{-1}(\frac{I_{ms}(R)}{I_{mc}(R)}). \end{aligned} \tag{2.2}$$

An important finding from Buta *et al.* (2006) is the single and double Gaussian forms of the radial variations of I_m/I_0 for some galaxies, especially early-types. The solid curves fitted to the amplitudes of the two early-type examples (Fig. 2.37) shows how well these representations work. The physical significance of these forms is unclear; however, similar forms have been seen in numerical simulations. For example, the relative Fourier profile for NGC 1452 is similar to a 'massive halo' bar model from Athanassoula & Misiriotis (2002). Note that more complex Fourier profiles are seen that can

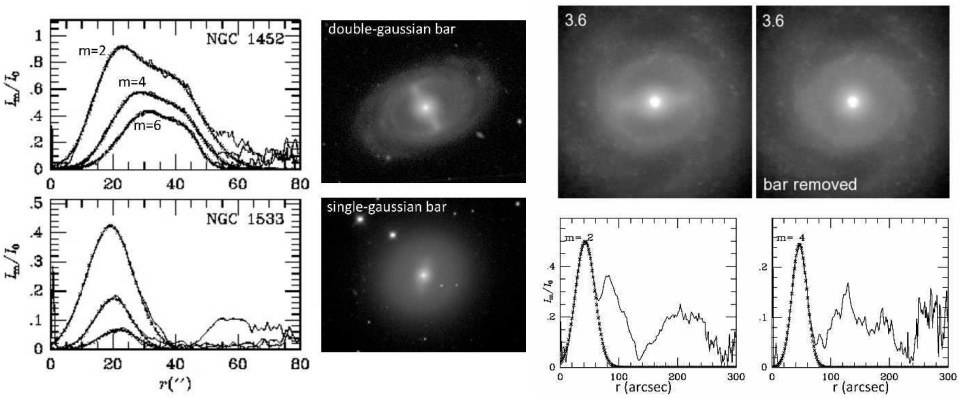

Fig. 2.37. Examples of single and double-Gaussian Fourier bar profiles. (Left frames): $m = 2$, 4, and 6 K_s-band relative Fourier intensity profiles and B-band images of early-type galaxies NGC 1452 and NGC 1533 (Buta *et al.* 2006). (Right frames): 3.6 μm Fourier profiles and images of NGC 3351, showing that a single Gaussian fits the $m = 2$ and 4 Fourier profiles well.

be described as multi-Gaussian in nature, often occurring when the bar is embedded in a massive oval.

Interestingly, single Gaussian bars are not restricted to early types like NGC 1533. The same kind of bar is seen in the SBb spiral NGC 3351. Figure 2.37, right, shows $m = 2$ and 4 Fourier profiles and their Gaussian representations for NGC 3351. Also shown is how effectively this representation removes the bar from an infrared image of the galaxy. Single Gaussian bars appear to be the simplest type, but remain to be explained.

2.5.2 Bar strength from maximum relative gravitational torques

Another way of quantifying bar strength is to use an infrared image to trace stellar mass and infer the gravitational potential Φ. Then the bar strength can be estimated in terms of the maximum relative tangential forcing. Using Fast Fourier Transform techniques (Binney & Tremaine 1987, Section 2.9), a two-dimensional image may be converted to a two-dimensional potential on a Cartesian grid (Quillen *et al.* 1994). From this potential we derive the parameter

$$Q_{\rm T}(R) = \left| \frac{F_T(R)}{F_{\rm 0R}} \right|_{\rm max}, \qquad (2.3)$$

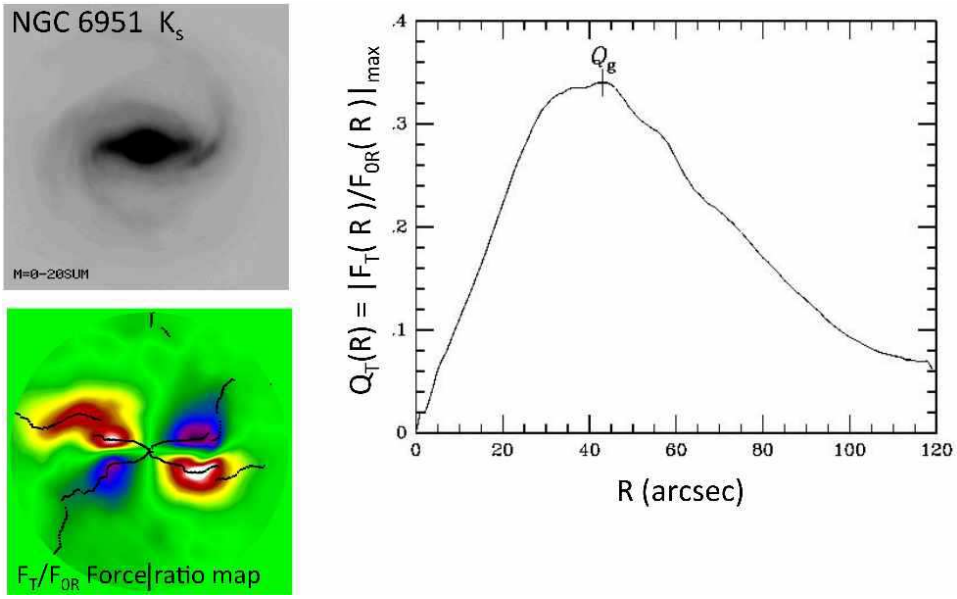

Fig. 2.38. Derivation of $Q_{\rm g}$ for NGC 6951, from Buta *et al.* (2003).

where $F_{\rm T} = \frac{1}{R}\frac{\partial \Phi}{\partial \phi}$ is the tangential force and $F_{\rm 0R} = \frac{\partial \Phi_0}{\partial R}$ is the mean radial force. This approach follows Sanders & Tubbs (1980) and Combes & Sanders (1981).

The actual application of this method is described by Buta *et al.* (2007) and highlighted in Fig. 2.38. Force ratio maps yield a 'butterfly' pattern defined by four 'islands' of high tangential forcing. Following the maximum of $F_T/F_{\rm 0R}$ through each quadrant (dotted curves, lower left of Fig. 2.38), and then averaging over the four quadrants, gives a curve like that in the right panel of Fig. 2.38. For the actual bar strength, we take the maximum of the average maxima, called $Q_{\rm g}$. Strictly speaking, $Q_{\rm g}$ is the bar strength only if there are no other perturbing features besides a bar, such as spiral arms. If arms are present, then $Q_{\rm g}$ can include contributions from these as well. Buta *et al.* (2003) describe a Fourier-based method of separating a bar from the surrounding spiral. This allows the true bar strength $Q_{\rm b}$ to be estimated, as well as an estimate of the spiral strength $Q_{\rm s}$. In general, if the bar is strong compared to the spiral, then $Q_{\rm b} \approx Q_{\rm g}$, while if the spiral is stronger than the bar, then $Q_{\rm s} \approx Q_{\rm g}$.

Although the $Q_{\rm g}/Q_{\rm b}$ method sounds like a physically reasonable approach to quantifying bar strength in galaxies, it has a number of problems that limit its accuracy. First, deriving potentials requires making assumptions

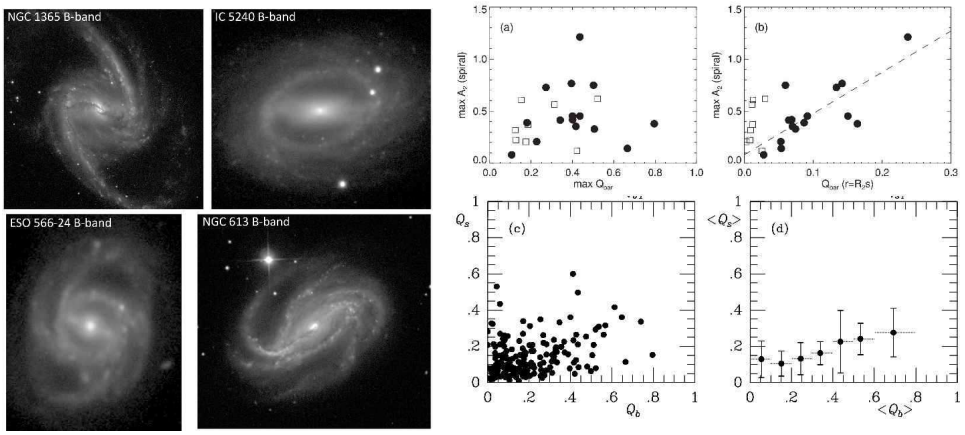

Fig. 2.39. Examples of global SB spirals (left) and correlations of bar and spiral strength from Buta *et al.* (2009, bottom-right panels) and Salo *et al.* (2010, upper-right panels).

about vertical thickness, and the thickness of bars may not be the same as that of the disk. The broad inner section may be more 3D than the bar ends. Second, since the method uses force ratios rather than light ratios, the impact of the dark matter halo becomes an issue that really only can be evaluated statistically. Finally, the method fails to distinguish different kinds of bars. Two bars can have the same $Q_{\rm g}$ value and look very different.

With these caveats in mind, let us examine how the strengths of spiral patterns correlate with bar strength. It is well-known that the spiral patterns in barred galaxies are generally global in nature (Kormendy & Norman 1979). Rare examples have flocculent spirals instead. Figure 2.39 shows several examples. An important question is, do the bars themselves 'drive' these patterns, or are the spirals mostly independent instabilities? In an article titled 'Do bars drive spiral density waves?', Buta *et al.* (2009) compared maximum relative spiral and bar torque strengths and detected a weak positive correlation. In a follow-up paper 'Bars do drive spiral density waves', Salo *et al.* (2010) compared local relative spiral and bar torque strengths and found a much better correlation, confirming the conclusion of Kormendy & Norman (1979). This does not mean that all the spirals in barred galaxies are necessarily driven by the bar. As will be described in Lecture 3 (see Section 2.6), potential-density phase shift studies suggest that some spirals are decoupled from their bars.

2.5.3 Inner ring shapes and bar strength

As described previously, inner SB rings have a mean intrinsic axis ratio of $q_o = 0.81 \pm 0.06$. However, individual cases suggest that inner rings can have a shape over the much broader range $q_o = 0.6$–1.0 (Buta 1986). Another question we can ask is: do inner ring shapes correlate with bar strength? Theoretically, such a correlation should exist because bar strength can determine the shapes of periodic orbits, and rings are thought to take on the shapes of specific orbits (e.g., Schwarz 1984b; Rautiainen & Salo 2000).

It is an interesting aspect of SB inner rings that the way HII regions are distributed around the rings is sensitive to intrinsic ring shape but not to maximum relative bar torque strength Q_g (Buta 2002; Buta *et al.* 2007). Nearly circular inner rings may be found around strong bars just as highly elongated rings are found. However, if you compare the ring radius with the radius of the bar torque maximum, then a correlation is found. Figure 2.40 shows that a highly elongated inner ring is found when the semi-major axis radius of the ring $a_r \approx R(Q_g)$, the radius of the relative bar torque maximum. In such a case, the ring essentially lies on the bar and can be considered a part of the bar. HII regions are seen to 'bunch up' around the ends of the bar, as in NGC 6782. In contrast, when $a_r > R(Q_g)$, the bar maximum is far enough inside the ring radius to allow the ring to be more circular, as in NGC 53. In this case, the HII regions are distributed more uniformly around the ring.

None of this really explains why some galaxies select one possible ring orbit over another. According to Schwarz (1984b), an inner ring takes on the shape of the largest 4:1 resonant orbit that is not cusped and which does not cross another orbit. However, simulated inner rings could have more diamond-like shapes if higher-order Fourier harmonics in the bar were important. Such a shape seems present in the inner ring of NGC 6782, and indeed Lin *et al.* (2008) interpreted the shape of this galaxy's inner ring in terms of an interaction between waves excited at the inner 4:1 resonance and waves excited at the inner Lindblad resonance, based on hydrodynamical simulations. These authors also attributed the distribution of HII regions around the bar ends as due to an interaction between the gas and curved shocks.

It is unclear how the shapes of inner rings might evolve over time. The likely evolution is from a pseudoring to a ring, while a change in ring shape might link more to changes in the bar pattern speed, which affects the actual location of resonances as I now describe. In a model galaxy having a significant halo and a moderately rising rotation curve, Rautiainen & Salo (2000) found a time sequence where a highly elongated inner ring becomes more circular.

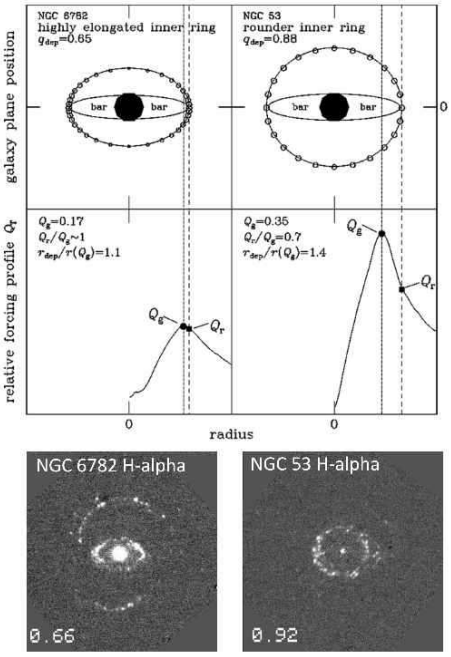

Fig. 2.40. How inner ring shape connects to bar torque strength. The Hα images are from Crocker *et al.* (1996) while the schematics are from Grouchy *et al.* (2010).

2.5.4 Resonances in barred galaxies

The presence of even a weak bar sets up a pattern speed $\Omega_{\rm p}$ and resonances in a differentially rotating disk. A perturbed orbit in a weak bar potential has this shape (Binney & Tremaine 2008):

$$R = R_{\rm o} + C_1 \cos[\kappa\phi/(\Omega - \Omega_{\rm p}) + \alpha] + C_2 \cos(m\phi)/[\kappa^2 - m^2(\Omega - \Omega_{\rm p})^2]. \quad (2.4)$$

The resonances are in the C_2 terms and are as follows:

(a) Corotation resonance (CR): $\Omega = \Omega_{\rm p}$
(b) Inner Lindblad resonance (ILR): $\Omega - \Omega_{\rm p} = \kappa/2$
(c) Outer Lindblad resonance (OLR): $\Omega - \Omega_{\rm p} = -\kappa/2$
(d) Inner 4:1 resonance (I4R): $\Omega - \Omega_{\rm p} = \kappa/4$
(e) Outer 4:1 resonance (O4R): $\Omega - \Omega_{\rm p} = -\kappa/4$

where $\kappa = 2\Omega[1 + \frac{1}{2}\frac{R}{\Omega}\frac{d\Omega}{dR}]^{\frac{1}{2}}$ is the epicyclic frequency and Ω is the circular angular velocity.

Are these resonances detectable in real galaxies? The answer is yes, and a variety of methods is available to detect them in both barred and spiral galaxies. Here we are mainly interested in how these resonances might be

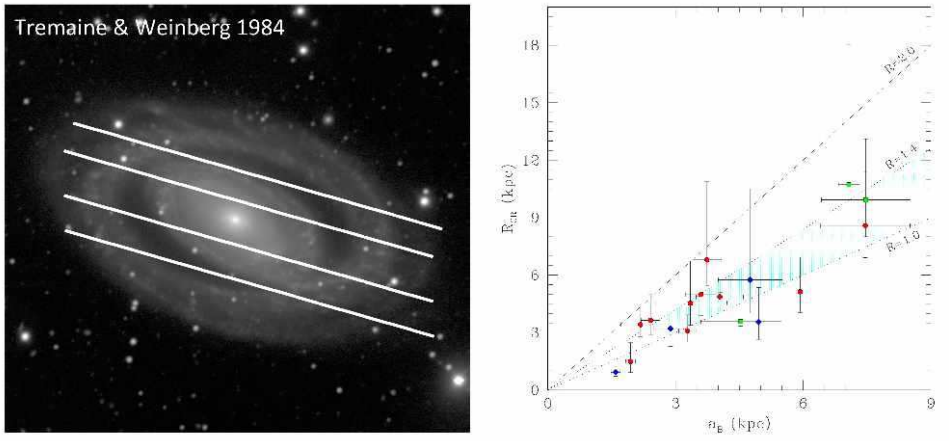

Fig. 2.41. (Left): NGC 7098 with a set of parallel slits along the major axis set up to estimate the pattern speed using the Tremaine-Weinberg method. (Right): graph from Corsini (2011) showing the preponderance of fast bars in a sample of mostly SB0 galaxies. Reproduced with permission.

manifested morphologically, and what their long-term impact on morphology might be.

The most direct method of locating resonances is to apply the Tremaine-Weinberg (1984) approach, which uses the equation of continuity to estimate the pattern speed $\Omega_{\rm p}$. Along a set of slits oriented parallel to the major axis (Fig. 2.41, left), one derives the luminosity-weighted averages of the line of sight velocity $\langle {\rm V} \rangle$ and the position $\langle {\rm X} \rangle$. A graph of $\langle {\rm V} \rangle$ versus $\langle {\rm X} \rangle$ has the slope $\Omega_{\rm p} \sin i$, where i is the inclination. Then the CR is located by using a rotation curve to calculate how Ω varies with galactocentric radius. The method has been mostly applied to SB0 galaxies to derive the parameter $\mathcal{R}$, where $\mathcal{R} = R_{\rm CR}/R_{\rm bar}$. The results have suggested that most bars in SB0 galaxies are fast with $\mathcal{R} \approx$1–1.4 (Corsini 2011; Fig. 2.41, right).

2.5.5 Rings and pseudorings as tracers of the bar pattern speed

Rings were tied early on to resonances in galaxies harbouring density waves. Many rings are zones of active star formation, and in colour index maps all ring types, inner, outer, and nuclear, can show enhanced blue colours (e.g., NGC 3081, Buta & Purcell 1998).

Schwarz (1981) made test-particle simulations of barred galaxies that led to the recognition of two morphologies that should be observed near the OLR. The first type involves outer arms that wind 180$^{\rm o}$ and close into a

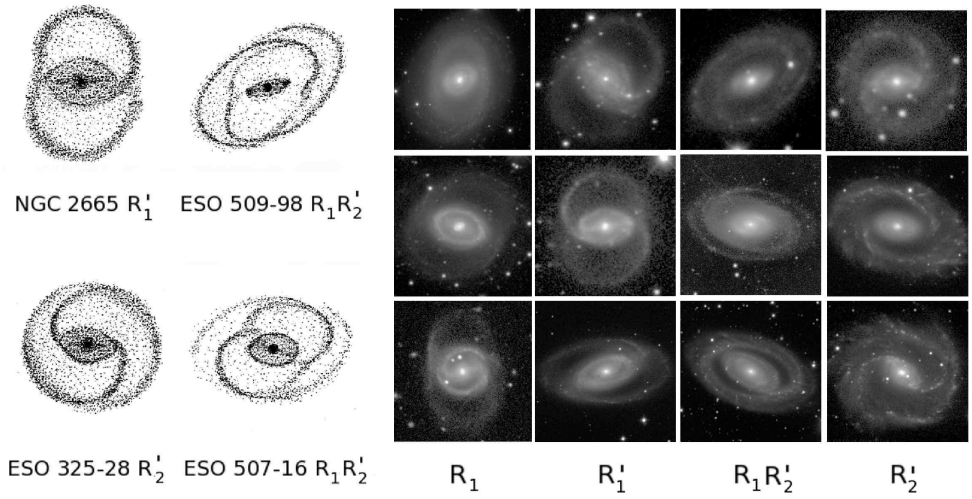

Fig. 2.42. Schematics of OLR morphologies and examples (from B13).

pseudoring aligned perpendicular to the bar, while the second type has arms winding 270° and is aligned parallel to the bar. Within the limitations of Schwarz's models, the first type was favoured if there was little gas outside the OLR, while the second was favoured if there was more gas outside the OLR. These types were searched for and found by Buta (1985, 1995), who called the first type R'_1 and the second type R'_2, implying these should be interpreted as outer pseudorings. The argument that these features trace the OLR was strengthened by the identification of galaxies showing a combination of these two types, called $R_1R'_2$ by Buta (1995). In these types, you can almost see the two families of OLR periodic orbits that Schwarz linked to the two main types originally. The Catalogue of Southern Ringed Galaxies (Buta 1995) includes many examples of all three categories, and many others can be found in the GalaxyZoo database (`www.galaxyzoo.org` forums). Figure 2.42 shows schematics of what are known as the 'OLR subclasses', while many examples are shown in Fig. 2.42, right, and the dVA.

Schwarz (1981) did not predict the existence of the $R_1R'_2$ morphology. How it might develop was shown by Byrd *et al.* (1994) in modified Schwarz-type simulations. These showed an evolution from R_1 to R'_2, and that an $R_1R'_2$ morphology develops mainly in cases where the pattern speed is relatively high and no inner resonances occur (Fig. 2.43). The more sophisticated N-body models of Rautiainen & Salo (2000) found an almost cyclic change between R_1 and R_2 morphologies, due to the presence of a slower spiral mode in the outer disk. These authors also explained the absence of

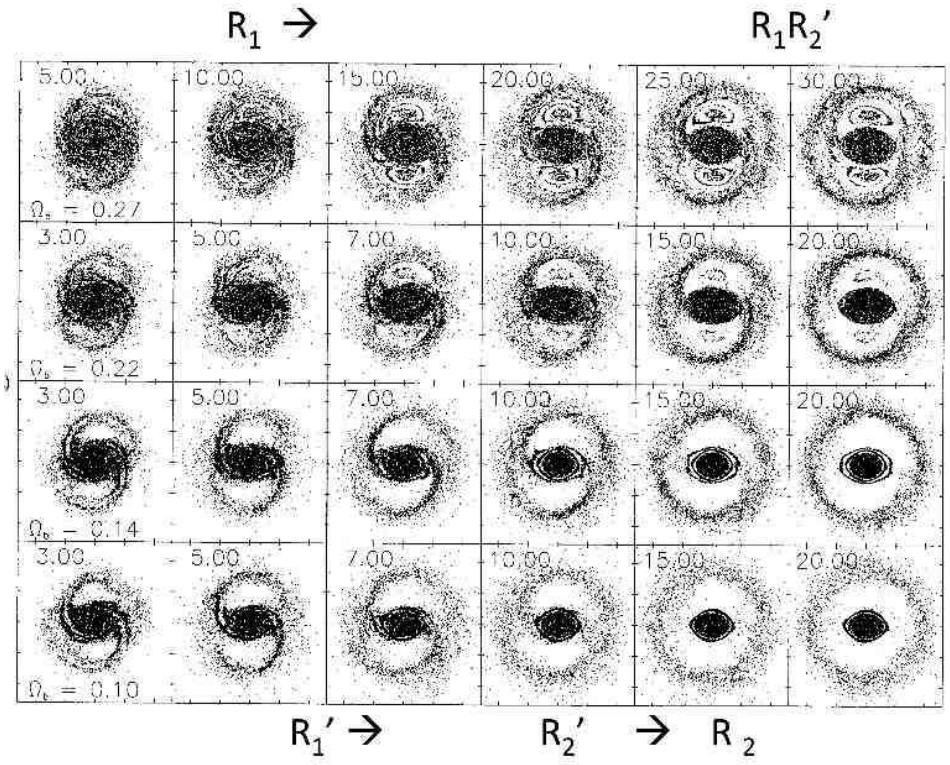

Fig. 2.43. High pattern speed simulations of barred galaxies from Byrd *et al.* (1994), showing the evolution of ring and pseudoring patterns at the OLR.

rings as being due either to the non-existence of a required resonance (like ILR) or, even when a resonance (like OLR) existed, to the greatly differing timescales of the different ring types.

The intrinsic shapes and orientations of rings also favour identification of rings with resonances. In the simulations of Simkin *et al.* (1980), a highly elongated inner ring aligned parallel to the bar forms at the inner 4:1 ultraharmonic resonance (I4R). This and the two alignments of outer pseudorings are consistent with CSRG statistics.

Up to four resonant ring features may be present in the same galaxy. Example: the remarkable 'resonance ring galaxy' NGC 3081 (Buta *et al.* 2004). Recognising all of its rings and a nuclear bar as well, here is a revised type for NGC 3081: (R_1R_2')SAB(r,nr,nb)0/a.

Can we use the rings in NGC 3081 to estimate the pattern speed? Using a Fabry-Perot velocity field and a representation of the rotation curve, Buta & Purcell (1998) derived Ω and the precession frequencies $\Omega \pm \kappa/2$ and

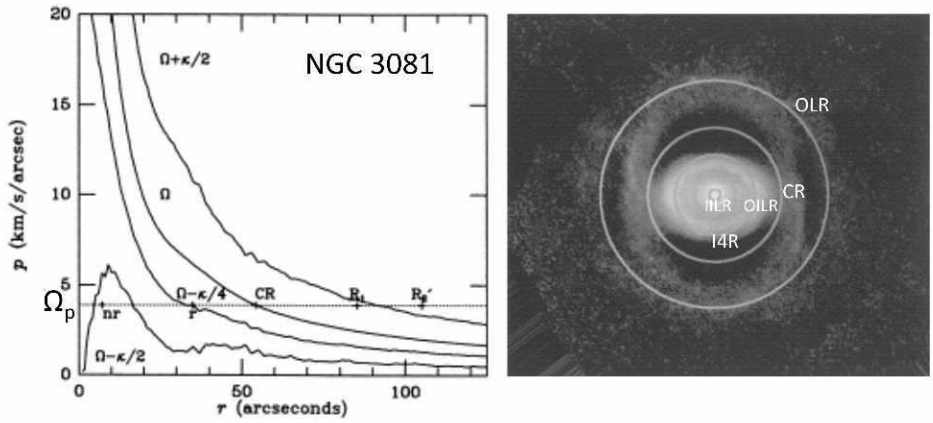

Fig. 2.44. (Left): Precession frequency curves for NGC 3081. (Right): Resonance locations from rotation curve analysis (Buta & Purcell 1998).

$\Omega - \kappa/4$ and set the OLR between the R_1 and R_2' features. The resulting value of Ω_p placed the inner ring near the I4R and the nuclear ring between two ILRs, consistent with the findings of Schwarz (1984a) and Simkin *et al.* (1980). Figure 2.44 shows how well NGC 3081 fits into barred spiral theory. The images show the deprojected galaxy after subtraction of an exponential disk model. If the R_1R_2' feature locates the OLR, then CR lies in the 'gap' between the inner ring and the R_1 outer ring.

A particularly interesting case with possible resonant features is the galaxy NGC 1433, which has an exceptionally well-defined and unusually highly elongated inner ring (dVA). In addition, the galaxy has two secondary spiral arcs off the leading sides of the bar called 'plumes' by Buta (1984). Treuthardt *et al.* (2008) were able to simulate both the inner ring and the plumes, as well as the outer R_1' pseudoring using a near-IR image to define the potential. These simulations demonstrated that the outer pseudoring in this case is likely related to the outer 4:1 resonance (O4R), not the OLR as would have been expected from Schwarz's simulations. A similar result was deduced for the outer R_1 ring of NGC 6782 by Lin *et al.* (2008).

As important as the 'OLR subclasses' are for understanding galaxy structure, there has been no systematic study of the global properties of these galaxies and how their structure (e.g., disk scalelengths, bulge-to-total luminosity ratios, etc.) compare with galaxies that lack these features. Interestingly, Pérez *et al.* (2012) have used R_2' pseudorings to examine the evolution of bar pattern speeds.

The possible evolution of nuclear rings might be evident in their observed

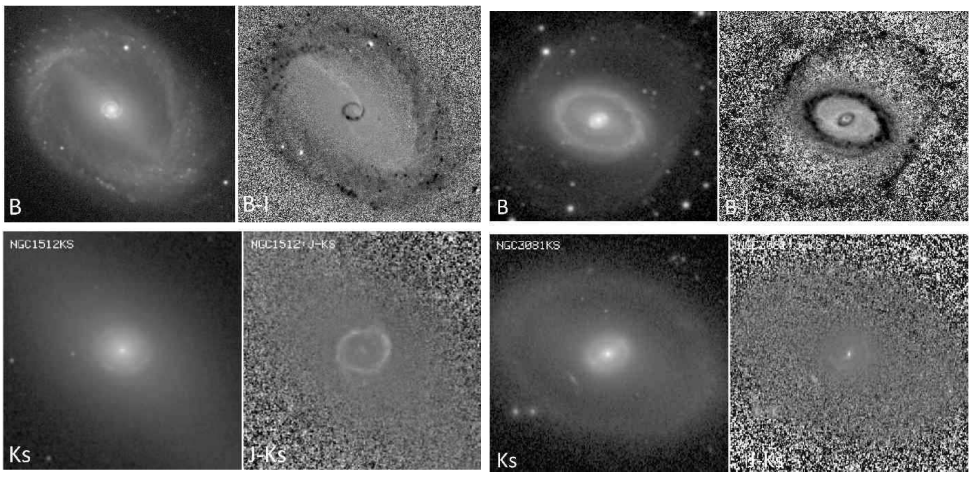

Fig. 2.45. Optical and near-IR colours of nuclear rings.

colours. Figure 2.45, left, shows optical and near-IR images and colour index maps of NGC 1512, an early-type barred galaxy that harbours both inner and nuclear rings. The nuclear ring in NGC 1512 is blue in a $B - I$ colour index map because of large numbers of young blue supergiants. However, the ring is 'red' in a $J - K_{\rm s}$ colour index map, implying the likely presence of a large number of young red supergiants as well. In contrast, the nuclear ring of NGC 3081 is also blue in a $B - I$ colour index map (Buta & Purcell 1998) but is largely invisible in a $J - K_{\rm s}$ map (Fig. 2.45, right), implying far fewer red supergiants (and probably a more evolved ring than the one in NGC 1512).

2.5.6 Are bars generally slightly skewed?

The final morphological question I want to ask about bars is, how straight are they? There is some indication that bars can be skewed in the form of very open spirals. In the SDSS galaxy shown in Fig. 2.46, the bar is skewed trailing, while in NGC 4596 in the same figure, the bar is slightly skewed leading, both after assuming trailing outer arms. The incidence and amplitude of bar skewness has not been determined, but some interesting cases have been identified. As shown in Fig. 2.46, the bar of NGC 3124 is distinctly skewed in a leading sense with little ambiguity. Bar skewness can lead to secular evolution by the potential-density phase shift that would result (Zhang 1996). This is described further in Lecture 3 (see Section 2.6).

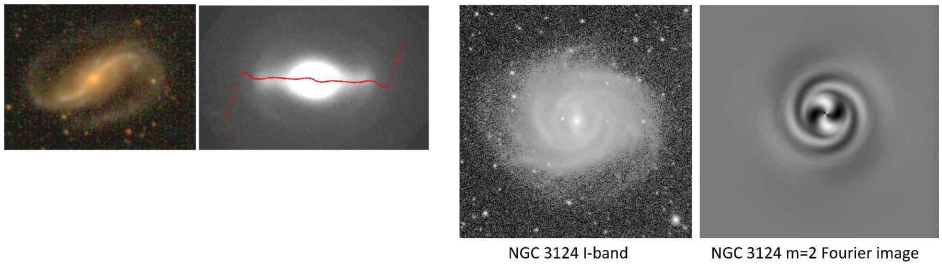

Fig. 2.46. Examples of skewed bars. The SDSS galaxy at left was selected from the GalaxyZoo Forum but its identity was not posted. The image of NGC 4596 is deprojected to face-on and the superposed curve shows the phase of the m=2 component. At right is NGC 3124, as it appears in an I-band image and an m=2 Fourier image.

2.5.7 Secular evolution in barred galaxies

The general view of secular evolution in barred galaxies is that the main effect is the ability of a bar to drive interstellar gas into the centres of galaxies, fuelling star formation and building up a pseudobulge (KK04). Figure 2.47 shows all of the types of features considered to be pseudobulges by KK04 as compared to 'classical' (merger-built) bulges. Pseudobulges include not only 'disky bulges' (as they are called by Athanassoula 2005; see top row of examples), but also nuclear bars and boxy-bulge galaxies. Pseudobulges generally have a low Sérsic index (see Lecture 3, Section 2.6), are flatter, and have a higher ratio of rotation to random motions compared to classical bulges.

Barred galaxies provide other possibilities for secular evolution:

(a) Can a 'normal' bar separate its middle section from its ends? Why would it do this? This is more a question of how ansae form and what they mean to galactic dynamics. If S0 galaxies are stripped or otherwise gas-depleted former spirals, and at the same time have a very different distribution of bar strengths from spirals, then bar evolution is a possible avenue to explore for the origin of ansae.

(b) What causes intrinsic bar-ring misalignment? Is this a phase in bar evolution? This is such a rare phenomenon that it is likely to be relatively short-lived. Nevertheless, bar-ring misalignment (which can also mean bar-oval misalignment) could point to an evolutionary mechanism: the destruction and rejuvenation of bars. If destruction of a bar can lead to formation of a lens-oval, and then external gas accretion cools the disk enough for bar rejuvenation, could the new bar have a different pattern speed from the old one? The misalignment

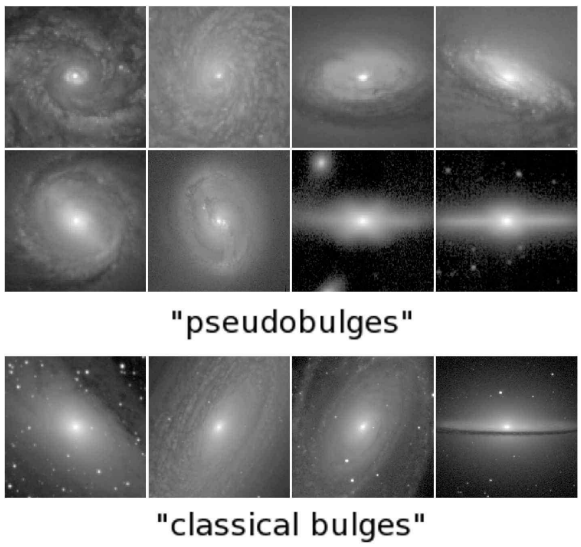

Fig. 2.47. Examples of pseudobulges and classical bulges. From B13 based on KK04.

between primary and secondary bars has also been attributed to different pattern speeds (e.g., Buta & Crocker 1993a).

(c) Why would a bar be skewed in a leading sense? I have shown that there are suggestive examples where a bar is curved like a very open spiral. When the mass associated with such spirals is converted into a gravitational potential, a small phase difference can result that has relevance to secular evolution (Lecture 3, Section 2.6). But what is determining the sense of spirality of the bar? Bar skewness supports the idea that a bar is a density wave like an ordinary spiral.

(d) What do double outer rings mean? Why should one ring be red and the other blue? Double outer rings seem much less common than double outer rings/pseudorings. The latter is usually found as the R_1R_2' morphology. But cases classified as '(RR)' as in the dVA (example: NGC 2273) are very rare. Could a double outer ring signify two episodes of ring formation at different values of the pattern speed?

(e) Is there an evolutionary connection between R_1 and R_2 outer rings? Did detached outer rings begin as pseudorings? The simulations of Byrd *et al.* (1994) showed a clear trend of evolution from an R_1' to an R_2' outer pseudoring, followed by a detached outer ring. At high pattern speeds, an R_1R_2' morphology developed. Rautiainen & Salo (2000) suggested a different evolutionary connection, in that the presence of a slower spiral mode in the outer disk would cause cyclic changes from R_1 to R_2.

2.6 Lecture 3: The infrared experience

I am titling this lecture as 'the infrared experience' because moving to the infrared (IR) opens such a big door to galactic studies. This is the wavelength domain that allows us to see what is often referred to as the 'backbone' of the stellar mass distribution. It is also the wavelength domain that exposes the interstellar medium (ISM) in a manner that no other domain can.

Observing at such wavelengths shows *dust-penetrated morphology*. At 2.2 microns, the extinction $A_{K_s} \approx 0.1 A_V$, where A_V is the visual extinction, at 3.6 microns, the extinction is $A_{3.6} \approx 0.05 A_V$. When we observe in the near- and mid-IR, we minimise the effects of these features on spiral galaxy morphology: bar dust lanes, spiral arm dust lanes, near-side dust lanes, dust rings, red planar dust lanes, and blue planar dust lanes (Fig. 2.48, which includes colour index maps that show these features). It is even advantageous to observe S0 galaxies in the IR, since extraplanar dust is often seen in such galaxies (Fig. 2.49). Colour index maps are not the only way to see the dust. In overlapping galaxy pairs, the dust is sometimes detected well beyond the standard isophotal radius, r_{25} (Fig. 2.50, Holwerda *et al.* 2009).

The near- and mid-IR may be mostly free of the effects of extinction but they are NOT completely free of the effects of star formation. Dust warmed by hot young stars becomes increasingly visible over 2–5 μm as shown in Fig. 2.51. In fact, the IR is an excellent domain for detailed studies of star-forming regions and especially star-forming galaxies. Spectral emission lines due to polycyclic aromatic hydrocarbons appear in three of the four mid-IR bands of the Infrared Array Camera (IRAC) on the *Spitzer Space Telescope* (e.g., Churchwell *et al.* 2004).

The IR can also provide a great deal of information on the properties of bulges and disks in galaxies. Because of the reduced effects of extinction, standard parameters of bulges and disks can be considered more characteristic of the stellar mass distribution than they are in the optical. Before describing IR galaxy morphology, let me first briefly describe the methods people are currently using to derive these parameters.

Most photometric decomposition today is 2D, meaning the whole image is fitted rather just the major or the minor axis as was once the standard method. The most popular parametric function to use is the Sersic Law.

Let R_e be the radius of the isophote enclosing half the total luminosity (called the effective radius) and let I_e be the surface brightness of this isophote. Define relative parameters $\rho = R/R_e$ and $J_n = I_n(R)/I_e$. The Sersic Law connects these parameters through

$$\log(J_n) = -0.434(2n - 0.324)(\rho^{\frac{1}{n}} - 1), \tag{2.5}$$

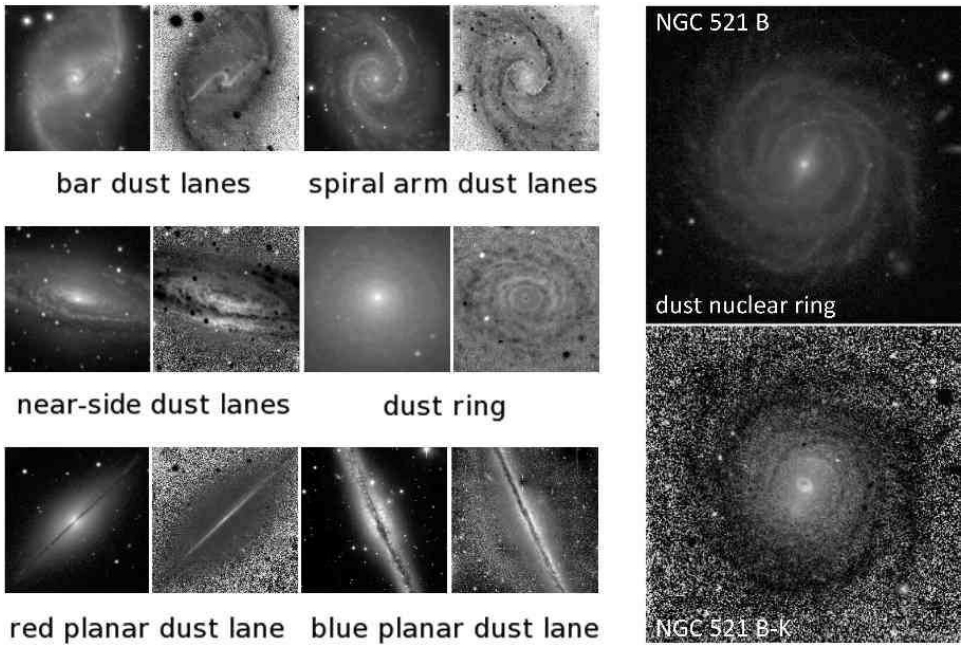

Fig. 2.48. Dust morphologies in normal galaxies based on colour index maps. The left panels are from B13 and show from top-left to lower-right: NGC 1530, NGC 1566, NGC 7331, NGC 7217, NGC 7814, and NGC 891. The images of NGC 521 are from Buta *et al.* (2009).

where n is a characteristic index that determines the shape of the radial profile. The Sersic law is a 'jack of all trades':

(a) n=1: exponential law,
(b) n=4: de Vaucouleurs $r^{\frac{1}{4}}$ law.

Two-dimensional decomposition today has gone well beyond merely bulges and exponential disks. Barred galaxies are no longer ignored because bars can be fitted and their contribution allowed for. For example, one can use a Ferrers bar model (e.g., Binney & Tremaine 2008):

$$\begin{aligned} I(m^2) &= I_0(1-m^2/a^2)^n, \quad (m \le a) \\ I(m^2) &= 0, \qquad\qquad\quad (m > a), \end{aligned} \tag{2.6}$$

where m is the radius along the bar axis. The Sersic law can also be used for bars. Values of $n<1$ can fit some bars well. Sersic fits have also been used for secondary bars and lenses. If these features are not fitted, then the bulge-to-total luminosity ratio B/T will tend to be overestimated (Laurikainen *et al.* 2006). With initial guesses of all parameters, the best fit uses

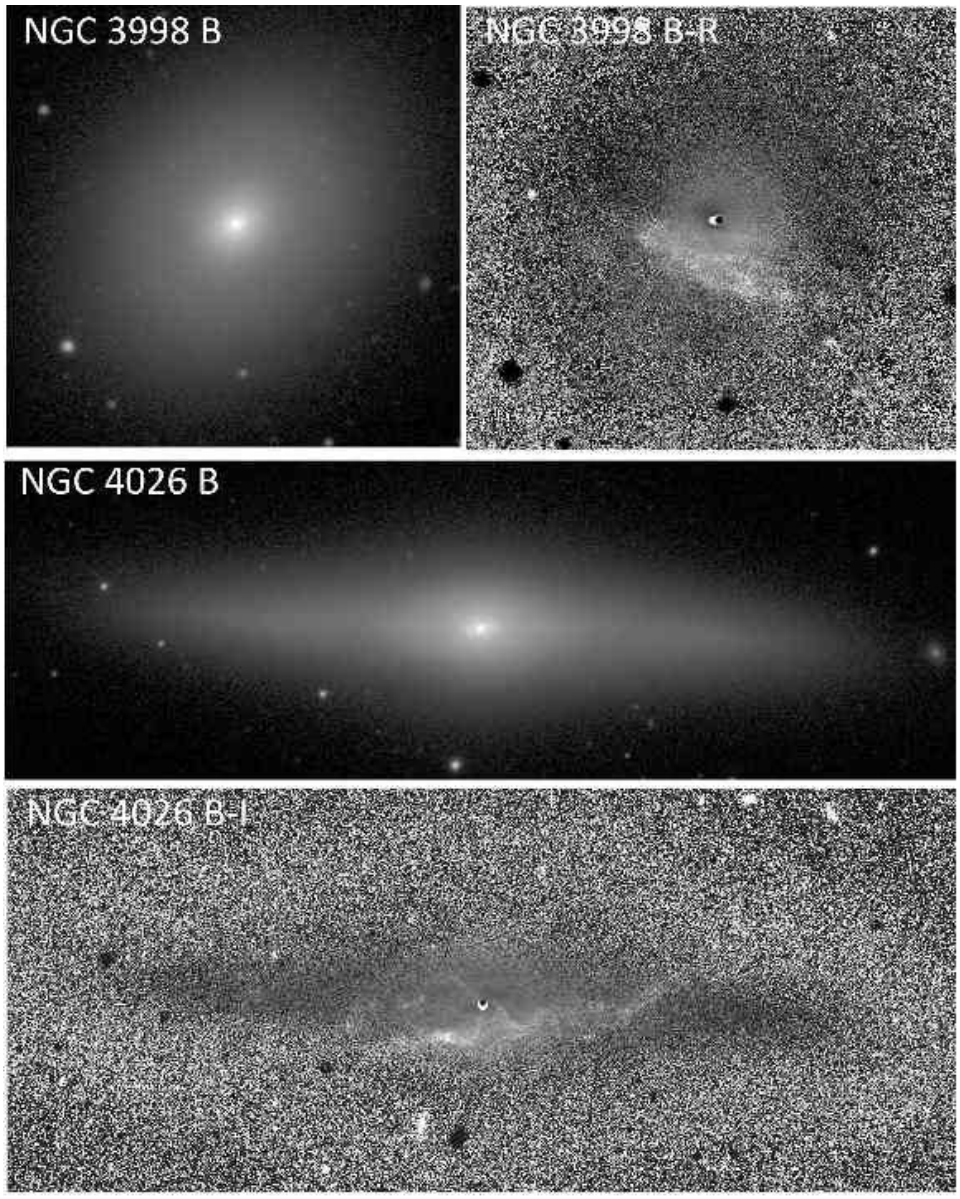

Fig. 2.49. Examples of dusty S0s.

χ^2 minimisation, usually with an adopted weighting scheme. Initial guesses can be based on 1D profile analysis.

Fig. 2.50. Example of an overlapping pair that reveals the significant extent of the dust disk of the foreground galaxy (from Holwerda *et al.* 2009, reproduced with permission).

2.6.1 Significant IR morphological surveys

I would like to describe now three recent extensive surveys that shed a great deal of light on IR galaxy morphology.

2.6.1.1 The Ohio State University Bright Spiral Galaxy Survey

The Ohio State University Bright Spiral Galaxy Survey (OSUBSGS, Eskridge *et al.* 2002) was a comprehensive imaging survey of 205 bright nearby spiral galaxies. The main IR imaging filter used was the H-band at 1.65 μm. The galaxies in the survey were classified in the de Vaucouleurs (1959) system and special attention was paid to how near-IR types differ from the optical classifications of galaxies. The authors found several galaxies classified as SA in the Third Reference Catalogue of Bright Galaxies (RC3) for which they assigned a classification of SB. They also estimated the frequency of bars in their sample (Lecture 2, Section 2.5). In general, it was found that intermediate-type spirals were classified approximately one stage interval earlier in the H-band than in the B-band. The authors also challenged

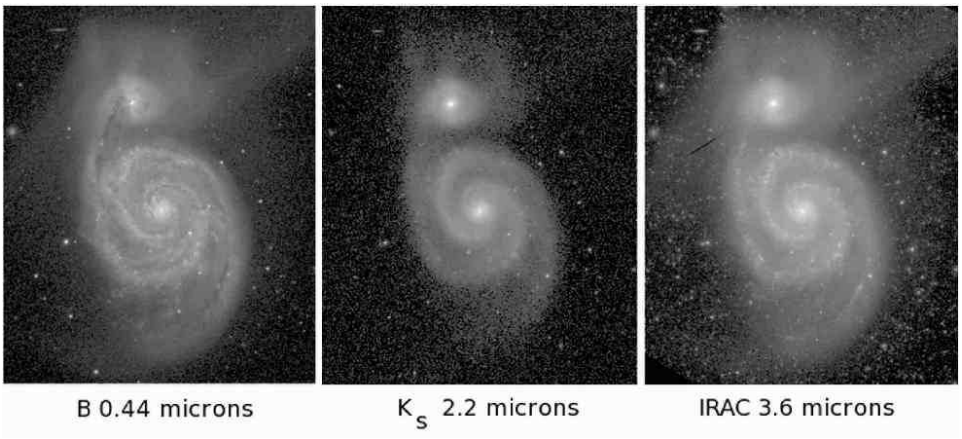

Fig. 2.51. M 51 from the B-band to the mid-IR.

the idea, implied by earlier IR studies based on lower-quality imaging, that the Hubble tuning fork breaks down in the near-IR.

2.6.1.2 The Near-Infrared S0 Survey

The Near-Infrared S0 Survey (NIRS0S, Laurikainen *et al.* 2011) provides a near-IR atlas (in the $K_{\rm s}$ or 2.15 μm bands) of 174 mostly S0 and some S0/a and Sa galaxies. The analysis described by Laurikainen *et al.* (2011) and in earlier papers in the series includes sophisticated 2D multi-component decompositions and classifications in a modified dVA system (with special recognition of lenses). A summary of the main findings of the NIRS0S is provided by Laurikainen *et al.* (2012).

NIRS0S 2D decompositions have modified our views of bulges along the Hubble sequence. Laurikainen *et al.* (2007) found that most bulges are pseudobulges and that B/T ratios of S0–Sa galaxies are much less than was determined in past studies (Fig. 2.52, left). Across the Hubble sequence, the average value of the Sersic index n is generally less than 2, consistent with one of the pseudobulge criteria adopted by KK04.

Two-dimensional decompositions allow a more reliable deprojection of galaxy images, because the bulge is modelled and can be removed from the image. Then the remaining disk light can be deprojected and the bulge added back. With such images, the bar strength parameter $Q_{\rm g}$ can be derived and the distribution of bar strengths for early-type galaxies can be compared with that for late-type galaxies. This was done by Buta *et al.* (2010a) who used NIRS0S deprojected images for S0 to Sa galaxies and OSUBSGS images for spirals (Buta *et al.* 2004). The histograms in Fig. 2.52, right,

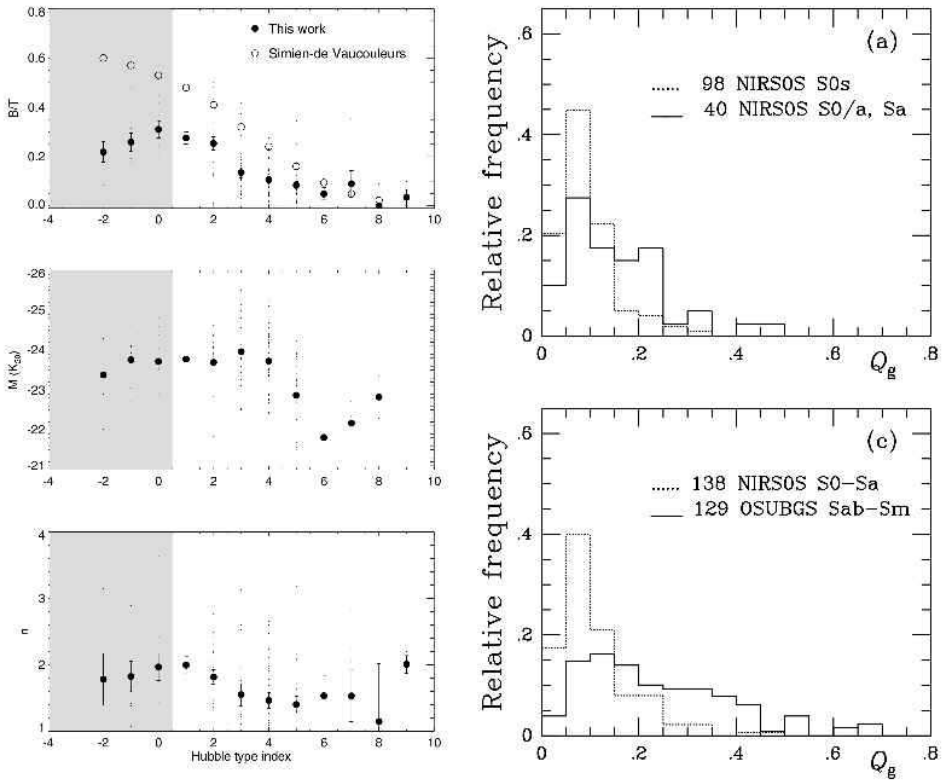

Fig. 2.52. NIRS0S results from Laurikainen *et al.* (2007, left frames) and Buta *et al.* (2010a, right frames).

show that S0 bars tend to be weak. This had been evident previously based on other bar strength indicators (e.g., Aguerri *et al.* 2009; Laurikainen *et al.* 2009). Part of the difference will be due to the presence of significant bulges in early-type galaxies, which add forcing to the axisymmetric background and thereby dilute the bar torques. However, all of the difference cannot be explained this way, and it is possible that there is a process that allows bar evolution to continue even after gas depletion in S0 galaxies. Laurikainen *et al.* (2006) showed that radial disk scalelengths of S0s correlate with bulge effective radii, which favours secular evolution of S0 bulges from disk material.

How could the bar of an S0 evolve? Block *et al.* (2002) argued that an S0 bar should be a fossil relic, capable of no further change. But if S0s are former spiral galaxies, why is it that S0 bars are weaker on average than those in spirals and why are ansae bars so prevalent among S0 galaxies? The answer could be secular evolution of the *stellar mass distribution*.

Another important finding from the NIRS0S is the recognition of a new type of lens: the 'barlens' or inner component of the bar (Laurikainen *et al.* 2011, 2012). In NGC 2787 (Fig. 2.53, top), the barlens is separated from the bar ends, leaving the familiar 'ansae' previously discussed (Lecture 2, Section 2.5). At first sight, the barlens looks like nothing more than a part of the bulge, but 2D decompositions do not support this interpretation. To show that a barlens is a distinct feature, the right panel of Fig. 2.53 shows a normal Kormendy-type lens in the face-on ringed galaxy NGC 1543. A normal lens envelops and is filled by the bar, while a barlens is *part of the bar* although it may not contribute much to the actual torquing action of the bar. Bar dissolution, if it occurs, would mainly mean the loss of the bar ends.

The nature of lenses also gains greater immediacy when we find them in multiple form in nonbarred early-type galaxies. Two important and very similar examples are shown in Fig. 2.53, bottom. In both NGC 524 and NGC 1411, three distinct lens features are detectable, and each galaxy is classified as (L)SA(l,nl)0°, where (L) refers to an *outer lens*, (l) to an *inner lens*, and (nl) to a *nuclear lens*. The (L) and (l) notations are due to Kormendy (1979), who also suggested that inner lenses (l) represent the dissolution of bars, so that in principle a lens in a nonbarred galaxy could imply that the galaxy was once barred. However, bar evolution cannot necessarily explain all types of lenses.

One way to possibly shed light on the origin of lenses is to measure their colours. Figure 2.54 shows a V-band image, a $B-V$ colour index map, and azimuthally averaged B, V, and $B-V$ surface brightness profiles for NGC 1411. On the graph, the radial locations of the 'edges' of the three lenses of the galaxy are indicated. The $B-V$ colour index profile shows two zones of slightly bluer colours, one between the (nl) and (l), and one between the (l) and (L). The apparent sharp edges appear to delineate zones with slight stellar population differences. The $B-V$ map also shows some reddening on the east side of the centre, which could signify a minor merger.

2.6.1.3 The Spitzer Survey of Stellar Structure in Galaxies

The *Spitzer* Survey of Stellar Structure in Galaxies (S^4G, Sheth *et al.* 2010) is a comprehensive survey of 2331 nearby galaxies in the 3.6 and 4.5 μm IRAC bands, the only filters that were usable for the *Spitzer* 'warm mission'. The images sample the Rayleigh-Jeans limit for all stars with $T > 2000$ K, and the [3.6]−[4.5] colour is roughly constant with radius, independent of stellar population (but see also the Peletier lectures, this volume). The goal of S^4G is to examine stellar structure in galaxies free of the effects of extinction and to a depth greater than groundbased near-IR imaging could achieve.

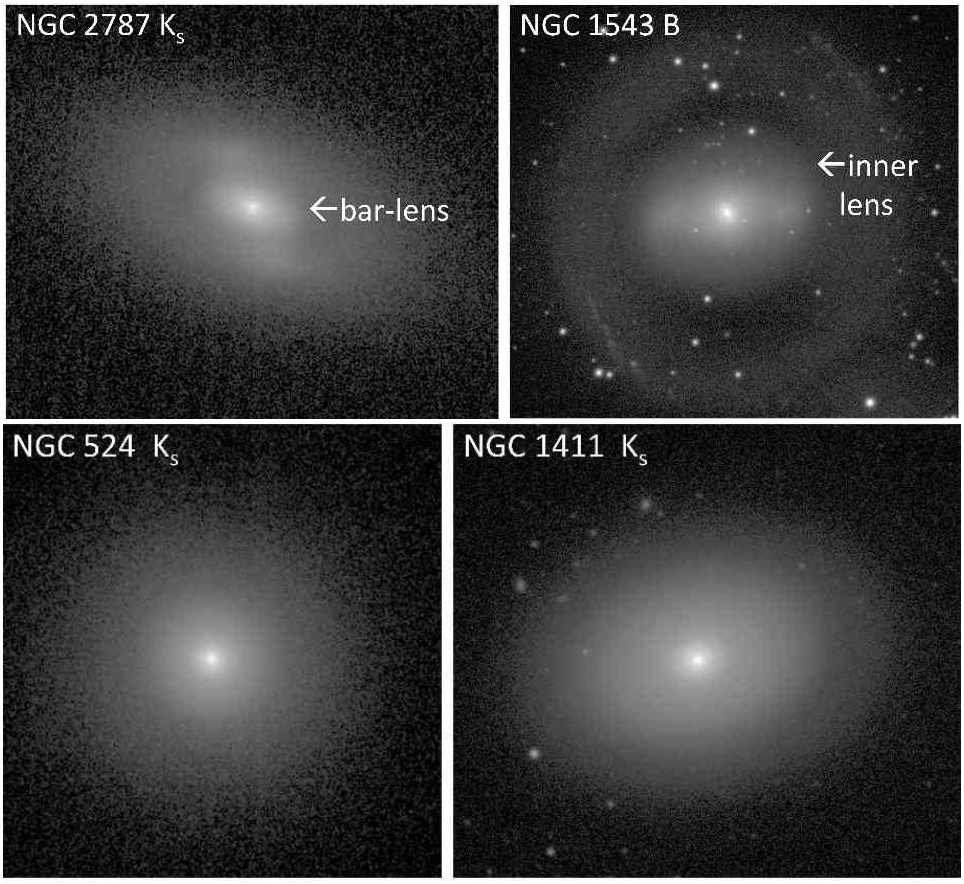

Fig. 2.53. NIRS0S results from Laurikainen *et al.* (2011). (Top): the 'barlens' as compared to a typical SB galaxy 'lens'. (Bottom): two examples of SA galaxies having multiple lenses.

The selection criteria for S^{4}G are as follows: galactic latitude $b \geq 30^{\rm o}$, isophotal diameter $D_{25} > 1.0$ arcmin, HI radial velocity $V > 3000$ km s^{-1}, and apparent photographic magnitude $m_B < 15.5$. The sample includes 1734 newly observed galaxies and 597 archival objects. Histograms presented in Sheth *et al.* (2010) show that the bulk of S^{4}G galaxies are of types Sb and later, a consequence of the use of an HI velocity as a selection criterion. The most statistically complete subset of S^{4}G galaxies is for masses $\log(M/M_\odot) < 9.2$.

In a preliminary analysis of 200 mostly archival S^{4}G galaxies, Buta *et al.* (2010b) showed that galaxies can be classified in 3.6 μm images in much the same manner as for the historically standard B-band images (essentially

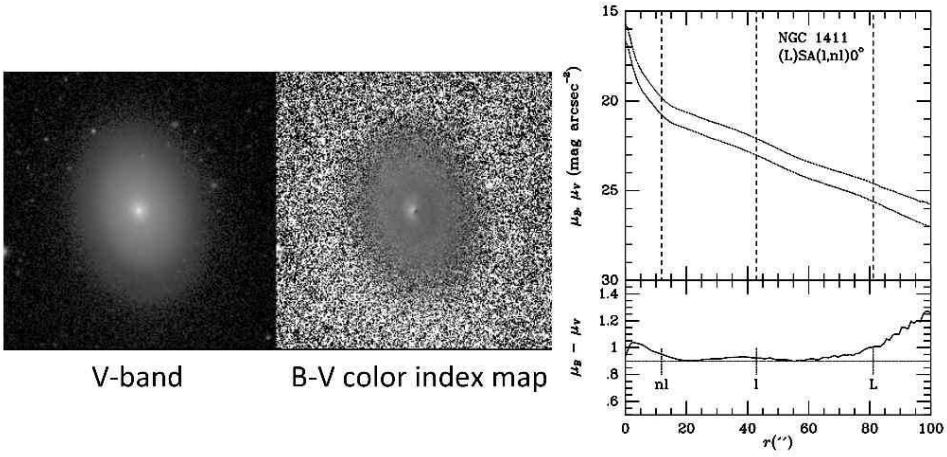

Fig. 2.54. This shows NGC 1411 and a colour index map that highlights the enhanced blue colours that lie between the apparent 'edges' of the lenses.

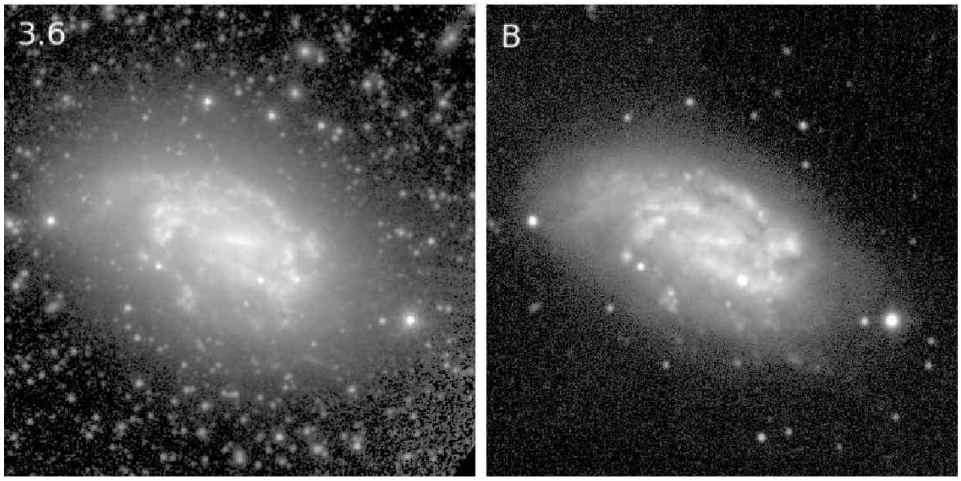

Fig. 2.55. The late-type spiral NGC 1559 has a very similar morphology in blue and 3.6 μm light.

the same as was found by Eskridge *et al.* 2002 for the H-band). In fact, for many galaxies, 3.6 μm morphology is very similar to blue light morphology, absent the effects of obscuring dust (Fig. 2.55). Because mid-IR galaxy morphology is so similar to optical morphology, we can apply the old classification systems to S^{4}G data as an exploratory step. The system being used is a further modified version of that outlined in the dVA. Figure 2.56 shows some classifications of S^{4}G galaxies in Buta *et al.* (2013).

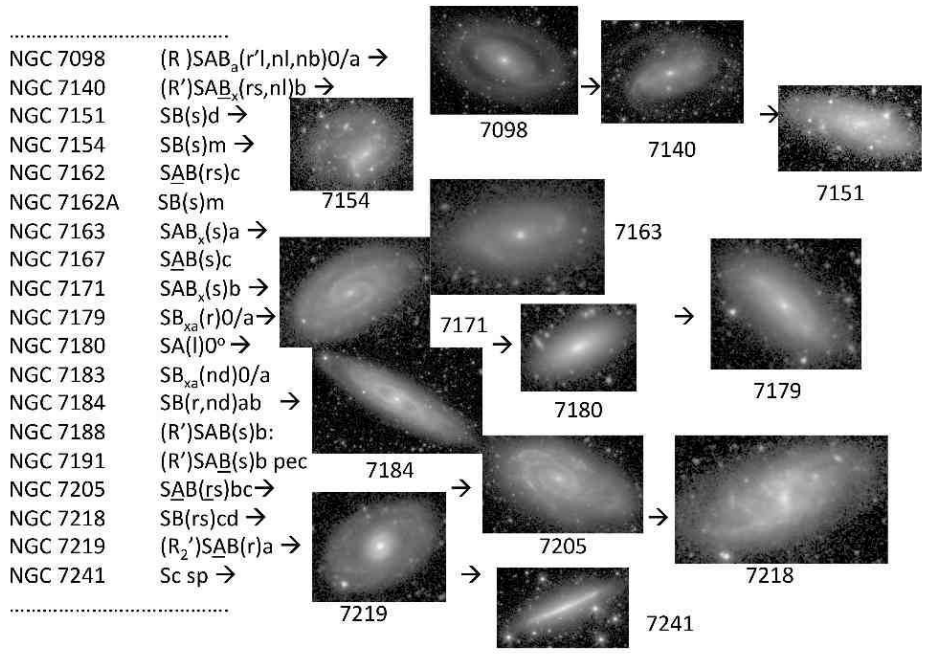

Fig. 2.56. A set of classifications of S^{4}G galaxies using a modified version of dVA types.

Buta *et al.* (2010b) also showed that galaxies of types S0/a to Sbc can appear about one stage interval 'earlier' at 3.6 μm compared to B. Types S0$^+$ and earlier and Sc and later can look almost the same. This is similar to what Eskridge *et al.* (2002) concluded for near-IR H-band images. The effect is shown for NGC 1433 in Fig. 2.57. Some B-band flocculent spirals look more globally armed at 3.6 μm; many do not change (Elmegreen *et al.* 2011). S^{4}G images also show many galaxies where a late-type spiral or irregular is embedded in an early-type disk. One example is NGC 5713, which has a clear SB(rs)m galaxy embedded in a background S0/a disk. Other examples shown by Buta *et al.* (2010b) are IC 750, IC 3392, and NGC 3769. Buta *et al.* (2010b) show two B-band Magellanic irregulars (Im) that appear more regular at 3.6 μm. If placed in a cluster environment, these could become progenitors of Kormendy spheroidal (Sph) or nucleated (Sph,N) galaxies. Also possible progenitors of spheroidals are Magellanic barred spirals like NGC 3906 and NGC 4618, shown also in Fig. 10 of Buta *et al.* (2010b).

The dust-penetrated nature of S^{4}G images also can reveal unusual optical misclassifications. NGC 5470 is classified as type Sb, but at 3.6 μm we

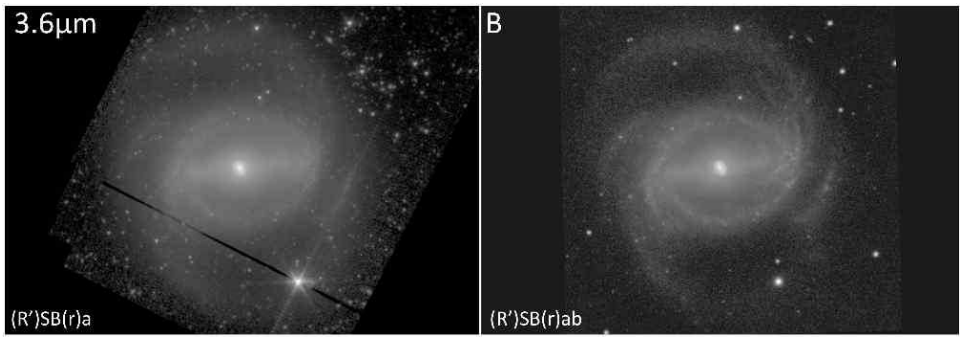

Fig. 2.57. NGC 1433 at 3.6 μm (left), showing the 'earlier' effect as compared to the B-band (right).

see an edge-on S0 with virtually no bulge and both thick and thin disks (Fig. 2.58). In the mid-IR the galaxy should be classified as type S0d, which alludes to the van den Bergh (1976) parallel sequence classification of S0s. Other interesting edge-on disks, some of which look like they are embedded in Kormendy spheroidals, are shown in Fig. 2.59.

Several special S^{4}G cases are shown in Fig. 2.60. NGC 3094 looks like a barred spiral with a dusty bar in optical images, but at 3.6 μm it shows an extremely bright starburst nucleus that was measured by Narayanan *et al.* (2005) to have $\log(L_{\rm IR}) = 10.73$. NGC 4250 looks like an early-type galaxy with an oval ring/lens, a very faint outer ring, and an exceptionally well-defined nearly circular nuclear lens. The type of the galaxy at 3.6 μm is (R)SAB(rl,nl)0$^+$. NGC 4572 is a very unusual case which at first sight appears to be a very open spiral, but which is more likely to be an extremely warped edge-on disk. IC 167 is an extreme case of an open spiral in the S^{4}G sample.

Figure 2.61, left, shows S^{4}G 3.6 μm images of two nearly edge-on galaxies showing a clear X-pattern in the central regions. Figure 2.61, right, shows unsharp-masked versions of the same images of NGC 2654 and NGC 2683, both optical Sb spirals. The X-pattern in NGC 2654 is more distinct than that in NGC 2683 and is detectable even in an optical SDSS image. These features point to the presence of a bar in each galaxy (see also Kuzio de Naray *et al.* 2009).

2.6.2 The S^{4}G bar fraction

The differing characteristics of bars along the de Vaucouleurs revised Hubble-Sandage sequence of types complicate the interpretation of the bar

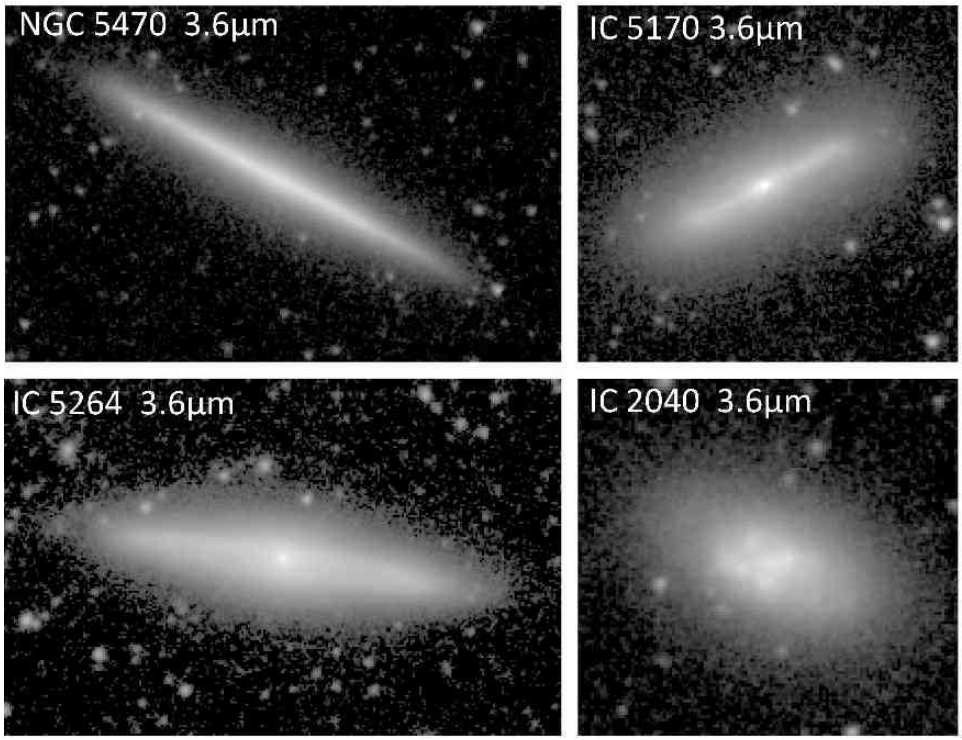

Fig. 2.58. Four S^{4}G galaxies showing dust-free views of edge-on disks and a Magellanic irregular.

fraction. Excluding highly inclined galaxies (spindles), here are some preliminary results from my classification of 2184 S^{4}G galaxies (and a few of their companions):

(a) Types S0$^-$ to Scd: bar fraction (SAB, SA<u>B</u>, and SB) = 57.2%,
(b) Types Sd and later: bar fraction (SAB, SA<u>B</u>, and SB) = 83.8%.

Thus, bars are very abundant in extreme late-type galaxies! This result is consistent with the recent SDSS study by Barazza *et al.* (2008), who found an optical bar fraction of ≈87% for what they called 'class 3' (bulgeless) galaxies.

2.6.3 Inferring stellar mass from S^{4}G images

The ultimate value of IR imaging is to infer stellar mass and the gravitational potential in galaxies. With such potentials you can, among other things:

(a) Estimate maximum relative bar torques $Q_{\rm b}$ (or $Q_{\rm g}$) and mass-flow rates;

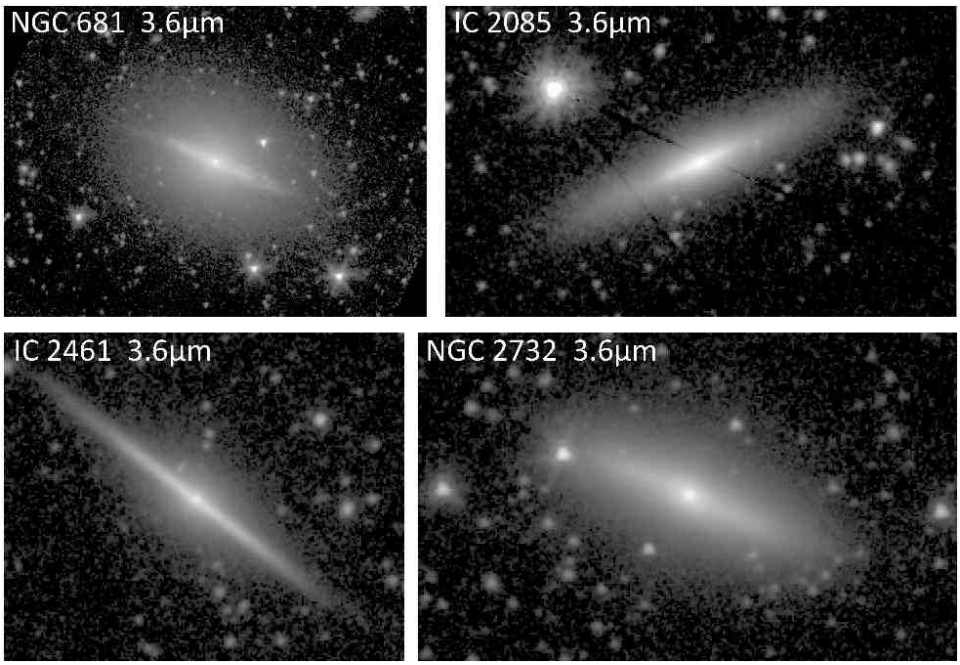

Fig. 2.59. Four S^{4}G galaxies showing 'embedded disks' in what appear to be spheroidal systems.

(b) Derive mass models and run simulations to estimate pattern speeds (e.g., Aguerri *et al.* 2001; Treuthardt *et al.* 2008; Kalapthorakis *et al.* 2010; Rautiainen *et al.* 2008; Lin *et al.* 2008);
(c) Measure potential-density phase shifts and infer locations of resonances (Zhang 1996, 1998, 1999, hereafter Z96, Z98, Z99).

Stellar surface mass density maps can be made from 2D images using surface colours as indicators of stellar mass-to-light ratio (Bell & de Jong 2001). Calibrated surface brightness maps can be converted to units of $L_\odot$ pc^{-2}, and then multiplied by colour-inferred M/L values in Solar units to give the surface mass density $\Sigma\ (i, j)$ in units of $M_\odot$ pc^{-2} at pixel coordinate (i, j).

Bell & de Jong (2001) give linear relationships between the logarithm of the M/L ratio in a given passband and a variety of colour indices in the Johnson-Cousins systems. Bell *et al.* (2003) give the same kinds of relations for SDSS filters, as well as an improved calibration for $B - V$ and $B - R$ colours that allows for the scatter in metallicities that affects near-IR mass-to-light ratios. For 3.6 μm images, colours such as $B - V$, $B - R$, $V - I$, or even $g - i$ can be used to give the stellar mass-to-light ratio in the K-band, depending on which of these colours is available. Then a simple relationship

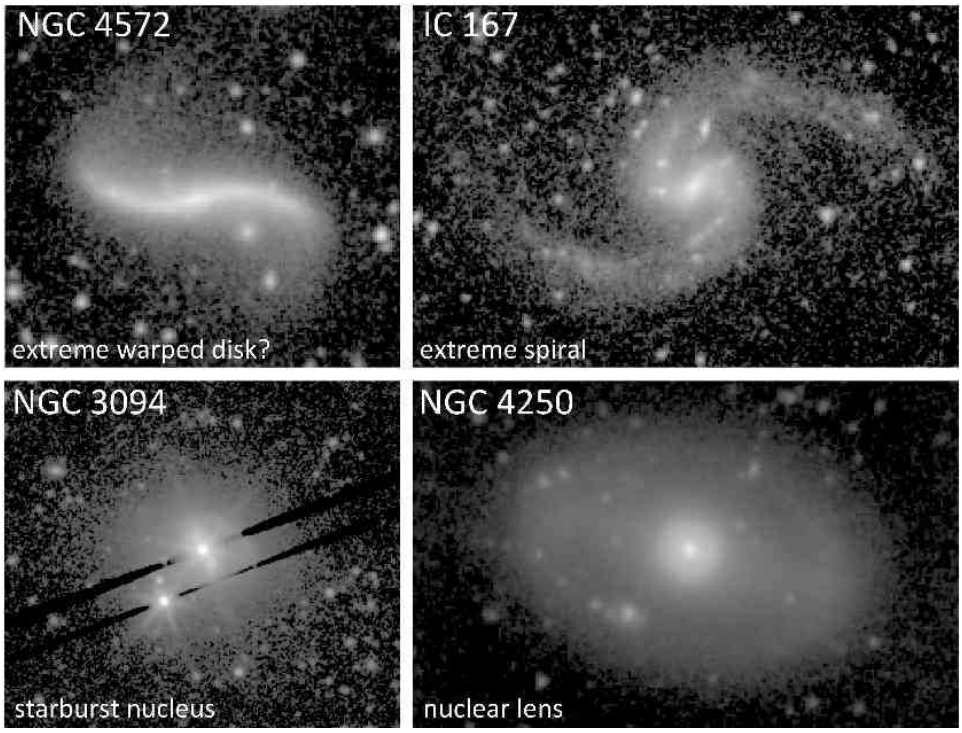

Fig. 2.60. Four extreme S^{4}G cases.

between M/L_K and $M/L_{3.6}$ (Oh *et al.* 2008) can be used to estimate the surface mass densities:

$$\frac{M}{L_{3.6}} = 0.92\frac{M}{L_K} - 0.05. \tag{2.7}$$

In practice, it is useful to use two colours and two base IR images to check for consistency of results. For example, X. Zhang and R.J. Buta (2013, in preparation) have used SINGS (Kennicutt *et al.* 2003) 3.6 μm images with $B-V$ or $B-R$ surface colours, and SDSS i-band images with $g-i$ surface colours, to estimate mass flow rates (see also Zibetti *et al.* 2009; Foyle *et al.* 2010).

As already noted, 3.6 μm images are affected by hot dust connected with star-forming regions and by a prominent 3.3 μm emission feature due to a polycyclic aromatic hydrocarbon compound that also is associated with star-forming regions. These star-forming regions appear as conspicuous 'knots' lining spiral arms in 3.6 μm images.

In practice, the star-forming region problems in the 3.6 μm band can be reduced using an 8.0 μm image if available. IRAC 8.0 μm images show mainly

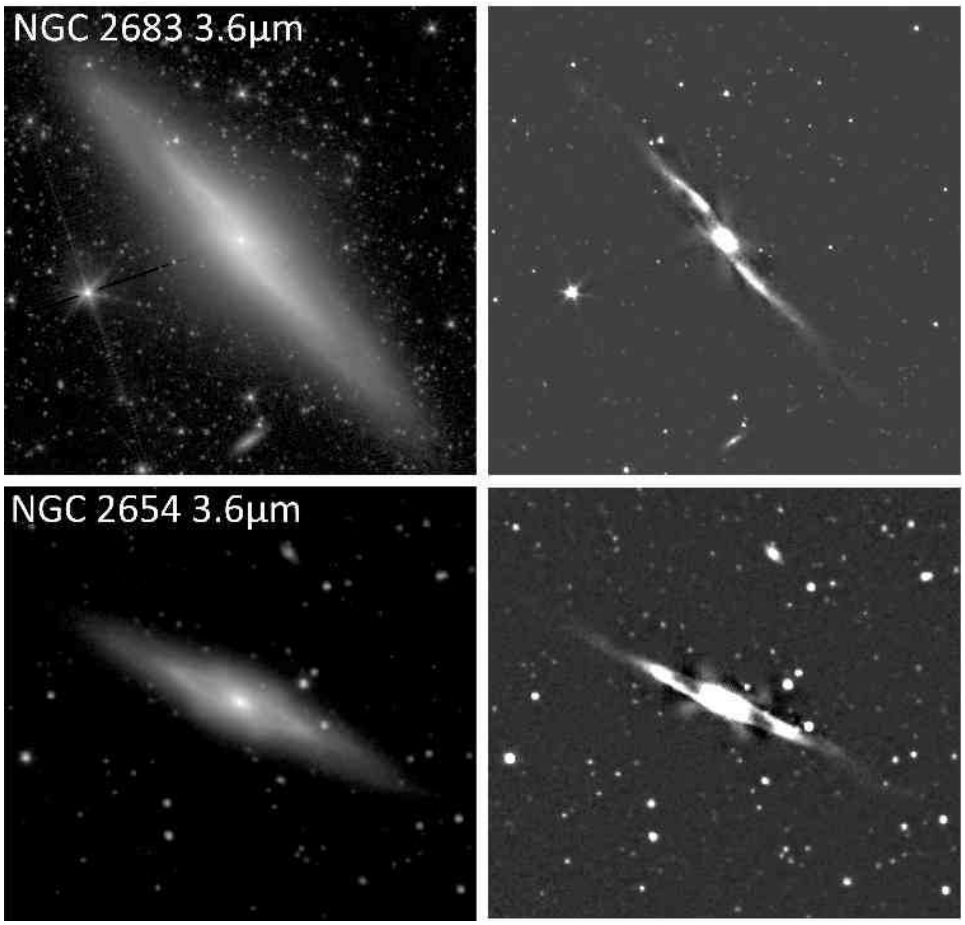

Fig. 2.61. S^{4}G X-galaxies NGC 2654 and NGC 2683.

the ISM with a small contribution from starlight. Kendall *et al.* (2008) describe how to correct the 3.6 μm image. The first step is to match the coordinate systems of the 3.6 and 8.0 μm images and then subtract a fraction (0.232) of the 3.6 μm flux from the 8.0 μm image to correct the latter for continuum emission (Helou *et al.* 2004). Then, a fraction (0.059–0.095; Flagey *et al.* 2006) of the net dust map is subtracted from the 3.6 μm map to give an image corrected for the hot dust emission. These 'contaminants' can also be eliminated using Independent Component Analysis and [3.6]−[4.5] colours (Meidt *et al.* 2012) if no 8.0 μm image is available. This is the case for most of the S^{4}G sample.

2.6.4 Secular evolution and the potential-density phase shift

The availability of large numbers of IR images that can be converted into stellar mass maps provides us with an opportunity to examine a promising new approach to understanding the actual *mechanism* of secular evolution in many galaxies. In any galaxy having a skewed bar, oval, or spiral perturbation, there will be a radius-dependent phase shift between the density perturbation and the potential perturbation (Zhang 1996). This phase shift distribution can drive secular stellar and gaseous mass redistribution because it leads to an interaction between the perturbation and the *basic state* of a galactic disk.† The approach interprets bars, ovals, and spirals as quasi-steady modes that arise spontaneously from an originally featureless disk. In the presence of such modes, the interaction resulting from the phase shift secularly evolves the basic state in the sense that a late-type spiral galaxy will evolve to an earlier-type galaxy. The actual interaction between the perturbation and the basic state involves collective effects that scatter and change stellar orbits without actual collisions (called 'collisionless shocks').

An important result from Zhang's studies is that the phase shift changes from positive (density spiral leads potential spiral) inside CR to negative (density spiral lags potential spiral) outside CR. Given a surface mass density map of a disk galaxy, one can convert the densities into a potential and measure the phase shift distribution directly. This provides a direct way of locating the CR resonance *without kinematic data*. Thus, in addition to providing information on secular mass flow in galactic disks, the potential-density phase shift can be used to interpret galaxy morphology, since CR is tied to a fundamental property of a spiral or bar/oval: its pattern speed $\Omega_{\rm p}$.

The method of locating CR using the potential-density phase shift (PDPS) method is outlined by Zhang & Buta (2007=ZB07) and Buta & Zhang (2011=BZ11). The result of this is that, if spirals and bars are quasi-steady modes, a single mode will be characterised by one positive phase shift hump followed by one negative hump. The negative part has to be there to take the angular momentum transferred outward by the positive part. Thus CR will be located at a positive-to-negative (P/N) crossing. The mode may end at a negative-to-positive (N/P) crossing, which then leads into the next mode if present. To measure phase shifts:

(a) First approx.: use IR image assuming constant M/L;
(b) Second approx.: use IR image and 2D colour-dependent variable M/L distribution;

† The basic state is defined by the radial distributions of mass density, velocity dispersion, and rotation speed of the bulge and disk components (Bertin *et al.* 1989).

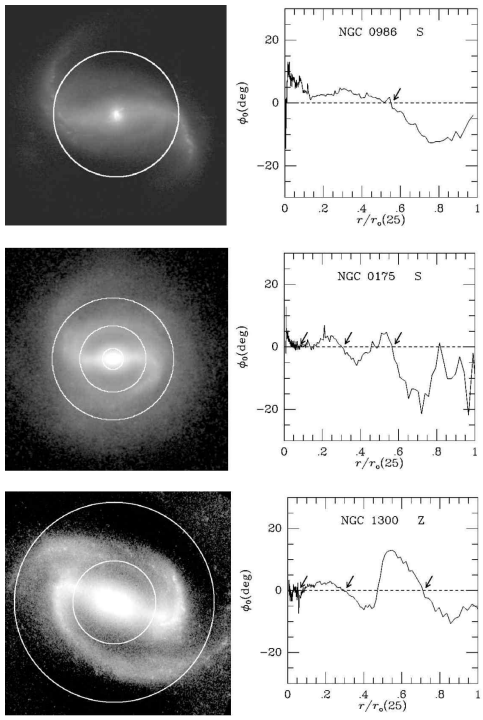

Fig. 2.62. K_s-band images and phase shift distributions of three galaxies: (top) NGC 986; (middle) NGC 175; (bottom) NGC 1300. The arrows on the phase shift plots show the main P/N crossings, and hence the implied CR radii. The circles superposed on the images show these radii.

(c) Third approx.: add in atomic and molecular gas.

BZ11 describe first approximation phase shift analyses of several well-known galaxies (Fig. 2.62). NGC 986, a barred galaxy with a strong spiral curving off the bar ends, shows a distribution with only a single major P/N crossing that places CR exactly around the bar ends. In this case, the bar and the spiral would have the same pattern speed, and BZ11 interpret NGC 986 as a genuine example of a 'bar-driven spiral'. In contrast, NGC 175 is a barred spiral with two clear P/N crossings. The first CR circles the ends of the bar and the mode includes the inner part of a bright spiral pseudoring, which is interpreted as being bar-driven. The second CR refers to an independent outer spiral pattern. In both of these cases, the ratio $\mathcal{R} = R_{\rm CR}({\rm bar})/R_{\rm bar} \approx 1$. Buta & Zhang (2009=BZ09) highlighted two cases, NGC 1493 and NGC 3686, which may be genuine examples having a 'slow bar', where $\mathcal{R} > 1.4$ (Debattista & Sellwood 2000).

The most enigmatic (and by default the most controversial) result from

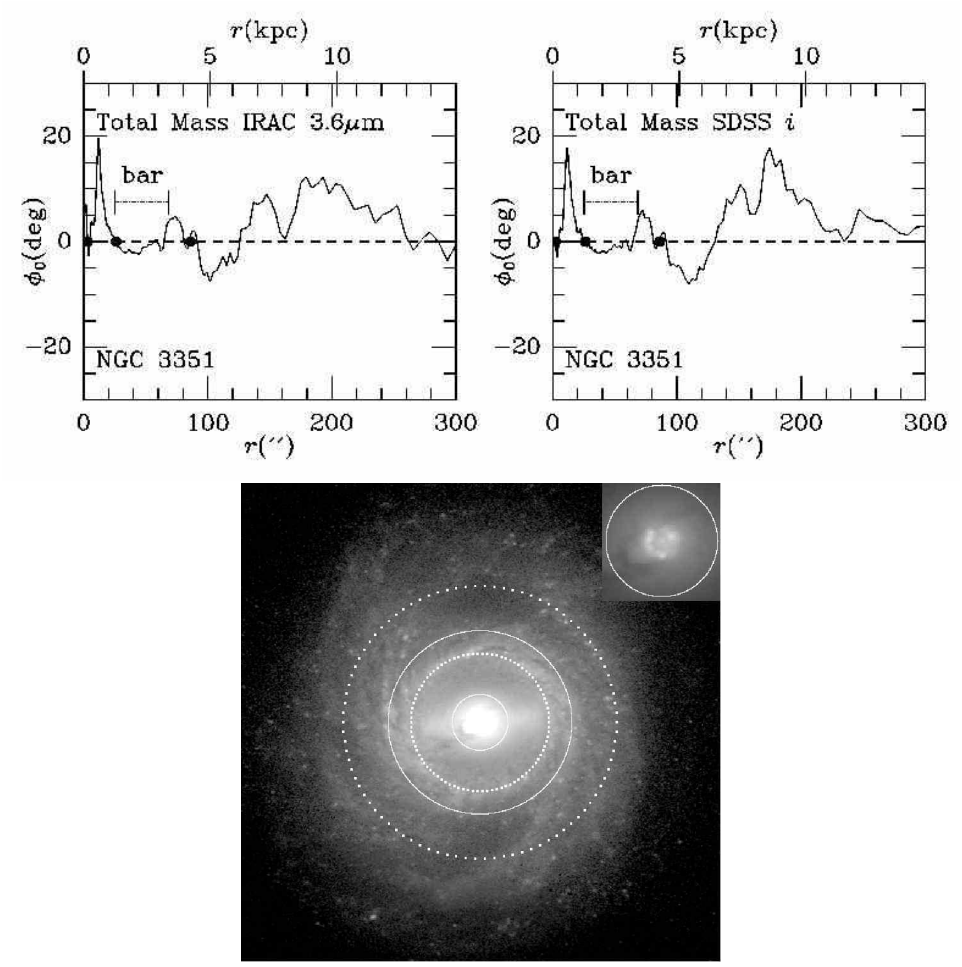

Fig. 2.63. (Top): Phase shift analysis of NGC 3351 based on IRAC 3.6μm and SDSS i-band total (star plus gas) mass maps. The bar extent is indicated. (Bottom): P/N (solid circles) and N/P (dotted circles) phase shift crossings superposed on a deprojected SDSS g-band image of NGC 3351, based on an average of the values derived from the IRAC and SDSS images. Since the bar extends to an N/P crossing, it is of the 'superfast' type (from ZB12).

the phase shift method of locating CR is the unusual 'superfast bars', where the bars extend *beyond the bar CR*. This appears to violate an almost cherished rule that bars cannot extend beyond their CR, because orbits outside CR cannot support the bar (Contopoulos 1980). This was a conclusion based on what ZB07 called 'passive orbit analysis', an analytic approach where the Jacobi integral is conserved along a stellar orbit and secular change in the

average radius of the orbit cannot occur. BZ11 describe the case of NGC 1300 as an example. In NGC 1300, there is a clear skewness to the apparently strong bar, meaning it is a very open spiral. In such a case, it is possible that the bar extends to its OLR and not to its CR. BZ09 show two other examples of superfast bars (NGC 4902 and NGC 5643). BZ11 also show the phase shift distribution for the strong grand-design spiral NGC 5247. In this case, CR lies at an intermediate position within the arms and the arms likely extend to their OLR.

Zhang & Buta (2012=ZB12) have carried out a more sophisticated (third approximation) analysis of the well-known ringed, barred spiral NGC 3351. An IRAC 3.6μm SINGS (Kennicutt *et al.* 2003) image and an SDSS i-band image were converted into surface mass density maps using colour-dependent M/L ratios as described above. The appearance of NGC 3351 can garner much preconception. The bar is surrounded by a bright inner spiral pseudoring that could easily be interpreted in terms of the inner 4:1 resonance of the bar, as suggested by Schwarz (1984a,b). This would imply that the bar CR is outside the inner pseudoring. The phase shift distributions, however, suggest a very different interpretation. Figure 2.63 shows the phase shift distributions for NGC 3351 based on total mass maps that include both HI and H_2 gas. The figure shows that the 3.6μm and SDSS i-band maps give very similar results: the phase shift is negative throughout the main part of the bar. This means that of the two CR radii indicated, CR_1 is the bar CR, and thus NGC 3351 is another example of a 'superfast' bar. In this circumstance, the spiral pseudoring around the bar is a *separate mode*, not a bar-driven spiral.

Why is the phase shift relevant to secular evolution? The phase shift brings attention to the role of collective effects on galactic dynamics, and may be the principal driver of secular evolution in disk galaxies. The idea is that if the basic state is changed by the presence of a spontaneous, self-sustaining density wave, then it means orbits of stars will migrate, slowly building up a 'pseudobulge' and spreading out the stellar disk.

2.6.5 Summary

(a) Near- and mid-IR images are goldmines for studies of galaxy morphology.
(b) The essential features of optical galaxy morphology are preserved in the IR, but are unambiguously detected because of the minimal effects of extinction.
(c) Morphological analysis of S^4G images confirms a high fraction of bars in extreme late-type galaxies, more than 80%.
(d) IR images offer a way to locate CRs and to probe secular evolution of the stellar mass distribution using the PDPS method.

2.7 Lecture 4: Environmental effects, exotic morphologies, and morphological databases

In my final lecture in this series, I want to cover a *potpourri* of topics to finish out the richness of galaxy morphology and to highlight some thoughts of what future studies of galaxy morphology and secular evolution might be like. Examining environmental effects may seem a little off the topic of secular evolution, but such effects do not have to be rapid or violent. Environmental effects can also produce exotic and very rare morphologies that are worthy of discussion. A few such morphologies (double detached outer rings, intrinsic bar-ring misalignment) have already been discussed in Lecture 2 (see Section 2.5).

2.7.1 Environmental effects in clusters

Gravitational interactions, ranging from minor, distant or fast encounters, to violent collisions and major/minor mergers, certainly play a role in galaxy morphology. Up to 4% of bright galaxies are currently involved in a major interaction (Knapen & James 2009).

The cluster environment offers a number of processes that can modify or even transform galaxy morphology. The cluster environment also brings attention to the idea of *environmental secular evolution* (see Kormendy's lectures, this volume), that adds a new dimension to morphological studies. The main processes or effects are:

(a) Gas stripping
(b) Star-forming disk truncation
(c) HI deficiency and truncated HI disks
(d) Harassment
(e) Starvation
(f) Transformation (morphology-density relation).

Gas stripping has long been thought to be one of the dominant mechanisms of transforming a spiral galaxy into an S0 galaxy. Spitzer & Baade (1951) suggested that repeated collisions with other galaxies can strip a galaxy clean of its ISM. An alternative idea is that, as a galaxy moves in a cluster, it interacts with the intracluster medium in the form of X-ray emitting gas and can be stripped clean of its own interstellar gas, causing star formation to cease and spiral arms to disappear (Gunn & Gott 1972). Van den Bergh (1998) has argued that perhaps even some of the stellar mass is lost during the transformation, which might explain why S0s tend to have a lower luminosity than spirals.

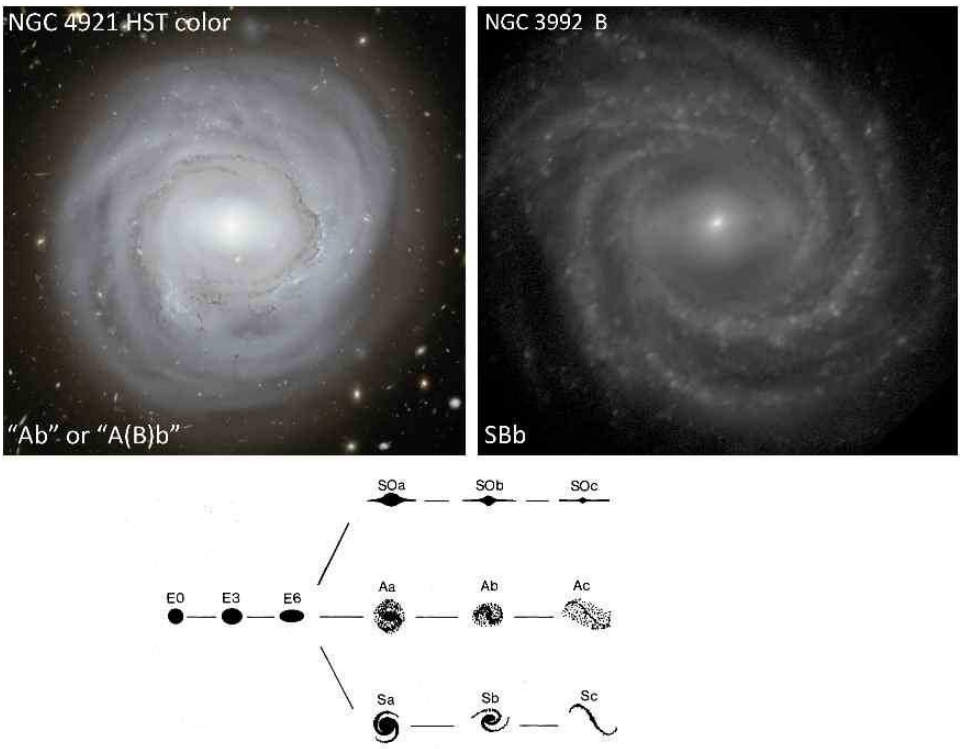

Fig. 2.64. Comparison between the 'anemic' barred spiral NGC 4921 and the more normal barred spiral NGC 3992. The van den Bergh (1976) parallel sequence classification is also shown.

If this process occurs and takes time, then partially stripped spiral galaxies ought to be observed. These are the galaxies referred to as 'anemic' by van den Bergh (1976), and morphologically, these seem to be a legitimate class of objects. Figure 2.64 shows an example of an anemic spiral identified by van den Bergh (1976). Anemic spirals are cluster spirals deficient in HI gas and as a result have a lower amount of dust and star formation. NGC 4921 is a Coma cluster spiral that strongly resembles a normal SBb spiral like NGC 3992, but has much smoother spiral arms. The smoothness indicates gas deficiency probably caused by stripping due to the intracluster medium. According to the hydrogen index parameter given in the RC3 (de Vaucouleurs *et al.* 1991), NGC 4921 is HI deficient compared to NGC 3992 by a factor of more than six. Bothun & Sullivan (1980) argue that the galactic anemia 'look' can be caused by other factors besides HI deficiency.

Environmental effects on the star-forming disks of Virgo cluster galaxies were examined by Koopmann & Kenney (2004) using Hα images. They

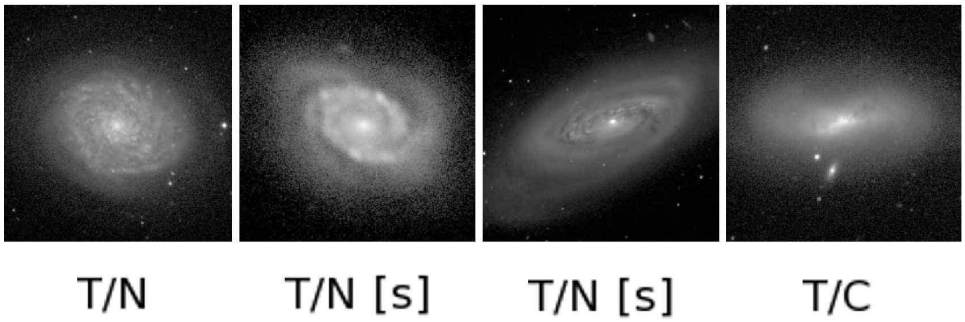

Fig. 2.65. Koopmann & Kenney (2004) environmental categories of Virgo cluster galaxies having truncated star-forming disks, illustrated using blue light images (from B13).

recognised seven environmental categories based on star formation rates and the Hα disk as compared to a field sample. Class N had normal star formation rates for the galaxy type. Class E had star formation enhanced by a factor of three or more over normal, while class A (anemic) had star formation a factor of three or more below normal. The remaining categories are the truncated star-forming disk morphologies, several examples of which are shown in Fig. 2.65. Class T/N is 'truncated/normal', meaning the star-forming disk is confined to the inner regions, but in those regions the star formation rates are normal. Class T/N[s] is similar but the truncation of the disk is severe. Class T/A is similar except that the star-forming part of the disk is anemic. Finally, class T/C is a truncated star-forming disk where the star formation is confined to a compact central area. Koopmann & Kenney (2004) illustrate the Hα images of all of these categories, while Fig. 2.65 (from B13) illustrates the truncated categories in blue light.

These optical categories translate into similar categories of HI distributions. The VLA (Very Large Array) imaging of Virgo spirals in Atomic gas (VIVA) survey (Chung *et al.* 2009) shows the interesting truncated morphologies that are found near the centre of the cluster (Fig. 2.66). Cases like NGC 4064, NGC 4405, and NGC 4457 are among the most extreme truncations. The survey also found evidence of ongoing stripping and fallback, the possibility that some galaxies have already fallen through the core and reached farther distances from the cluster centre as stripped spirals, as well as signs of gravitational interactions.

Yagi *et al.* (2010) identified a dozen galaxies in Coma that show ionised gas clouds mostly outside their disks. They suggest that these galaxies are likely to be 'new arrivals' to the core region of Coma in different phases of

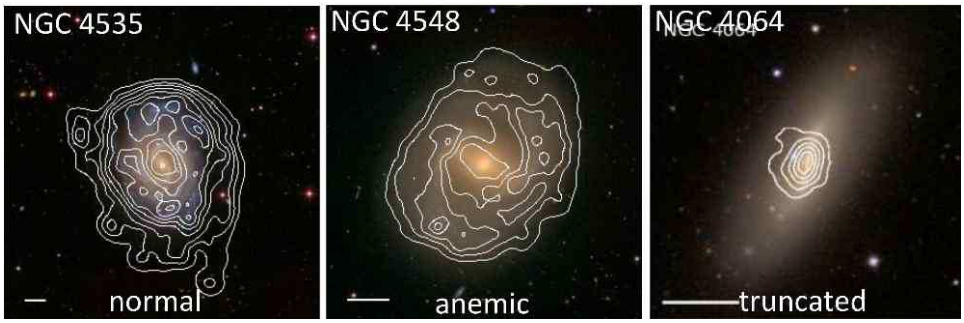

Fig. 2.66. VIVA images of HI disks of Virgo cluster galaxies (from Chung *et al.* 2009, reproduced with permission).

stripping. These authors identified three morphological gas stripping categories:

(a) connected Hα clouds with disk star formation, thought to be in an early phase of stripping,
(b) connected Hα clouds without disk star formation,
(c) detached Hα clouds, thought to be a later phase of stripping.

A summary illustration of these categories can be found in B13.

2.7.2 Gravitational encounter phenomena

Among gravitational encounter morphologies, ring phenomena have captured a great deal of attention. Here I discuss what I will refer to as 'catastrophic rings', or rings that have formed because of a collision between two galaxies. The main classes of catastrophic rings: accretion, polar, and collisional, must first be distinguished from the background of normal rings, usually referred to as 'resonance rings' which were discussed in Lecture 2 (see Section 2.5). Figure 2.67 shows an example of each ring type.

'Resonance rings' constitute the *vast majority* of all rings observed. They are interpreted as features which form by gas accumulation at resonances, owing to continuous action of gravity torques from a bar (Buta & Combes 1996). The main resonances theoretically linked to rings are (Schwarz 1981, 1984a, b):

(a) nuclear rings: ILR,
(b) inner rings: I4R, and
(c) outer rings: OLR.

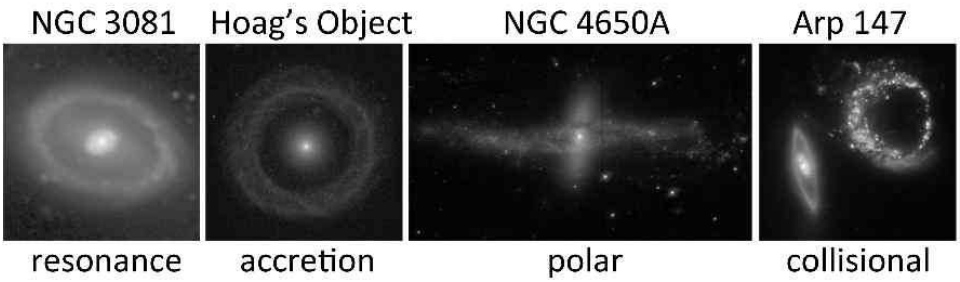

Fig. 2.67. Examples of different galactic ring categories.

These theoretical links found strong support in statistics of intrinsic ring shapes and orientations, as well as in morphology (Lecture 2, see Section 2.5). However, there have been alternative interpretations suggested over the years. Regan & Teuben (2004) noted that the concept of a 'resonance radius' (i.e., a single radius where a resonance occurs) is not really valid for strong bars because the epicyclic approximation breaks down. In the inner regions of a strongly barred galaxy, one instead has a broad 'ILR region'. Because rings in models seem to be connected more to orbit transitions (i.e., orbit family changes, which are usually accompanied by orientation changes), Regan & Teuben (2004) preferred the term 'orbit transition rings' for inner and nuclear rings at least, but still leaving outer rings and pseudorings in the 'resonance' category.

A second alternative interpretation of rings is that they are connected to 'invariant manifolds', or collections of orbits which emanate from the L_1 and L_2 Lagrangian points of a bar potential (Athanassoula *et al.* 2009a, b). This interpretation can successfully predict broad aspects of the morphologies of inner and outer rings in barred galaxies. Please see the lectures by Athanassoula (this volume) for more details.

The PDPS provides additional interpretations of normal rings. As described in Lecture 3 (Section 2.6), the nearby barred galaxy NGC 3351 has a bright inner ring whose morphology fits well into the resonance idea, yet the PDPS method suggests that the ring is a spiral mode with a different pattern speed from the bar. ZB12 interpret the ring as a spiral located at its own inner 4:1 resonance (not the bar's 4:1 resonance, because the bar in NGC 3351 is 'superfast').

Accretion rings are thought to be made of material from an accreted satellite (Schweizer *et al.* 1987). Evidence for this is sometimes *counter-rotation*, where the material in the ring rotates in the opposite sense from the material

in the main galaxy (Schweizer *et al.* 1989; de Zeeuw *et al.* 2002). The host galaxy can be an elliptical or disk galaxy. Examples of the former are Hoag's object (Schweizer *et al.* 1987) and IC 2006 (Schweizer *et al.* 1989), while an example of the latter is NGC 7742 (de Zeeuw *et al.* 2002). In the case of a disk galaxy like NGC 7742, the ring material mostly lies in the same plane as the receiving disk. It is also possible, as shown by the interesting case of NGC 1211 (Lecture 2, see Section 2.5), that a 'dead' resonance ring galaxy could accrete a satellite in its outer regions and have a blue second outer ring.

Polar rings are also accretion features, except that the accreting object is usually a disk system, like an S0 (Schweizer *et al.* 1983). The most stable configuration is an accretion angle close to 90°. This limits the ability of differential precession to cause the ring to settle into the main disk (Schweizer *et al.* 1983). S0s are preferred probably because the disk is generally clean of interstellar gas and dust, allowing the high-inclination orbital material to pass unimpeded through the plane.

The most easily recognisable polar ring galaxies are those where the two disks are seen nearly edge-on (Whitmore *et al.* 1990). Cases where only one disk is edge-on are less obvious unless the main disk is a spiral rather than an S0. Cases like NGC 660 (Whitmore *et al.* 1990) and ESO 235−58 (Buta & Crocker 1993b) both have been classified as barred spirals, but both show an aligned dust lane along their apparent 'bar' that demonstrates convincingly that their bars are actually edge-on disks. Thus, these galaxies show what the accreted high-inclination ring material looks like in a more face-on view. Cases where neither disk is edge-on are also possible but even harder to recognise. Some possibilities include NGC 1808, NGC 4772, and NGC 6870.

Collisional ring galaxies (also simply called 'ring galaxies') are cases where a small galaxy has crashed down the rotation axis of a larger disk galaxy, triggering a radially expanding density wave (Lynds & Toomre 1976). Multiple rings are possible. Different morphologies represent different encounter parameters and different time frames. To be classified as collisional, there must be a viable intruder (Madore *et al.* 2009). Struck (2010) provides a useful overview of ring galaxy theoretical studies as compared with the limited observational material available.

The three catastrophic ring types are all much rarer than resonance rings. For example, according to Madore *et al.* (2009), only one in a thousand galaxies is a ring galaxy.

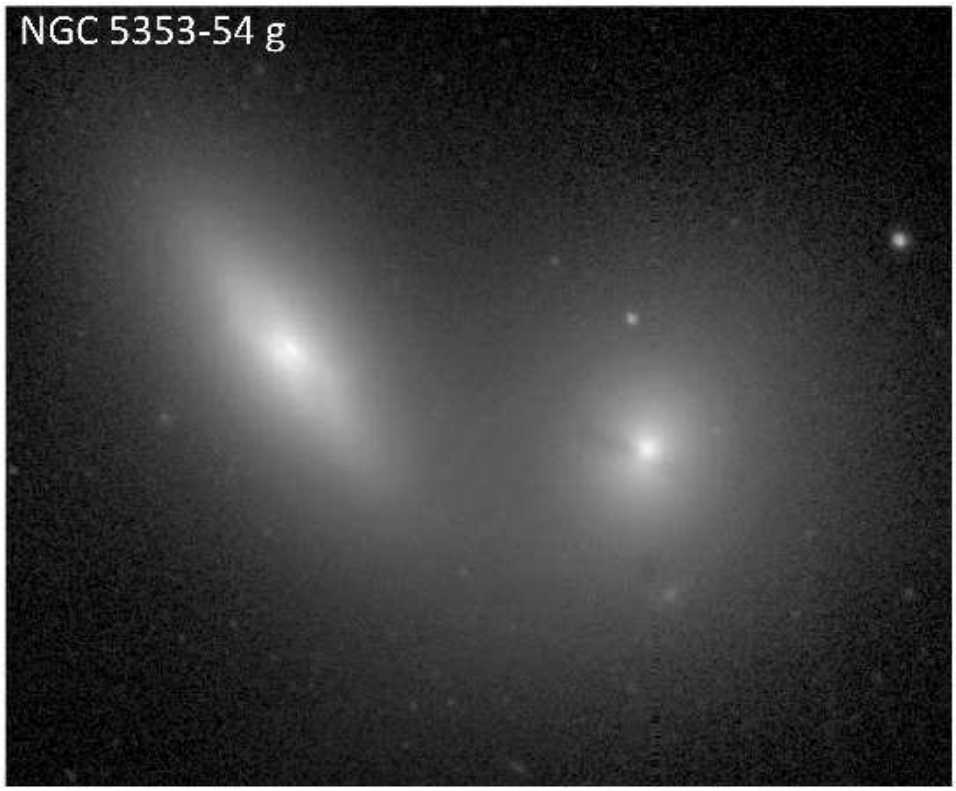

Fig. 2.68. NGC 5353 (right) is an example of a minor axis dustlane ETG. Its companion, NGC 5354, also has an inner dustlane.

2.7.3 Interaction and merger morphologies

There are several categories of interaction and merger-driven morphologies. A *dustlane* elliptical is an E or E-like galaxy showing lanes of obscuring dust (Fig. 2.68). Minor axis, major axis, and misaligned lanes are found. Whether these should be classified as 'ellipticals' or not was controversial, as de Vaucouleurs had once quipped: 'If an elliptical shows dust, then it's not an elliptical'. Bertola (1987) established dustlane Es as a class of interacting galaxies where a small gas-rich companion undergoes a minor merger with a more massive E galaxy (Oosterloo *et al.* 2002). The current general view of these objects is to call them 'dustlane early-type galaxies' (or dustlane ETGs; Kaviraj *et al.* 2011).

A shell galaxy is a normal elliptical or S0 galaxy showing faint ripples or ellipsoidal, sharp-edged features in its outer regions. Well-known examples are NGC 1344 and NGC 3923 (Fig. 2.69). Shells are likely to be 3D in

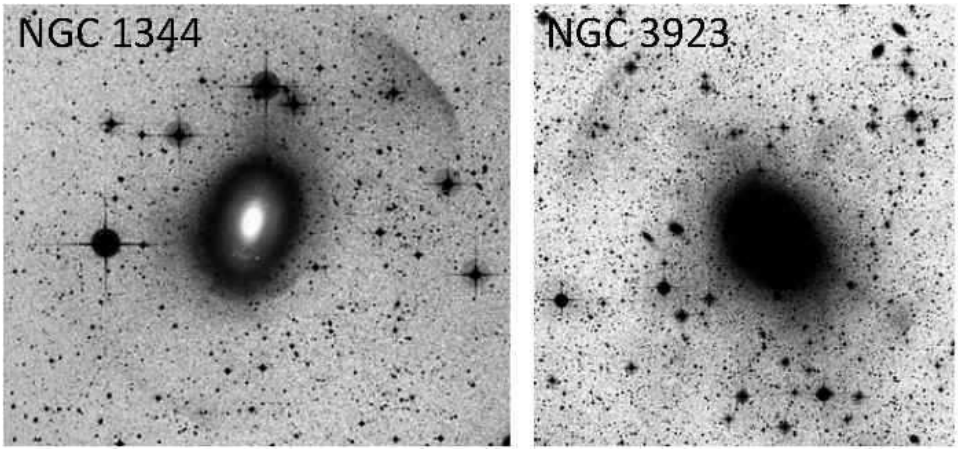

Fig. 2.69. Two 'shell' elliptical galaxies (copyright David Malin, reproduced with permission).

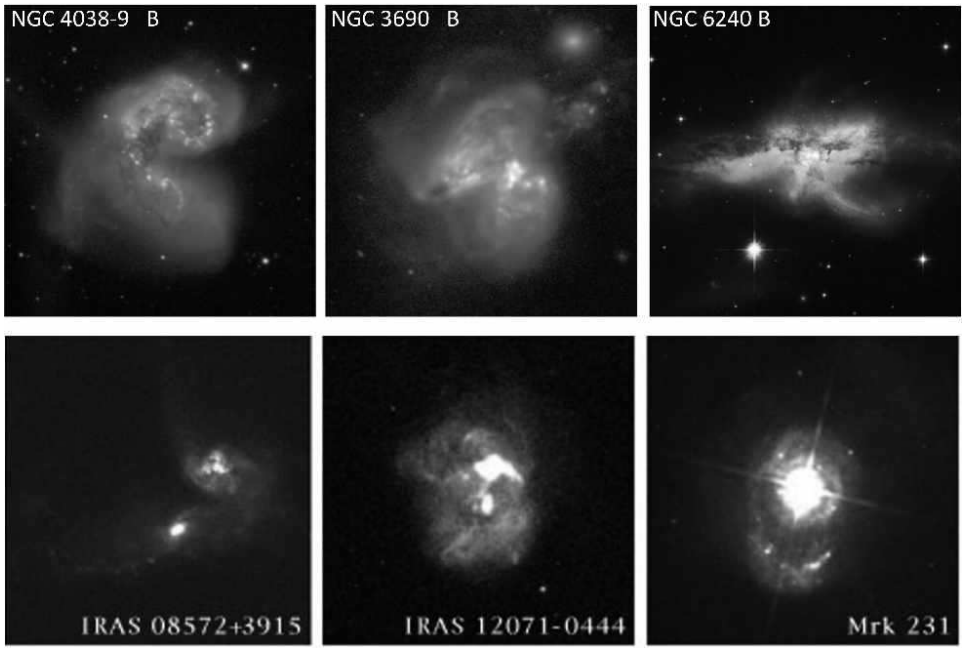

Fig. 2.70. Three cases of advanced and ongoing mergers (top row, from B13) and three ULIRGs (bottom row, from Surace *et al.* 1988, reproduced with permission).

geometry, not parts of a disk. Schweizer & Seitzer (1988) considered the term 'shell' as imposing an unjustified interpretation on the shapes of the features, and suggested the term 'ripples' instead. The extent of shells is

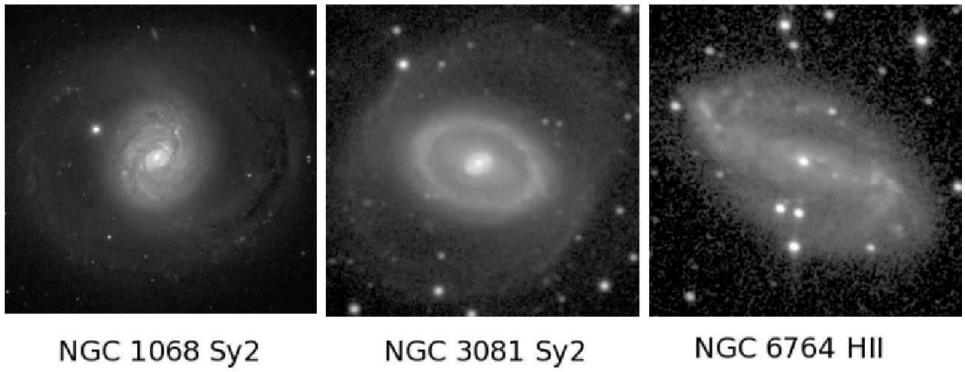

Fig. 2.71. Three active galaxies (B13).

huge, >100 kpc in some cases. Typically, the features are interleaved in radius, although some may have an 'all around' pattern (Prieur 1988). The best theory suggests that shells/ripples are remnants of a minor merger between a massive E galaxy and a small, cold, disk-shaped galaxy (e.g., Quinn 1984). The shells/ripples are thought to represent the maximum excursions of the disrupted orbits of the small companion's stars.

Tidal tails and bridges are common features of closely interacting but not necessarily merging disk galaxies. Tidal tails are a consequence of the tidal field due to the interaction and the shearing off of stars from the rotating disks. In M 51-type interacting pairs, a small companion is seen near the end of a bright spiral arm, as in M 51.

Figure 2.70 shows three examples of ongoing and advanced mergers. In these cases, the identities of the two separate galaxies are becoming less distinct, although the two separate nuclei may still be seen. The most extreme of such interactions may lead to ultra-luminous infrared galaxies (ULIRGs) (Fig. 2.70, lower frames). These objects have $L_{\rm IR} > 10^{12}\, L_\odot \approx L_{\rm bol}$ of QSOs. As shown by Surace *et al.* (1988), high-resolution *HST* images of ULIRGs reveal clear evidence of likely strong interactions. These authors suggest that warm ULIRGs are transition cases to optical QSOs.

2.7.4 The morphology of active galaxies

The global morphology of active galaxies has always been of interest as people seek to understand the triggering mechanism of active galactic nuclei (AGN). Figure 2.71 shows three examples of active galaxies that highlight some of the features that have been implicated: rings, bars, and interactions.

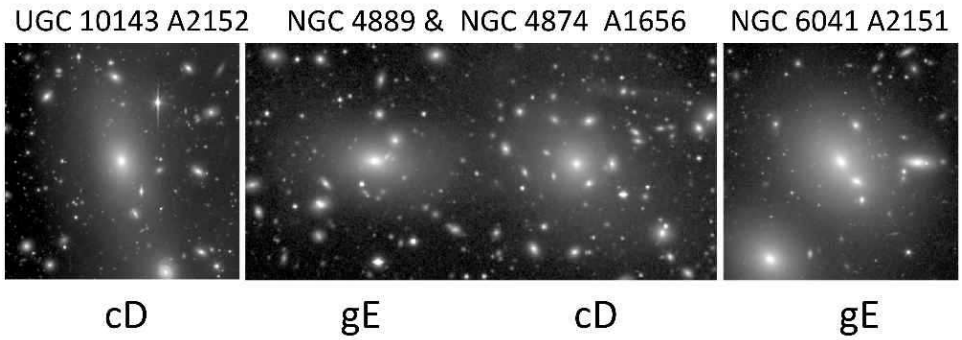

Fig. 2.72. Four brightest cluster members as seen in optical images (B13). Classifications are from Schombert (1986).

Hunt & Malkan (1999) found that the frequencies of outer rings and inner/outer ring combinations are three to four times higher in Seyferts than in normal spirals. Knapen *et al.* (2000) also showed that bars are more frequent in active galaxies than in non-active galaxies.

With *HST* resolution, the details of the host galaxies of quasars have been imaged. Bahcall *et al.* (1997) obtained *HST* images of quasars that show a variety of host morphologies, including Es, interacting pairs, systems with obvious tidal disturbances; and normal-looking spirals. These authors concluded that interactions may trigger the quasar phenomenon.

2.7.5 The morphology of brightest cluster members

These are the extremely luminous galaxies often found in the centres of rich galaxy clusters. Two of these were shown in Lecture 1 (see Section 2.3, Fig. 2.10). Figure 2.72 shows several more examples. Schombert (1986, 1987, 1988) classified the brightest cluster members according to luminosity profile shape:

(a) gE, giant ellipticals,

(b) D, larger and more diffuse, with shallower profiles, than gEs, and

(c) cD, same as D but with a larger extended envelope. These are the Morgan supergiant types.

The properties of the brightest cluster members fit well with merger simulations, including accretion and cannibalism (Schombert 1988).

Fig. 2.73. The warped disk galaxy ESO 510-13 (Hubble Heritage).

2.7.6 Warped disks

Edge-on views of many disk galaxies reveal a clear warping of the outer disk light. An excellent example is found in ESO 510-13 (Fig. 2.73). B13 shows three additional examples: NGC 4762, NGC 4452, and UGC 3697. These are all extreme cases detectable in optical light. Many more cases are found when the HI layer is considered. The most promising interpretation of warps is that they are connected to the properties of dark matter haloes. For example, the stellar disk may be slightly misaligned with the equatorial symmetry axis of the dark halo. In this circumstance, the inner, more tightly bound part of the disk remains perfectly flat, while the outer parts of the disk are bent towards the equatorial plane of the halo, leading to warping of the disk at large radii (Binney & Tremaine 2008).

Do warps secularly evolve? Debattista & Sellwood (1999) argued that a warp would have a 'winding problem' if the effects of a misaligned halo are not taken into account. Dynamical friction with a misaligned halo can drive a long-lived warp. Still, warps so driven are expected to be transient, because the friction force decays over time.

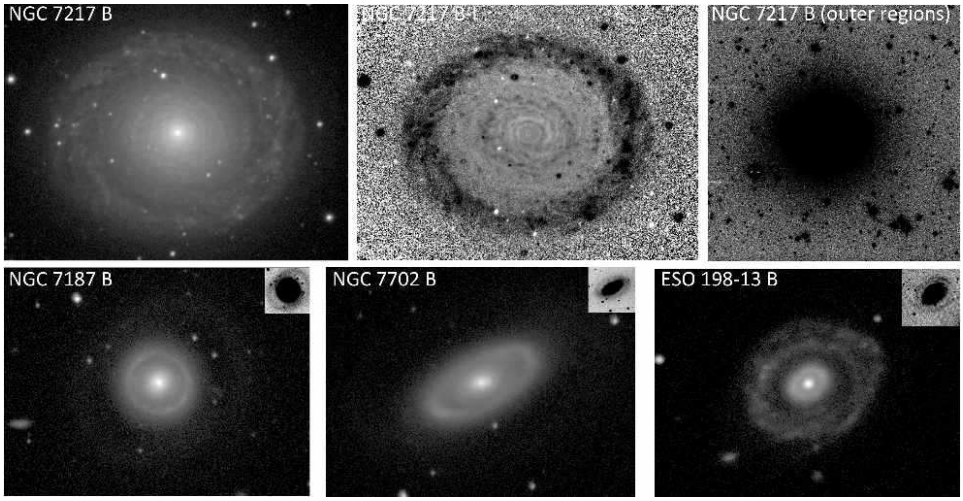

Fig. 2.74. Examples of non-barred ringed galaxies.

2.7.7 Non-barred ringed galaxies

This is an important but mostly neglected class of galaxies. While the majority of ringed galaxies are barred, a non-negligible fraction of non-barred ringed galaxies exists. Unlike barred galaxy rings, which are fairly homogeneous in metric and morphological properties, non-barred galaxy rings have a larger dispersion in properties that seems to point to a variety of mechanisms of ring formation.

NGC 7217 is a well-studied nearby example showing a spectacular blue outer ring in colour index maps (Buta *et al.* 1995b; Fig. 2.74, top row). At low light levels, the isophotes in NGC 7217 become almost exactly round, suggesting an extreme bulge-dominated system like the Sombrero Galaxy, NGC 4594. The strong bulge could therefore be the reason NGC 7217 is non-barred. Buta *et al.* (1995b) suggested that the strong outer ring formed in response to a subtle broad oval in the mass distribution.

Other examples appear to be cases of former barred galaxies that in the course of secular evolution lost their primary bars. A good possible example of this is NGC 7702, a double-ringed late S0 that looks very much like an early-type barred galaxy with inner and outer rings and a nuclear bar (Buta 1991; Fig. 2.74, bottom row). However, no clear primary bar crosses the bright inner ring, although this ring is undoubtedly oval in intrinsic shape and therefore bar-like. Bar dissolution is a real possibility that may be tied to the gradual build-up of a strong central mass concentration (e.g., Hasan & Norman 1990).

Other non-barred ringed galaxies could involve galaxies that accreted a small companion, as described in Lecture 3 (see Section 2.6). Hoag's Object, IC 2006, and NGC 7742 would all be described as non-barred, and it is clear that a mixture of such objects, ex-barred galaxies, and possibly tidally driven rings like in NGC 4622 could account for the larger dispersion in the properties of non-barred galaxy rings.

2.7.8 Counter-winding spirals

This is a very rare, possibly interaction- or minor merger-driven morphology where a disk-shaped galaxy has two non-overlapping spiral patterns that wind outward in opposite senses. While the bulk of spirals have been demonstrated to be trailing the direction of rotation (de Vaucouleurs 1958), and the Toomre (1981) swing amplification mechanism (as well as the Lynden-Bell & Kalnajs 1972 mechanism) seems to explain why (Binney & Tremaine 2008), counter-winding spirals appear to present genuine examples of *leading* spiral arms.

Determining the sense of winding of spiral arms has typically depended on two things: knowing which half of the galaxy is receding from us, and which side of the galaxy is nearer to us. From the schematic in Fig. 2.75, right, it can be seen that on the near side, the bulge is viewed through the dust layer, while on the far side, the dust layer is viewed through the bulge. This leads to a reddening and extinction asymmetry that can be seen in the colour index map of NGC 7331 in Fig. 2.48 of Lecture 3 (see Section 2.6). Once the near-side is established, the velocity field tells us which way the galaxy must be turning. With these two pieces of information together, the sense of winding of the spiral arms can be reliably judged. Of course, the less inclined a galaxy is, the less evident is the nearside extinction and reddening effect.

The first counter-winding spiral identified, and the one that is best studied, is the nearly face-on SA(r)a spiral NGC 4622 located in the Centaurus cluster (Byrd *et al.* 1989). The galaxy has two high-contrast outer arms and a single lower-contrast inner arm, with no overlap between the patterns (Fig. 2.75, top row). Instead, the single inner arm and the two outer arms blend at the position of a conspicuous, offset inner ring. Buta *et al.* (2003) obtained *HST* imaging and a ground-based Hα velocity field, and used the dust distribution to judge the near-side and the velocity field to judge the sense of rotation (Fig. 2.75, bottom frames). A *V*–*I HST* colour index map showed thin curved dust lanes all lying on one side of the line of nodes, which can be identified as the near side. With the velocity field telling us that the north side is receding relative to the nucleus, this implied a

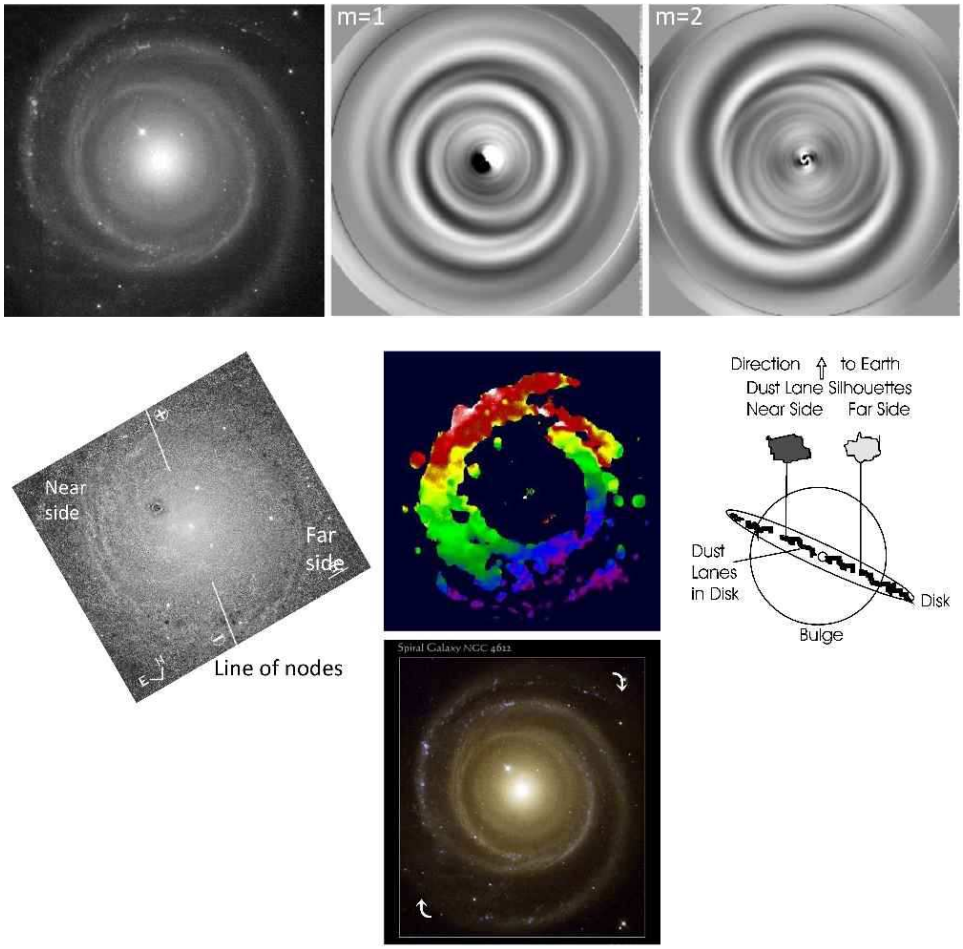

Fig. 2.75. (Top row): V-band image of NGC 4622 with $m = 1$ and 2 Fourier decompositions (Buta *et al.* 2003). (Bottom frames): V–I colour index map (left), Fabry-Perot velocity field (upper, middle), colour image (lower, middle), all from Buta *et al.* (2003). Also shown at right is a schematic illustrating how tilt leads to an extinction and reddening asymmetry across the galaxy minor axis. The arrows on the colour image indicate the implied sense of rotation.

clockwise rotation of the disk. This gave the surprising and unexpected result that the two strong outer arms, not the weaker inner arm, have the leading sense, a result that is difficult to accept. In the centre a small edge-on dust lane is found that suggests the galaxy has suffered a recent minor merger that could be responsible for the peculiar morphology.

A second example of a counter-winding spiral was identified by Buta (1995). This was the Sb-Sbc spiral ESO 297-27. Although not in a cluster

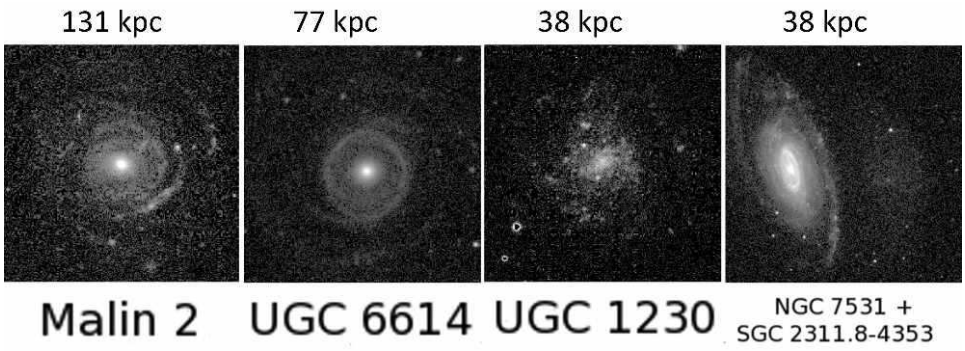

Fig. 2.76. Giant low surface brightness galaxies, from B13 and references therein. The number above each box is the length of the top side at the distance of the galaxy.

environment, ESO 297-27 has similarities to NGC 4622. In this case, the inner arm leads and the outer arms trail (Grouchy *et al.* 2008). Other galaxies with leading spiral structure:

(a) NGC 3124 (bar in ring; Purcell 1998). See Fig. 2.46 (Section 2.5),
(b) NGC 6902 (bar in ring), and
(c) IRAS 182933413 (two leading arms, not counter-winding; Vaisanen *et al.* 2008).

What causes counter-winding spiral structure? The phenomenon is very rare, so perhaps an unusual circumstance is at work. If the two outer arms of NGC 4622 are really leading, they would be difficult to explain in current theories of spiral structure. Swing amplification depends on the swing of a leading density wave. Also, the comprehensive study of Lynden-Bell & Kalnajs (1972) showed that only a trailing spiral pattern can transfer angular momentum outwards, which allows the wave itself to be maintained.

2.7.9 Giant low-brightness galaxies and stellar streams

Giant low surface brightness galaxies were first identified by Bothun *et al.* (1987). They are galaxies having a relatively normal bulge and an extremely low surface brightness, very large disk. The first example found was Malin 1 (Bothun *et al.* 1987). Figure 2.76 shows other examples: Malin 2, UGC 6614, UGC 1230, and in addition a strange possibly unrelated case called SGC 2311.8−4353, which was first studied in detail by Buta (1987). SGC 2311.8−4353 is a very low surface brightness companion to the giant spiral NGC 7531, and is notable for having an isophotal diameter 2/3 the size of NGC 7531. If at the same distance as NGC 7531, SGC 2311.8−4353

Fig. 2.77. The LMC, the prototype of classification SB(s)m. Reproduced with permission from de Vaucouleurs & Freeman (1972).

would be a dwarf in luminosity but not in size. That is, it would be a large low surface brightness galaxy, but not a giant. In a recent study of tidal streams in late-type spirals, Martínez-Delgado *et al.* (2010) have interpreted SGC 2311.8−4353 as a companion in the act of tidal disruption by NGC 7531. These authors show how commonly 'normal' late-type galaxies can show extremely low surface brightness tidal features that are analogous to the streams found around the Milky Way.

2.7.10 Magellanic barred spiral galaxies

These were identified as a distinct morphological class by de Vaucouleurs & Freeman (1972; Fig. 2.77; see also Lundmark 1927 and Lecture 1, Section 2.3). The class is characterised by a bar with no bulge, a single main spiral arm, shorter spiral features, and an offset of the centre of the bar from the centre of outer isophotes. De Vaucouleurs & Freeman noted that SBm galaxies often come in pairs (e.g., the large Magellanic cloud [LMC] and small Magellanic cloud [SMC], NGC 4618 and NGC 4625, NGC 2537 and

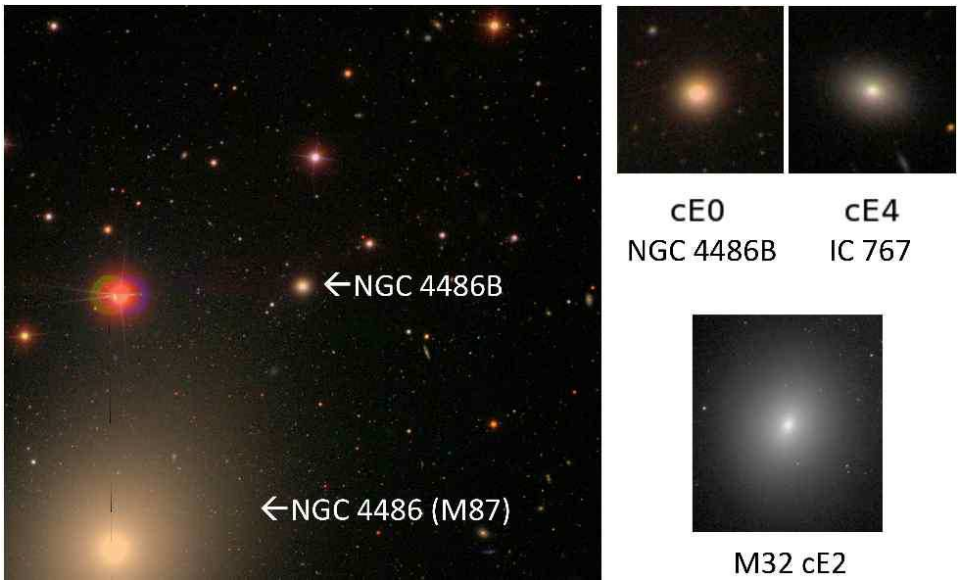

Fig. 2.78. Examples of compact elliptical galaxies.

NGC 2537A), suggesting that the morphology may be interaction-driven. Although the bar is usually offset in these galaxies, and in the LMC and SMC the bar is also kinematically offset from the rotation centre, prominent cases like NGC 4027 were found to have a rotation centre coincident with the centre of the bar (Pence *et al.* 1988). Too few cases have been observed to definitively prove that an offset rotation centre is characteristic of these galaxies.

2.7.11 Compact ellipticals

Compact galaxies (Fig. 2.78) have been known since Zwicky & Zwicky (1971) published a major catalogue. The departure of three compact elliptical (cE) galaxies, M 32, NGC 4486B, and NGC 5846A, from the norm in a graph of V-band surface brightness versus absolute V-band magnitude for E galaxies led Faber (1973) to suggest that these galaxies could be the stripped cores of formerly larger elliptical galaxies. However, it is now known that cE galaxies are simply the lower-luminosity tail of normal elliptical galaxies, based on photometric parameter correlations (Kormendy 1985; Kormendy *et al.* 2009). That is, cE galaxies are true 'dwarf ellipticals'. These are to be contrasted with a large number of Virgo cluster objects classified as type 'dE' by Bingelli *et al.* (1985) that have photometric properties more akin to dwarf irregulars than to normal ellipticals. As I have already noted in

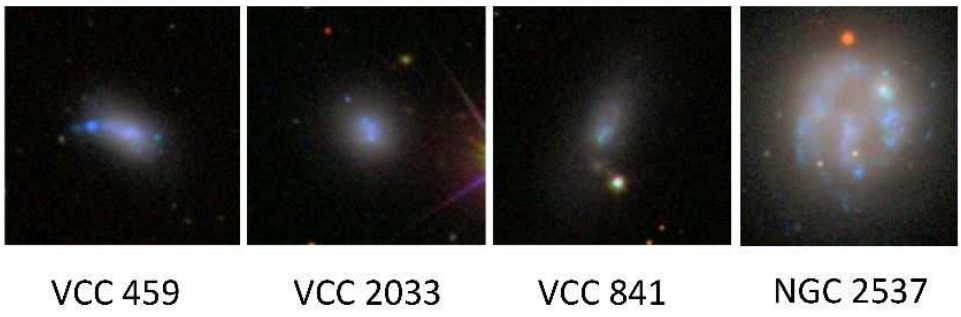

Fig. 2.79. Examples of blue compact dwarf galaxies.

Lecture 1 (see Section 2.4), Kormendy & Bender (2012) have interpreted the Bingelli *et al.* (1985) dE, dE,N, dS0, and dS0,N types as environmentally driven morphologies, former irregular and very late-type galaxies that were stripped, harassed, or otherwise windblown to lose their gas.

2.7.12 Blue compact dwarf galaxies

These are small, high surface brightness galaxies experiencing a strong starburst (Fig. 2.79). As defined by Gil de Paz *et al.* (2003), blue compact dwarf (BCD) galaxies have $(\mu_B - \mu_R)_{\rm peak} \leq 1$, $\mu_B < 22$ mag arcsec^{-2}, and $M_K > -21$. On average, BCDs have $B-R = 0.7 \pm 0.3$, $M_B = -16.1 \pm 1.4$, and $\log L_{\rm H\alpha} = 40.0 \pm 0.6$. BCDs have been identified in the Virgo cluster by Bingelli *et al.* (1985; three examples are shown in Fig. 2.79), but are also known in field environments. In the Local Group, IC 10 has been identified as a BCD (Richer *et al.* 2001). Figure 2.79 shows an SDSS colour image of BCD NGC 2537.

The BCD class has brought to light some of the most extreme cases of star-forming galaxies. For example, the BCD I Zw 18 was once thought to be a genuine young galaxy with a high level of star formation and an optical morphology greatly affected by stellar winds and supernovae from an earlier starburst. However, deep imaging with *HST* revealed a definite older stellar population in I Zw 18 (Contreras-Ramos *et al.* 2011).

2.7.13 Ultra-compact dwarf galaxies

These are very compact, star-like galaxies with luminosities comparable to dE galaxies (Drinkwater *et al.* 2000, 2003). Hilker (2011) reviews the properties of a significant population of ultra-compact dwarf galaxies (UCDs) in

the Fornax cluster. These objects have absolute magnitudes in the range $-13.4 < M_V < -11.4$, and are brighter than the brightest Milky Way globular cluster but fainter than compact ellipticals. One interpretation of these objects is that they are the threshed nuclei of dE,N galaxies (that is, environmentally driven morphologies where a dE,N galaxy has lost all of its stars, except for the 'N').

2.7.14 Isolated galaxies

For investigations of the connection between morphology and secular evolution, there can probably be no better sample than isolated galaxies. For such galaxies, internal processes would have to be largely driving evolution.

A significant effort into establishing a reliable isolated galaxy sample was made by Karachentseva (1973) and was further improved by the Analysis of the Interstellar Medium in Isolated Galaxies (AMIGA) project (Verdes-Montenegro *et al.* 2005). Out of about 1000 galaxies in a final sample, Sulentic *et al.* (2006) found that the majority are Sb-Sc spirals, a few of which were shown in Fig. 2.4. The most striking thing about many of these galaxies is how regular and well-defined their spiral patterns are. AMIGA galaxies are selected to not have had a close encounter with a major galaxy in more than 3 Gyr. Do these galaxies support the idea that spiral structure can arise spontaneously, independent of an interaction?

2.7.15 Ultraviolet galaxy morphology

The ultraviolet (UV) is an important window into star formation in galactic disks. The recent launch of the *Galaxy Evolution Explorer* (*GALEX*, Martin *et al.* 2005) has provided an extensive database of images at 0.15 μm (far-UV, or FUV) and 0.22 μm (near-UV, or NUV). Gil de Paz *et al.* (2007) outline what can be learned from such images:

(a) young stars are mostly what you see at UV wavelengths in any star-forming galaxy,
(b) massive early-type galaxies can show significant UV flux due to the 'UV-upturn', caused by hot low-mass horizontal branch stars,
(c) UV flux is an excellent tracer of the star formation rate, and
(d) UV flux absorbed by dust is re-emitted in the IR.

Figure 2.80 shows the *GALEX* FUV image of M 51 compared to a normal B-band image. The FUV image shows mainly hot stars younger than 10^8 years, while the B-band shows older stars in addition to dust and star-forming regions. Most interesting is how the companion galaxy, NGC 5195,

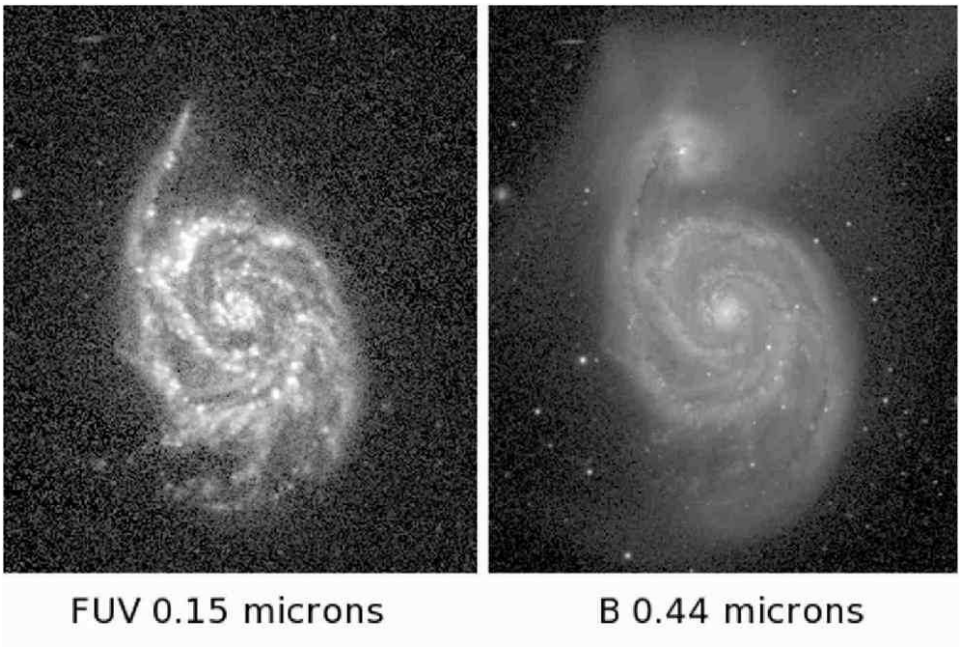

Fig. 2.80. *GALEX* UV image of M 51 as compared to a typical B-band image.

and the extensive tidal debris around it, are mostly invisible at FUV wavelengths. This galaxy does not have a UV upturn that would make it more prominent in the FUV image.

The NUV morphology of a spiral like M 83 strongly resembles an Hα image but with an older background disk.

B13 shows a montage of *GALEX* NUV images of galaxies of different types. In early-type galaxies, significant UV flux may occur if the galaxy has a star-forming nuclear ring, as in NGC 1317 and NGC 4314. In an intermediate type barred galaxy like NGC 3351, the inner ring, nuclear ring, and outer arms are conspicuous, while the bar is invisible. In the SBc galaxy NGC 7479, both the bar and the arms are seen, while the late-type galaxies NGC 628 and NGC 5474 have extensive UV disks. Most interesting was the discovery of an extensive UV disk around the diminutive Sm galaxy NGC 4625, which suggests that the galaxy is currently forming most of its stars (Gil de Paz *et al.* 2005). Finally, the intriguing star-forming galaxy NGC 5253 shows bright UV emission even from its extended diffuse disk.

2.7.16 The morphology of the interstellar medium

The ISM in galaxies has distinctive morphological qualities that are surely, in some cases, tied to secular evolution. The HI Survey of Nearby Galaxies (THINGS, Walter *et al.* 2008) provides some of the best information on the HI morphology of normal galaxies. In such galaxies we see:

(a) extended HI disks with spiral structure (NGC 628),
(b) central holes (NGC 2841) or central spots (M 81),
(c) large gaseous rings (NGC 2841) or pseudorings (NGC 2903),
(d) small rings (NGC 4736),
(e) supernova-blown holes (WLM), and
(f) sometimes huge HI/optical sizes (DDO 154).

Other galaxies, possibly because of their environment, have HI disks comparable in extent to their optical disks, such as NGC 1433 (Ryder *et al.* 1996) and NGC 5850 (Higdon *et al.* 1998). In these cases, the HI morphology follows the optical morphology closely. I have already described previously the HI morphology of galaxies in the central regions of the Virgo cluster, where stripping has not only truncated the HI disk significantly, but also has erased morphological structures so thoroughly that the diversity of HI morphologies is greatly reduced.

The morphology of molecular hydrogen, H_2, is also of interest. The Berkeley-Illinois-Maryland CO Survey of Nearby Galaxies (BIMA-SONG, Helfer *et al.* 2003) is one of the most extensive databases of molecular galaxy morphology available. Using CO 2.6 mm emission as a tracer of H_2, BIMA-SONG maps reveal the following:

(a) inner spiral arms (NGC 628),
(b) large rings (NGC 2841, NGC 7331),
(c) scattered giant molecular clouds (GMCs; NGC 2403),
(d) primary bars (NGC 7479),
(e) nuclear gas bars (NGC 3351),
(f) central spots (NGC 4535), and
(g) small pseudorings (NGC 1068).

CO morphology does not necessarily mimic HI morphology and the CO disk may not extend as far as the HI disk.

Figure 2.81 shows several examples of HI and CO maps of nearby galaxies, with a corresponding optical image for comparison.

Especially interesting morphology is revealed by 8 μm emission maps obtained with IRAC. This mid-IR wavelength is sensitive to the warm dust associated with spiral arms and shows no near-side/far-side asymmetry, as

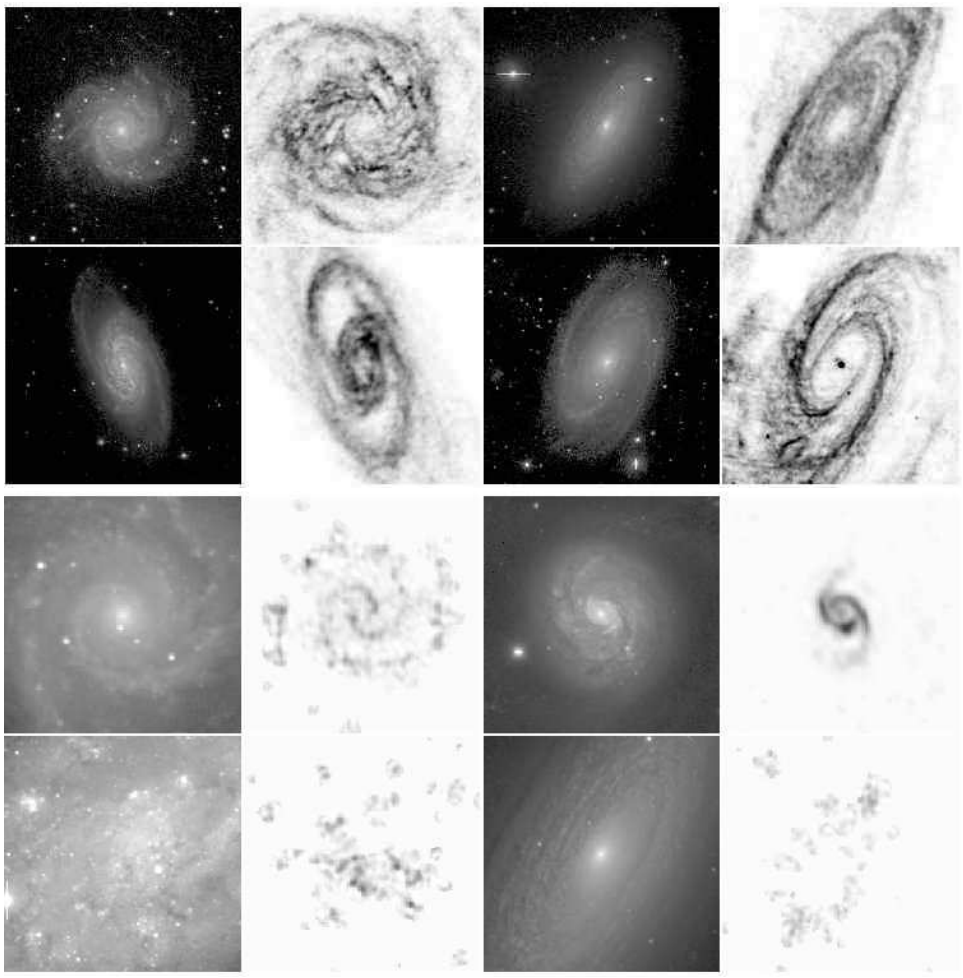

Fig. 2.81. (Top rows): HI maps of NGC 628, NGC 2841, NGC 2903, and NGC 3031 from THINGS (Walter *et al.* 2008); (bottom rows): CO maps of NGC 628, NGC 1068, NGC 2403, and NGC 2841 from the BIMA-SONG (Helfer *et al.* 2003).

the comparison in Fig. 2.82 shows. IRAC maps at 8 μm reveal the distribution of dust directly, instead of partly depending on how the dust layer projects against the bulge. In optical images, the spiral structure of M 81 appears to nearly terminate in a large pseudoring in the outer parts of the bright bulge. Spiral structure inside this pseudoring appears mainly in near-side extinction arcs. In contrast, at 8 μm there is complex spiral structure inside the apparent pseudoring that continuously winds outward.

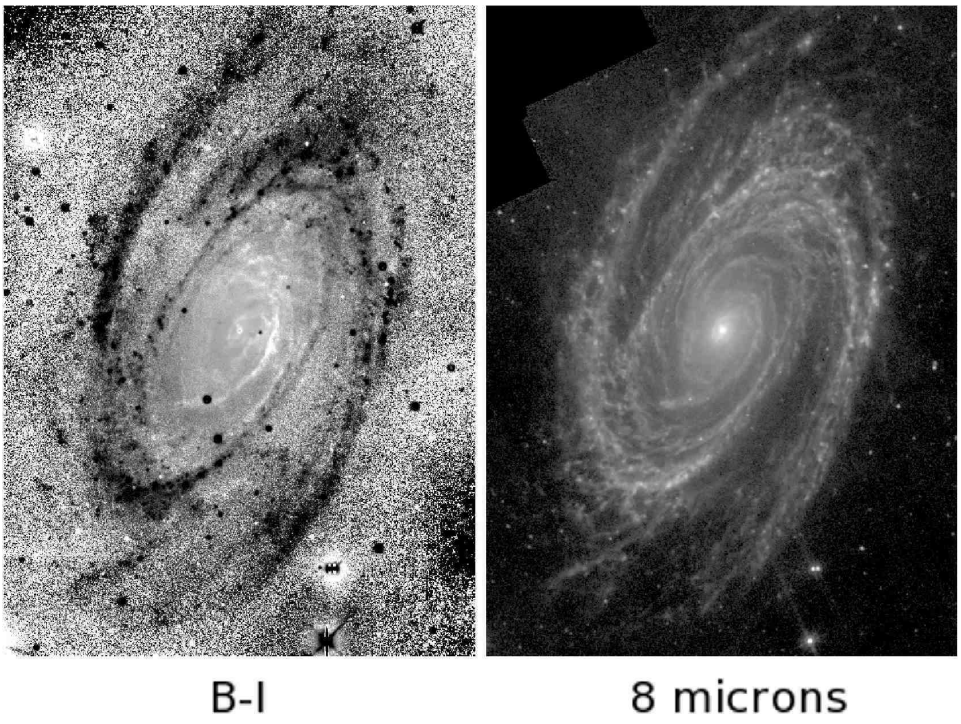

Fig. 2.82. A $B-I$ colour index map of M 81 as compared to an IRAC 8 μm image (from B13).

2.7.17 High-redshift galaxy morphology

There is no doubt that high-redshift galaxy morphology has come of age during the past 10–15 years. The resolution provided by *HST* with the Wide Field Camera and the Advanced Camera for Surveys (ACS) has provided morphological information on thousands of high-redshift galaxies. Using both spectroscopy and photometric techniques, significant redshift ranges can be isolated to examine galaxy evolution firsthand.

B13 reviews many papers on high-redshift galaxy morphology. One of the first results found from the early surveys is that high-redshift galaxies reveal morphological categories that would fit poorly within the various modern classification systems. Unusual irregular shapes dominate the high-z population. Normal spirals and ellipticals can be recognised to $z \approx 0.6$, but as $z \rightarrow 1$, the number of irregular-looking objects becomes more significant. Clump clusters, linear and bent chains, 'tadpoles', catastrophic rings, and mergers are identified in papers by Elmegreen *et al.* (2004, 2007), van den

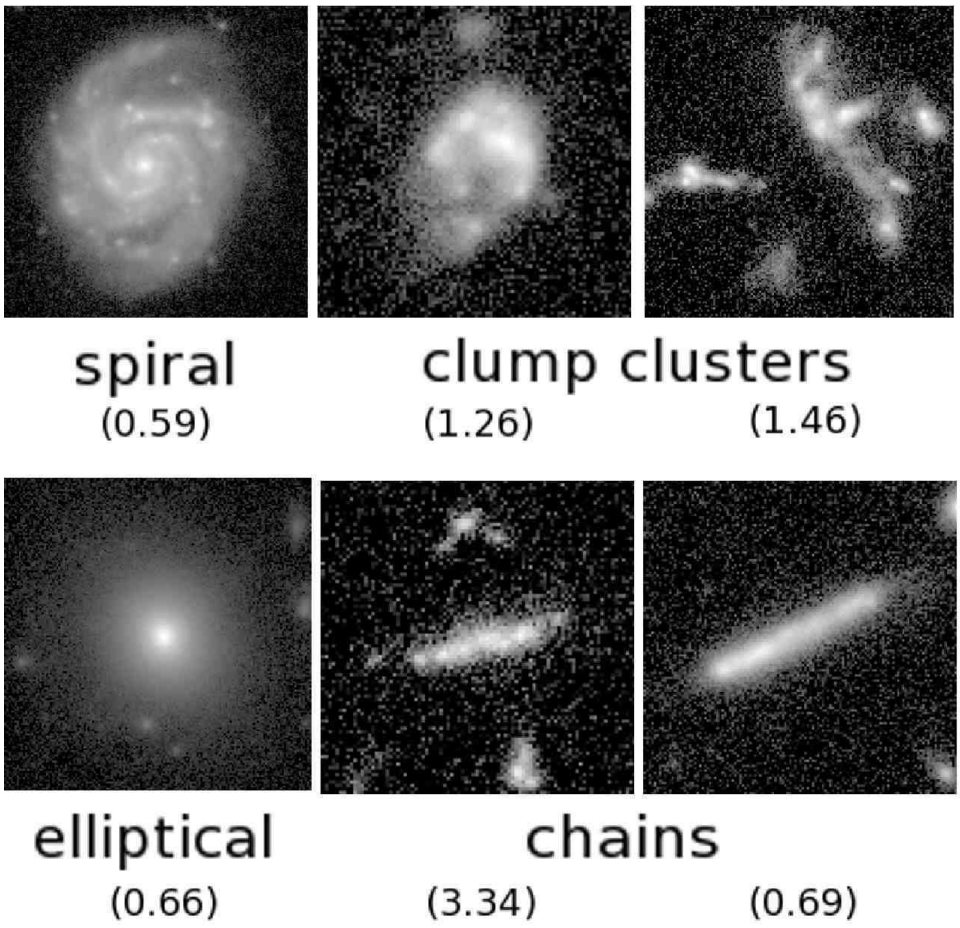

Fig. 2.83. Several high-redshift morphological categories, from B13 and references therein. The number in parentheses is the redshift.

Bergh *et al.* (1996,2000), and Cowie *et al.* (1995). Clump clusters and chains are shown in Fig. 2.83.

2.7.18 The Sloan Digital Sky Survey

The SDSS (Gunn *et al.* 1998; York *et al.* 2000) is without a doubt one of the most important assemblages of morphological information on galaxies since the Palomar Sky Survey. The survey includes morphological, photometric, and spectroscopic data for a million galaxies, and opened up the new era of huge extragalactic digital databases of medium-high resolution

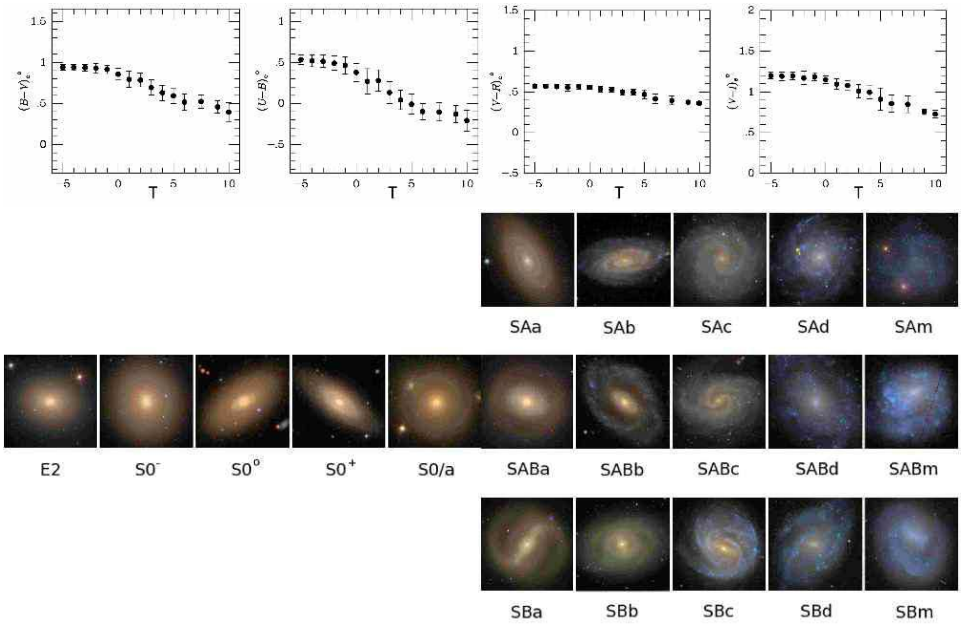

Fig. 2.84. (Top row): quantitative colour versus type relations, from Buta *et al.* (1994); from left to right, the colours are $(B-V)_{\rm eo}$, $(U-B)_{\rm eo}$, $(V-R)_{\rm eo}$, and $(V-I)_{\rm eo}$, where the subscripts mean the colours are within an effective (half-power) aperture and are corrected for extinction. (Bottom): a colour tuning fork based on SDSS colour images.

imagery. The SDSS also represents the advent of large-scale colour imagery for galaxies of all types.

Figure 2.84, top, shows several colour-type relations based on effective colour indices derived as outlined by Buta *et al.* (1994) and Buta & Williams (1995). All show the same general trend: colours of E-S0 galaxies are the same within the scatter, but there is a smooth decrease in colour indices from stage S0/a to Im. This morphology-colour relation is beautifully illustrated with SDSS colour images in Fig. 2.84, bottom. The transition from redder to bluer colours begins with spiral arms, leaving only bulges and bars remaining relatively red. However, as type advances, bulges decrease in relative importance and bars become bluer. By type Sm, the old stellar background is muted against the bright blue star-forming disk.

The most famous result from SDSS multi-colour imaging is the 'galactic Hertzsprung-Russell diagram', or colour-absolute magnitude diagram. This is shown in schematic form in Fig. 2.85. Galaxies that are made almost uniformly of old stars lie along the 'red sequence', the familiar colour-absolute

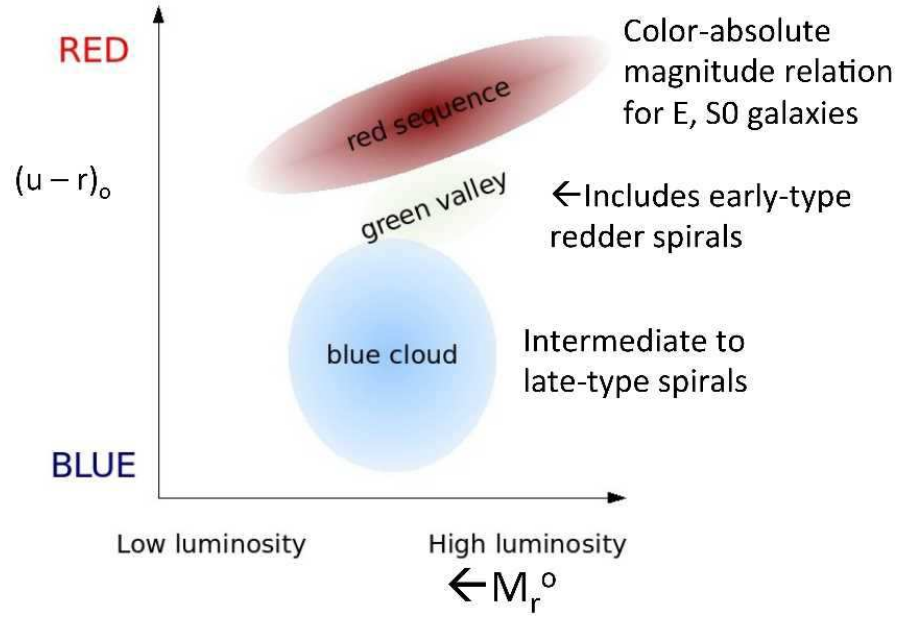

Fig. 2.85. A 'galactic Hertzsprung-Russell diagram' showing the three main groupings of galaxies, the 'red sequence', the 'blue cloud', and the 'green valley'. (Adapted from Wikipedia).

magnitude relation for early-type galaxies that was used extensively for distance scale studies in the 1980s. Star-forming galaxies, including spirals and irregulars, lie mainly in the 'blue cloud'. The 'green valley' is the name given to the zone intermediate between the red sequence and the blue cloud, and it is here where redder, early-type spirals are usually found. Galaxies in the green valley are thought to be evolving from the blue cloud to the red sequence, positioning themselves according to their absolute luminosity.

2.7.19 Galaxy Zoo and citizen science

As I noted earlier, the SDSS is a goldmine for galaxy morphology. Not only are the images of high quality for classification, but the sheer number of images, on the order of a million, is beyond the capability of a small number of experts. An important question is, how to tap the information contained in the survey in a reasonable amount of time? This is what Galaxy Zoo (GZ) was designed to deal with: outsource galaxy morphology and classification to the Internet, and allow non-professional volunteers to participate. The

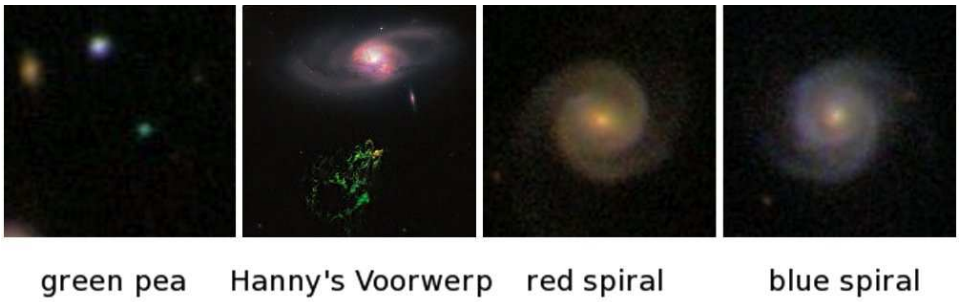

Fig. 2.86. Highlights from GZ1 (B13). Hanny's Voorwerp reproduced with permission from Keel *et al.* (2012).

history of how the project got started, and a summary of its results so far, is provided by Fortson *et al.* (2011).

Launched in 2006, GZ quickly became a model example of scientists giving something back to the general public: an opportunity to do science. The enlisted volunteers became known as 'citizen scientists', and although not a new concept, the sheer number of such scientists who volunteered, more than 200 000 forming a tight-knit community of galaxy morphologists, was surely a wonder to behold. Eventually, two Zoo projects were activated: GZ1, which asked very basic questions about morphology, and GZ2 which was slightly more advanced. Some results from GZ1 are (see also Fig. 2.86):

(a) decoupling of colour and morphology with high statistical significance,
(b) finding that 80% of galaxies follow the usual colour-morphology correlation (meaning red early-types and blue late-types),
(c) attention brought to a significant number of red (passive) spirals and blue early-types,
(d) studies showed that transformation from blue to red is faster than from spiral to early-type,
(e) no evidence for a preferred rotation direction in the Universe,
(f) local fraction of mergers is 1–3%, and
(g) correlations between morphology and black hole growth.

One thing that GZ offered to its volunteers was a real chance for discovery. When examining so many images of galaxies that had not been studied in much detail before, someone was bound to find something new and unusual. This was the case with 'Hanny's Voorwerp (Object)', a colourful cloud of ionised material and some active star formation located near a faint spiral galaxy, IC 2497. Figure 2.86 shows an *HST* image from Keel *et al.* (2012).

Follow-up studies suggest that the Voorwerp is tidal debris from a past encounter between IC 2497 and another galaxy that drew out a tidal tail and triggered infall into a supermassive black hole, producing a transient quasar episode. The Voorwerp's light is an echo of the quasar phase acting on tidal debris (Lintott *et al.* 2009).

A second unusual type of object found in GZ is 'green peas', which are compact star-forming galaxies having a high equivalent width of [OIII] emission (Cardamone *et al.* 2009). A recent study by Amorín *et al.* (2010) showed that green peas are a distinct class of metal-poor galaxies, possibly affected by interaction-driven gaseous inflow over a short phase of evolution.

Another result from GZ is that bars and bulge-dominated galaxies tend to be found in denser environments than unbarred and disk-dominated counterparts (Skibba *et al.* 2012). Also, tidal dwarf galaxies, formed from ejected debris during a merger, were studied by Kaviraj *et al.* (2012) using the GZ merger sample.

2.7.20 Advanced galaxy morphology and classification

While GZ took large-scale galaxy classification to the public, which led to visual morphological information for hundreds of thousands of galaxies and useful information for follow-up studies, the need for more detailed and sophisticated types has led several professional groups to try and get more information on fine structure details with the ultimate goal of facilitating automated galaxy classification. The key to success in such studies has been the development of an interface that allows visual classification to be more efficiently and more accurately carried out. This can be done either in web-based fashion or off-web.

One of the first such studies was by Nair & Abraham (2010), who used SDSS g-band images to visually record morphological information on 14 034 galaxies brighter than magnitude $g' = 16$ and having $z < 0.1$. The survey went beyond RC3-style T-types to include recognition of rings, bars (regular and ansae types), spiral arm morphology, dust, and tidal features.

Another advanced morphological project was the Extraction of the Idealised Shapes of Galaxies from Imagery (EFIGI) survey (Baillard *et al.* 2011), which uses SDSS DR4 images of 4458 RC3 galaxies to get information on 16 morphological attributes, including features such as bulges, arms, bars, rings, dust, flocculence, hotspots, inclination, and environment. The procedure for doing the 'morphometry' was for 11 astronomers to first classify a common subset of 100 galaxies to estimate relative biases and get each observer on a common scale compared to the scale of morphological

T-types in the RC3. Then each observer individually classified 445 galaxies, or 0.1 of the final sample. The final sets were then homogenised to give final classifications on the RC3 scale. The visual classification was done using a sophisticated interface called 'Manclass'. De Lapparent *et al.* (2011) analysed the statistical properties of the final EFIGI catalogue. The goal of the EFIGI catalogue is to set the stage for automated morphometry of the same attributes for a much larger sample.

Another sophisticated morphology project was the Wide-field Nearby Galaxy-clusters Survey (WINGS, Fasano *et al.* 2012). This survey provides morphological types of nearly 40 000 galaxies in 76 nearby galaxy clusters. The classification procedure began with 233 RC3 galaxies classified by two astronomers to evaluate the reliability of visual T-types. Then a single astronomer classified nearly a thousand randomly selected galaxies from the cluster sample to train an automated tool called MORPHOT, which uses neural networks and maximum likelihood techniques to extract types for the full cluster samples.

All of these studies highlight much of the future of galaxy morphology and classification, but most of all, they show that classical morphology still has relevance to modern extragalactic research and still has much to offer as we seek better understanding of galactic evolution.

2.8 Summary

Far from giving way to pure quantitative classification, galaxy morphology today is a vibrant subject with a huge database of material.

The Hubble tuning fork is being seriously modified. The placement of S0s and the interpretation of dwarf early-types has led to the resurrection of parallel sequence classification.

The high quality of digital images has allowed the old classification systems to be modified to recognise the features of current interest in galactic structure.

High-quality IR galaxy classification and morphology is now possible with NIRS0S and the S^4G.

Early-type galaxies continue to be the focus of a great deal of research. $ATLAS^{3D}$ has been a major advance in understanding these galaxies.

S^4G provides an opportunity to study the properties of extreme late-type galaxies in great detail.

Various large imaging surveys, like SDSS, the *Hubble* archives, deep surveys like COSMOS, GOODS, HDF, HUDF, etc., continue to richly add to morphological studies an evolutionary component.

The processes of secular evolution lie in the fine details of galaxy morphology. Interpreting those details is the challenge of the coming years.

Acknowledgments

I am deeply grateful to the organisers of this Winter School for giving me the opportunity to participate as a lecturer in one of the most interesting topics of astronomy today. It was an honour and a privilege to speak to the younger astronomers and to be with such a great group of colleagues. I am also grateful to Gerard de Vaucouleurs and Allan Sandage for inspiring my interest in galaxy morphology almost 40 years ago, and for their encouragement and support over the years that I knew them. Finally, I am grateful to the US National Science Foundation and to the National Aeronautics and Space Administration for past financial support of my extragalactic studies.

This chapter uses images from the Sloan Digital Sky Survey (SDSS). Funding for the creation and distribution of the SDSS Archive has been provided by the Alfred P. Sloan Foundation, the Participating Institutions, NASA, NSF, the U.S. Department of Energy, the Japanese Monbukagakusho, and Max Planck Society. This chapter has also made use of THINGS, "The HI Nearby Galaxy Survey" (Walter *et al.* 2008), and BIMA-SONG, the Berkeley-Illinois-Maryland Survey of Nearby Galaxies" (Helfer *et al.* 2003). Other images are from the archives of the *Hubble Space Telescope*, the *Spitzer Space Telescope*, and the *Galaxy Evolution Explorer* (GALEX). Observations with the NASA/ESA *Hubble Space Telescope* were obtained at the Space Telescope Science Institute, which is operated by the Association of Universities for Research in Astronomy, Inc., under contract NAS 5-26555. The *Spitzer Space Telescope* is operated by the Jet Propulsion Laboratory, California Institute of Technology, under NASA contract 1407. GALEX is a NASA mission operated by the Jet Propulsion Laboratory. GALEX data is from the Multimission Archive at the Space Telescope Science Institute (MAST). Support for MAST for non-HST data is provided by the NASA Office of Space Science via grant NNX09AF08G and by other grants and contracts.

References

Aguerri, J., Hunter, J., Prieto, M. *et al.* (2001), *A&A*, **373**, 786
Aguerri, J. A. L., Méndez-Abreu, J., Corsini, E. M. (2009), *A&A*, **495**, 491
Amorín, R. O., Pérez-Montero, E., Vílchez, J. M. (2010), *ApJL*, **715**, 128
Athanassoula, E. (2005), *MNRAS*, 358, 1477
Athanassoula, E., Bureau, M. (1999), *ApJ*, **522**, 699

Athanassoula, E., Misiriotis, A. (2002), *MNRAS*, **330**, 35
Athanassoula, E., Romero-Gómez, M., Masdemont, J. J. (2009a), *MNRAS*, **394**, 67
Athanassoula, E., Romero-Gómez, M., Bosma, A., Masdemont, J. J. (2009b), *MNRAS*, **400**, 1706
Athanassoula, E., Morin, S., Wozniak, H. *et al.* (1990), *MNRAS*, **245**, 130
Baade, W. (1963), *Evolution of Stars and Galaxies*, Cambridge: Harvard University Press
Bahcall, J. N., Kirhakos, S., Saxe, D. H., Schneider, D. P. (1997), *ApJ*, **479**, 642
Baillard, A., Bertin, E., de Lapparent, V. *et al.* (2011), *A&A*, **532**, 74
Barazza, F., Jogee, S., Marinova, I. (2008), *ApJ*, **675**, 1194
Bell, E. F., de Jong, R. S. (2001), *ApJ*, **550**, 212
Bell, E. F., McIntosh, D. H., Katz, N., Weinberg, M. D. (2003), *ApJS*, **149**, 289
Bertin, G., Lin, C. C., Lowe, S. A., Thurstans, R. P. (1989), *ApJ*, **338**, 78
Bertola, F. (1987), in *Structure and dynamics of elliptical galaxies*, IAU Symp., **127**, 135
Binggeli, B., Sandage, A., Tammann, G. A. (1985), *AJ*, **90**, 1681
Binney, J., Tremaine, S. (1987), *Galactic Dynamics*, Princeton: Princeton University Press
Binney, J., Tremaine, S. (2008), *Galactic Dynamics*, Second edition, Princeton: Princeton University Press
Block, D. L., Bournaud, F., Combes, F. *et al.* (2002), *A&A*, **394**, 35
Block, D. L., Freeman, K. C., Puerari, I. *et al.* (2004), in *Penetrating Bars Through Masks of Cosmic Dust*, D. L. Block, I. Puerari, K. C. Freeman, R. Groess, & E. Block, eds., Astrophysics and space science library (ASSL) vol. 319. Dordrecht: Kluwer Academic Publishers, p. 15
Bothun, G., Impey, C. D., Malin, D. F., Mould, J. R. (1987), *AJ*, **94**, 23
Bothun, G. D., Sullivan, W. T. (1980), *ApJ*, **242**, 903
Bournaud, F., Combes, F. (2002), *A&A*, **392**, 83
Bureau, M., Aronica, G., Athanassoula, E. *et al.* (2006), *MNRAS*, **370**, 753
Bureau, M., Athanassoula, E. (1999), *ApJ*, **522**, 686
Bureau, M., Freeman, K. C. (1999), *AJ*, **118**, 126
Buta, R. (1984), *Proc. Astr. Soc. Australia*, **5**, 472
Buta, R. (1985), *Proc. Astr. Soc. Australia*, **6**, 56
Buta, R. (1986), *ApJS*, **61**, 609
Buta, R. (1987), *ApJS*, **64**, 1
Buta, R. (1991), *ApJ*, **370**, 130
Buta, R. (1995), *ApJS*, **96**, 39
Buta, R. (2002), in *Disks of Galaxies: Kinematics, Dynamics and Peturbations*, E. Athanassoula, A. Bosma, and R. Mujica, eds., ASP Conf. Ser., **275**, 185
Buta, R. (2013), in *Planets, Stars, and Stellar Systems. Volume 6: Extragalactic Astronomy and Cosmology*, T. D. Oswalt, W. C. Keels, eds., Springer, p. 1
Buta, R., Block, D. L., Knapen, J. H. (2003), *AJ*, **126**, 1148
Buta, R., Byrd, G., Freeman, T. (2003), *AJ*, **125**, 634
Buta, R., Byrd, G., Freeman, T. (2004), *AJ*, **127**, 1982
Buta, R., Combes, F. (1996), *Fund. Cosmic Phys.*, **17**, 95
Buta, R., Corwin, H. G., Odewahn, S. C. (2007), *The de Vaucouleurs Atlas of Galaxies*, Cambridge: Cambridge University Press
Buta, R., Crocker, D. A. (1991), *AJ*, **102**, 1715
Buta, R., Crocker D. A. (1993a), *AJ*, **105**, 1344
Buta, R., Crocker D. A. (1993b), *AJ*, **106**, 939

Buta, R., Crocker, D. A., Byrd, G. G. (1999), *AJ*, **118**, 2071
Buta, R. *et al.* (2013), in preparation
Buta, R., Laurikainen, E., Salo, H. (2004), *AJ*, **127**, 279
Buta, R., Laurikainen, E., Salo, H., Block, D. L., Knapen, J. H. (2006), *AJ*, **132**, 1859
Buta, R., Laurikainen, E., Salo, H., Knapen, J. H. (2010a), *ApJ*, **721**, 259
Buta, R., Purcell, G. B. (1998), *AJ*, **115**, 484
Buta, R., Purcell, G. B., Crocker, D. A. (1995a), *AJ*, **110**, 1588
Buta, R., Mitra, S., de Vaucouleurs, G., Corwin, H. G. (1994), *AJ*, **107**, 118
Buta, R., Knapen, J. H., Elmegreen, B. G. *et al.* (2009), *AJ*, **137**, 4487
Buta, R., Ryder, S. D., Madsen, G. J. *et al.* (2001), *AJ*, **121**, 225
Buta, R., Sheth, K., Regan, M. *et al.* (2010b), *ApJS*, **190**, 147
Buta, R., van Driel, W., Braine, J. *et al.* (1995b), *ApJ*, **450**, 593
Buta, R., Williams, K. L. (1995), *AJ*, **109**, 543
Buta, R., Zhang, X. (2009), *ApJS*, **182**, 559B
Buta, R., Zhang, X. (2011), *MSAIS*, **18**, 13
Byrd, G. G., Rautiainen, P., Salo, H., Buta, R., Crocker, D. A. (1994), *AJ*, **108**, 476
Byrd, G. G., Thomasson, M., Donner, K. J., Sundelius, B., Huang, T. Y., Valtonen, M. (1989), *Celestial Mechanics*, **45**, 31
Cappellari, M., Emsellem, E., Krajnović, D. *et al.* (2011), *MNRAS*, **416**, 1680
Cardamone, C., Schawinski, K., Sarzi, M. *et al.* (2009), *MNRAS*, **399**, 1191
Chung, A., van Gorkom, J. H., Kenney, J. D. P., Crowl, H., Vollmer, B. (2009), *AJ*, **138**, 1741
Churchwell, E., Whitney, B. A., Babler, B. L. *et al.* (2004), *ApJS*, **154**, 322
Combes, F. (1991), in *Dynamics of Galaxies and Their Molecular Cloud Dstributions*, IAU Symp. 146, F. Combes & F. Casoli, eds., Dordrecht, p. 255
Combes, F., Sanders, R. H. (1981), *A&A*, **96**, 164
Comerón, S., Knapen, J. H., Beckman, J. E. *et al.* (2010), *MNRAS*, **402**, 2462
Contopoulos, G. (1980), *A&A*, **81**, 198
Contreras-Ramos, R., Annibali, F., Fiorentino, G. *et al.* (2011), *ApJ*, **739**, 74
Corsini, E. (2011), *MSAIS*, **18**, 23
Corsini, E. M., Debattista, V., Aguerri, J. (2003), *ApJ*, **599**, 29
Cowie, L., Hu, E., Songaila, A. (1995), *AJ*, **110**, 1576
Crocker, D. A., Baugus, P. D., Buta, R. (1996), *ApJS*, **190**, 147
Curtis, H. D. (1918), *Pub. Lick Obs. XIII*, Part I, 11
Debattista, V., Sellwood, J. A. (1999), *ApJL*, **513**, 107
Debattista, V., Sellwood, J. A. (2000), *ApJ*, **543**, 704
de Lapparent, V., Baillard, A., Bertin, E. (2011), *A&A*, **532**, 75
de Vaucouleurs, G. (1958), *ApJ*, **127**, 487
de Vaucouleurs, G. (1959), *Handbuch der Physik*, **53**, 275
de Vaucouleurs, G. (1963), *ApJS*, **8**, 31
de Vaucouleurs, G., de Vaucouleurs, A., Corwin, H. G., Buta, R., Paturel, G., Fouque, P. (1991), *Third Reference Catalogue of Bright Galaxies*, New York, Springer (RC3)
de Vaucouleurs, G., Freeman, K. C. (1972), *Vistas in Astronomy*, **14**, 163
Drinkwater, M., Gregg, M., Hilker, M. *et al.* (2003), *Nature*, **423**, 519
Drinkwater, M., Jones, J., Gregg, M, Phillips, S. (2000), *Publ. Astr. Soc. Australia*, **17**, 227
de Zeeuw, P. T., Bureau, M., Emsellem, E. *et al.* (2002), *MNRAS*, **329**, 513
Dressler, A. (1980), *ApJ*, **236**, 351

Elmegreen, D., Elmegreen, B. G., Ferguson, T. E., Mullan, B. (2007), *ApJ*, **663**, 734
Elmegreen, D., Elmegreen, B. G., Sheets, C. (2004), *ApJ*, **603**, 74
Elmegreen, D., Elmegreen, B. G., Yau, A. *et al.* (2011), *ApJ*, **737**, 32
Emsellem, E., Cappellari, M., Krajnović, D. *et al.* (2007), *MNRAS*, **379**, 401
Emsellem, E., Cappellari, M., Krajnović, D. *et al.* (2011), *MNRAS*, **414**, 888
Erwin, P. (2004), *A&A*, **415**, 941
Erwin, P. (2011), *MSAIS*, **18**, 145
Eskridge, P. B., Frogel, J. A., Pogge, R. W. *et al.* (2000), *AJ*, **119**, 536
Eskridge, P. B., Frogel, J. A., Pogge, R. W. *et al.* (2002), *ApJS*, **143**, 73
Faber, S. (1973), *ApJ*, **179**, 423
Fasano, G., Vanzella, E., Dressler, A. *et al.* (2012), *MNRAS*, **420**, 926
Firmani, C., Avila-Reese, V. (2003), *RMxAC*, **17**, 107
Flagey, N., Boulanger, F., Verstraete, L., Miville Deschenes, M. A., Noriega Crespo, A., Reach, W. T. (2006), *A&A*, **453**, 969
Fortson, L., Masters, K., Nichol, R. *et al.* (2011), arXiv/1104.5513
Foyle, K., Rix, H.-W., Zibetti, S. (2010), *MNRAS*, **407**, 163
Gil de Paz, A., Boissier, S., Madore, B. F. *et al.* (2007), *ApJS*, **173**, 185
Gil de Paz, A., Madore, B. F., Boissier, S. *et al.* (2005), *ApJL*, **627**, 29
Gil de Paz, A., Madore, B. F., Pevunova, O. (2003), *ApJS*, **147**, 29
Grouchy, R. D., Buta, R. J., Salo, H., Laurikainen, E. (2010), *AJ*, **139**, 2465
Grouchy, R. D., Buta, R., Salo, H., Laurikainen, E., Speltincx, T. (2008), *AJ*, **136**, 980
Gunn, J. E., Carr, M., Rockosi, C. *et al.* (1998), *AJ*, **116**, 3040
Gunn, J. E., Gott, J. R. (1972), *ApJ*, **176**, 1
Hasan, H., Norman, C. (1990), *ApJ*, **361**, 69
Helfer, T. T., Thornley, M. D., Regan, M. W. *et al.* (2003), *ApJS*, **145**, 259
Helou, G., Roussel, H., Appleton, P. *et al.* (2004), *ApJS*, **154**, 253
Herschel, J. (1864), *Catalogue of Nebulae and Clusters of Stars*, Philosophical Transactions of the Royal Society of London, Volume 154
Higdon, J. L., Buta, R. J., Purcell, G. B. (1998), *AJ*, **115**, 80
Hilker, M. (2011), *European Astron. Society Publication Series*, **48**, 219
Holwerda, B. W., Keel, W. C., Williams, B., Dalcanton, J. J., de Jong, R. S. (2009), *AJ*, **137**, 3000
Hoskin, M. (1982), *Journal for the History of Astronomy*, **13**, 97
Hubble, E. (1922), *ApJ*, **56**, 162
Hubble, E. (1926), *ApJ*, **64**, 321
Hubble, E. (1936), *The Realm of the Nebulae*, Yale: Yale University Press
Hubble, E., Humason, M. (1943), *ApJ*, **74**, 43
Hunt, L. K., Malkan, M. A. (1999), *ApJ*, **516**, 660
Jeans, J. (1928), *Astronomy and Cosmogony*, Cambridge: The University press
Jedrzejewski, R. (1987), *MNRAS*, **226**, 747
Jerjen, H., Kalnajs, A., Binggeli, B. (2000), *A&A*, **358**, 845
Kalapotharakos, C., Patisi, P., Grosbol, P. (2010), *MNRAS*, **408**, 9
Karachentseva, V. E. (1973), *Astrofiz. Issled-Izv. Spets. Astrofiz. Obs.*, **8**, 3
Kaviraj, S., Darg, D., Lintott, C., Schawinski, K., Silk, J. (2012), *MNRAS*, **419**, 70
Kaviraj, S., Ting, Y. S., Bureau, M. *et al.* (2012), *MNRAS*, **423**, 49
Keel, W. C., Lintott, C., Schawinski, K. *et al.* (2012), *AJ*, **144**, 66
Kendall, S., Kennicutt, R. C., Clarke, C., Thornley, M. D. (2008), *MNRAS*, **387**, 1007
Kennicutt, R. C., Armus, L., Bendo, G. *et al.* (2003), *PASP*, **115**, 928

Knapen, J. H. (2005), *A&A*, **429**, 141
Knapen, J. H. (2010), in *Galaxies and their Masks*, D. L. Block, K. C. Freeman, & I. Puerari, eds., Springer, p. 201
Knapen, J. H., James, P. A. (2009), *ApJ*, **698**, 1437
Knapen, J. H., Shlosman, I., Peletier, R. F. (2000), *ApJ*, **529**, 93
Koopmann, R., Kenney, J. D. P. (2004), *ApJ*, **613**, 866
Kormendy, J. (1979), *ApJ*, **227**, 714
Kormendy, J. (1984), *ApJ*, **286**, 116
Kormendy, J. (1985), *ApJ*, **295**, 73
Kormendy, J., Bender, R. (1996), *ApJL*, **464**, 119
Kormendy, J., Bender, R. (2012), *ApJS*, **198**, 2
Kormendy, J., Fisher, D. B., Cornell, M. E., Bender, R. (2009), *ApJS*, **182**, 216
Kormendy, J., Kennicutt, R. C. (2004), *ARA&A*, **42**, 603
Kormendy, J., Norman, C. A. (1979), *ApJ*, **233**, 539
Kuzio de Naray, R., Zagursky, M. J., McGaugh, S. S. (2009), *AJ*, **138**, 1082
Laurikainen, E., Salo, H., Buta, R., Knapen, J. (2007), *MNRAS*, **381**, 401
Laurikainen, E., Salo, H., Buta, R., Knapen, J. (2009), *ApJL*, **692**, 34
Laurikainen, E., Salo, H., Buta, R., Knapen, J. (2011), *MNRAS*, **418**, 1452
Laurikainen, E., Salo, H., Buta, R., Knapen, J. (2011), *Advances in Astronomy*, vol. 2011, id.516739
Laurikainen, E., Salo, H., Buta, R., Knapen, J., Speltincx, T., Block, D. L. (2006), *MNRAS*, **132**, 2634
Lin, L.-H., Yuan, C., Buta, R. (2008), *ApJ*, **684**, 1048
Lintott, C., Schawinski, K., Keel, W. *et al.* (2009), *MNRAS*, **399**, 129
Lundmark, K. (1927), *Medd. Astr. Obs. Uppsala*, No. 30
Lynden-Bell, D., Kalnajs, A.J. (1972), *MNRAS*, **157**, 1
Lynds, C. R., Toomre, A. (1976), *ApJ*, **209**, 382
Madore, B. F., Nelson, E., Petrillo, K. (2009), *ApJS*, **181**, 572
Martin, D. C., Fanson, J., Schiminovich, D. *et al.* (2005), *ApJL*, **619**, 1
Martínez-Delgado, D., Gabany, R. J., Crawford, K. *et al.* (2010), *AJ*, **140**, 962
Martínez-Valpuesta, I., Knapen, J. H., Buta, R. (2007), *AJ*, **134**, 1863
Martínez-Valpuesta, I., Shlosman, I., Heller, C. (2006), *ApJ*, **637**, 214
Mateo, M. (1998), *ARA&A*, **36**, 435
Meidt, S., Schinnerer, E., Knapen, J. H. *et al.* (2012), *ApJ*, **744**, 17
Morgan, W. W. (1958), *PASP*, **70**, 364
Nair, P. B., Abraham, R. G. (2010), *ApJS*, **186**, 427
Narayanan, D., Groppi, C. E., Kulesa, C. A., Walker, C. A. (2005), *ApJ*, **630**, 269
Oh, S., de Blok, W. J. G., Walter, F., Brinks, E., Kennicutt, R. C. (2008), *AJ*, **136**, 2761
Oosterloo, T. A., Morganti, R., Sadler, E. M., Vergani, D., Caldwell, N. (2002), *AJ*, **123**, 729
Parsons, W. (1880), *Observations of Nebulae and Clusters made with the 6 foot Reflector, from 1848 to about the year 1878*, Scientific Transactions of the Royal Dublin Society
Pence, W. D., Taylor, K., Freeman, K. C. *et al.* (1988), *ApJ*, **326**, 564
Peng, C.-Y., Ho, L. C., Impey, C. D., Rix, H.-W. (2002), *AJ*, **124**, 294
Pérez, I., Aguerri, J. A. L., Méndez-Abreu, J. (2012), *A&A*, **540**, 103
Purcell, G. B. (1998), *PhD Thesis*, Univ. of Alabama
Quillen, A. C., Frogel, J. A., González, R. A. (1994), *ApJ*, **437**, 162
Quinn, P. J. (1984), *ApJ*, **279**, 596

Rautiainen, P., Salo, H. (2000), *A&A*, **362**, 465
Rautiainen, P., Salo, H., Laurikainen, E. (2008), *MNRAS*, **388**, 1803
Regan, M., Teuben, P. (2004), *ApJ*, **600**, 595
Reynolds, J. H. (1920), *MNRAS*, **80**, 746
Richer, M., Bullejos, A., Borissova, J. *et al.* (2001), *A&A*, **370**, 34
Ryder, S. D., Buta, R. J., Toledo, H., Shukla, H., Staveley-Smith, L., Walsh, W. (1996), *ApJ*, **460**, 665
Salo, H., Laurikainen, E., Buta, R., Knapen, J. H. (2010), *ApJL*, **715**, 56
Sandage, A. (1961), *The Hubble Atlas of Galaxies*, Carnegie Inst. of Wash. Publ. No. 618
Sandage, A. (2005), *ARA&A*, **43**, 581
Sandage, A., Bedke, J. (1994), *The Carnegie Atlas of Galaxies*, Carnegie Inst. of Wash. Pub. No. 638
Sandage, A., Tammann, G. A. (1981), *A Revised Shapley-Ames Catalog of Bright Galaxies*, Carnegie Institute of Washington Publ. No. 635 (first edition) (RSA)
Sanders, R. H., Tubbs, A. D. (1980), *ApJ*, **235**, 803
Schombert, J. (1986), *ApJS*, **60**, 603
Schombert, J. (1987), *ApJS*, **64**, 643
Schombert, J. (1988), *ApJ*, **328**, 475
Schwarz, M. P. (1981), *ApJ*, **247**, 77
Schwarz, M. P. (1984a), *MNRAS*, **209**, 93
Schwarz, M. P. (1984b), *Proc. Astr. Soc. Aust.*, **5**, 464
Schweizer, F., Ford, W.K., Jedrzejewski, R., Giovanelli, R. (1987), *ApJ*, **320**, 454
Schweizer, F., Seitzer, P. (1988), *ApJ*, **328**, 88
Schweizer, F., van Gorkom, J., Seitzer, P. (1989), *ApJ*, **338**, 770
Schweizer, F., Whitmore, B. C., Rubin, V. C. (1983), *AJ*, **88**, 909
Sheth, K., Regan, M., Hinz, J. L. *et al.* (2010), *PASP*, **122**, 1397
Shlosman, I., Frank, J., Begelman, M. C. (1989), *Nature*, **338**, 45
Simkin, S. M., Su, H. J., Schwarz, M. P. (1980), *ApJ*, **237**, 404
Skibba, R., Masters, K. L., Nichol, R. C. *et al.* (2012), *MNRAS*, **423**, 1485
Spitzer, L., Baade, W. (1951), *ApJ*, **113**, 413
Struck, C. (2010), *MNRAS*, **403**, 1516
Sulentic, J. W., Verdes-Montenegro, L., Bergond, G. *et al.* (2006), *A&A*, **449**, 937
Surace, J. A., Sanders, D. B., Vacca, W. D., Veilleux, S., Mazzarella, J. M. (1998), *ApJ*, **492**, 116
Tremaine, S., Weinberg, M. D. (1984), *ApJL*, **282**, 5
Treuthardt, P., Salo, H., Rautinainen, P., Buta, R. (2008), *AJ*, **136**, 300
Vaisanen, P., Ryder, S., Mattila, S., Kotilainen, J. (2008), *ApJL*, **689**, 37
van den Bergh, S. (1960a), *ApJ*, **131**, 215
van den Bergh, S. (1960b), *ApJ*, **131**, 558
van den Bergh, S. (1976), *ApJ*, **206**, 883
van den Bergh, S. (1980), *PASP*, **92**, 409
van den Bergh, S. (1998), *Galaxy Morphology and Classification*, Cambridge, Cambridge University Press
van den Bergh, S., Abraham, R. G., Ellis, R. S., Tanvir, N. R., Santiago, B. X., Glazebrook, K. G. (1996), *AJ*, **112**, 359
van den Bergh, S., Cohen, J. G., Hogg, D. W., Blandford, R. (2000), *AJ*, **120**, 2190
Verdes-Montenegro, L., Sulentic, J., Lisenfeld, U. *et al.* (2005), *A&A*, **436**, 443
Walter, F., Brinks, E., de Blok, W. J. G. *et al.* (2008), *AJ*, **136**, 2563
White, S. D. M., Rees, M. J. (1978), *MNRAS*, **183**, 341

Whitmore, B. C., Lucas, R. A., McElroy, D. B., Steiman-Cameron, T. Y., Sackett, P. D., Olling, R. P. (1990), *AJ*, **100**, 1489
Wolf, M. (1908), *Pub. Ap. Inst. König. Heidelberg*, Vol. 3, No. 5
Yagi, M., Yoshida, M., Komiyama, Y. *et al.* (2010), *AJ*, **140**, 1814
York, D. G., Adelman, J., Anderson, J. E. *et al.* (2000), *AJ*, **120**, 1579
Zhang, X. (1996), *ApJ*, **457**, 125
Zhang, X. (1998), *ApJ*, **499**, 93
Zhang, X. (1999), *ApJ*, **518**, 613
Zhang, X., Buta, R. (2007), *AJ*, **133**, 2584
Zhang, X., Buta, R. (2012), *MNRAS*, submitted (arxiv:1203.5334)
Zibetti, S., Charlot, S., Rix, H.-W. (2009), *MNRAS*, **400**, 1181
Zwicky, F., Zwicky, M. (1971), *Catalogue of Selected Compact Galaxies and Post-eruptive Galaxies*, Guemligen